Experimental Investigation of Void Fraction During Refrigerant Condensation in Horizontal Tubes

H. R. Kopke, T. A. Newell, and J. C. Chato

ACRC TR-142 August 1998

For additional information:

Air Conditioning and Refrigeration Center
University of Illinois
Mechanical & Industrial Engineering Dept.
1206 West Green Street
Urbana, IL 61801

(217) 333-3115

Prepared as part of ACRC Project 74
Experimental Investigation of Void Fraction
During Refrigerant Condensation and Evaporation
T. A. Newell and J. C. Chato, Principal Investigators

The Air Conditioning and Refrigeration Center was founded in 1988 with a grant from the estate of Richard W. Kritzer, the founder of Peerless of America Inc. A State of Illinois Technology Challenge Grant helped build the laboratory facilities. The ACRC receives continuing support from the Richard W. Kritzer Endowment and the National Science Foundation. The following organizations have also become sponsors of the Center.

Amana Refrigeration, Inc.
Brazeway, Inc.
Carrier Corporation
Caterpillar, Inc.
Copeland Corporation
Dayton Thermal Products
Delphi Harrison Thermal Systems
Eaton Corporation
Ford Motor Company
Frigidaire Company
General Electric Company
Hill PHOENIX
Hydro Aluminum Adrian, Inc.
Indiana Tube Corporation
Lennox International, Inc.
Modine Manufacturing Co.
Peerless of America, Inc.
The Trane Company
Whirlpool Corporation
York International, Inc.

For additional information:

Air Conditioning & Refrigeration Center
Mechanical & Industrial Engineering Dept.
University of Illinois
1206 West Green Street
Urbana IL 61801

217 333 3115

Abstract

EXPERIMENTAL INVESTIGATION OF VOID FRACTION DURING REFRIGERANT CONDENSATION IN HORIZONTAL TUBES

Helmut Ronald Kopke
Department of Mechanical and Industrial Engineering
University of Illinois at Urbana-Champaign, 1998
Ty Newell and John Chato, Advisors

This research on the condenser loop involves the experimental determination of void fractions for both R134a and R410A in various sizes and types of horizontally mounted copper tubes. The test sections are a 6.04 mm i.d. smooth tube, an 8.89 mm i.d. axially grooved tube, and an 8.93 mm i.d. helically grooved (18° helix angle) tube. Refrigerant R134a, a primary replacement for R12, is being tested because it is used extensively. R410A is being tested because it is being considered as one of the replacement refrigerants for R22.

The test matrix for the condenser loop covers a large range of mass fluxes and qualities. The test section inlet temperature is always set to 35 °C. The different inlet qualities are 10%, 30%, and 50%. The four mass fluxes which are tested are 75, 150, 300 and 450 kg/m^2-s.

There are many different existing correlations for void fraction; however, they exhibit little consistency for our refrigerant condenser conditions. For this reason, new, more accurate correlations were developed from the experimental data.

Table of Contents

List of Tables

List of Figures

Nomenclature

a	Helical tube correlation parameter	
b	Axial tube correlation parameter	
D_i	Tube inside diameter	
F_1	Premoli correlation variable	Equation 2.18
F_2	Premoli correlation variable	Equation 2.19
F_{td}	Modified Froude number of Taitel and Dukler	Equation 5.1
Fr	Froude number	Equation 2.14
Ft	Froude Rate	Equation 2.25
$F(X_{tt})$	Function of Lockhart-Martinelli parameter	Equation 2.24
G	Mass flux	
g_c	gravitational constant	
i.d.	inner diameter	
K	Smith's entrainment ratio	
K_H	Hughmark correction factor	Table 2.3
$\dot{m}_l$	mass flow rate of liquid phase	
$\dot{m}_v$	mass flow rate of vapor phase	
P	Pressure	
Re_l	Liquid Reynolds number	$=\frac{GD_i}{\mu_l}$
Re_α	Reynolds number as defined by Hughmark	Equation 2.13
S	Slip-ratio	Equation 2.2
V	Velocity	
V_l	Velocity of liquid phase	
V_v	Velocity of vapor phase	
We_l	Liquid Weber number	Equation 2.20

x	Quality	
x_S	Static quality	Equation 4.1
X_{tt}	Lockhart-Martinelli correlating parameter	Equation 2.8
Y	Premoli correlation variable	Equation 2.21
y_L	Hughmark liquid volume fraction	Equation 2.15
Z	Hughmark correlation parameter	Equation 2.12
α	Void fraction	
β	Volumetric quality	$=\frac{1}{1+\left(\frac{1-x}{x}\right)\left(\frac{\rho_v}{\rho_l}\right)}$
δ	Taitel-Dukler angle of inclination	
μ_l	Liquid viscosity	
μ_v	Vapor viscosity	
ρ_l	Liquid density	
ρ_v	Vapor density	
σ	Surface tension	

Chapter 1

Introduction

One of the fundamental quantities needed to describe two-phase flow is void fraction. For this reason, studies of void fraction are numerous in technical literature. The importance of void fraction to the refrigeration industry lies in its ability to help predict the amount of refrigerant charge in an operating component such as a condenser, which was used in this study, or an evaporator.

Many of the studies performed in the past have been for a bounded set of fluids under a range of operating conditions suitable for a particular application. Due to the complicating factors in two-phase flow, many correlations have been developed, both theoretically and empirically. However, these correlations have not shown agreement with the data gathered in this study or with each other.

The aim of this study is to provide a new, more accurate void fraction correlation. A review of existing literature and past correlations is presented in Chapter 2. Chapter 3 includes a topical, yet detailed description of the experimental apparatus used to collect data. The experimental procedures used to gather data are described in Chapter 4. In Chapter 5, the data which was gathered for the 6.04 mm i.d smooth tube is presented and analyzed. In addition, the data are compared to several existing void fraction correlations. Similar analyses are provided for the 8.93 mm i.d. helical tube and 8.89 axial tube in Chapters 6 and 7, respectively. Correlations involving the Froude rate are presented in Chapter 8. Lastly, the work is concluded in Chapter 9.

Chapter 2

Literature Review

Throughout the last half century, void fraction has been studied extensively by a number of independent researchers. Their interest in void fraction is due to its applications in heat transfer, fluid flow characteristics, and refrigerant charge prediction. Since void fraction is very difficult to measure directly, correlations are typically used. Numerous correlations are available in technical literature. Most of the correlations which will be discussed here are theoretically based, but there are several empirical correlations as well. The correlations can be grouped into the following categories: homogenous, slip-ratio, Lockhart-Martinelli, and mass flux dependent.

This literature review will examine the various correlations of ten separate researchers. It should be noted that many of the correlations mentioned here are overviewed by Rice [1987] and Graham [1998]. The purpose of this literature review is to provide a more in-depth look at these correlations relative to data collected in this investigation.

2.1 Homogenous Correlation

The homogenous void fraction model assumes that the vapor and liquid phases travel at the same velocity, thus creating a homogenous mixture. In this simple model, the relationship between void fraction, α, and quality, x is:

$$\alpha = \frac{1}{1+\left(\frac{1-x}{x}\right)\left(\frac{\rho_v}{\rho_l}\right)} \tag{2.1}$$

2.2 Slip-Ratio Correlations

The slip-ratio dependent correlations are slightly more complicated than the homogenous relationship in that they do not assume that the liquid and vapor phases are traveling at the same velocity. The slip-ratio, S, is defined as the ratio of vapor velocity to liquid velocity and is shown below.

$$S = \frac{V_v}{V_l} \tag{2.2}$$

The slip-ratio is estimated differently by various investigators and is applied to the homogenous correlation as follows:

$$\alpha = \frac{1}{1+\left(\frac{1-x}{x}\right)\left(\frac{\rho_v}{\rho_l}\right)\cdot S} \tag{2.3}$$

2.2.1 Zivi Correlation

One of the earliest theoretical void fraction correlations was proposed by Zivi [1964]. Zivi based his correlation on the principle of minimum entropy generation as applied to a steady state thermodynamic process. He formulated energy dissipation as a function of void fraction, and then sought the void fraction which would minimize the energy dissipation. In order to do this, it was assumed that there were no time variations in void fraction, pressure, quality, and local velocities. In addition, it was assumed that wall friction is negligible, that the flow is annular, and that there is no liquid entrained in the vapor flowing through the tube. Using the above assumptions to solve for the void fraction, Zivi formulated his correlation which is shown below.

$$\alpha = \frac{1}{1+\left(\frac{1-x}{x}\right)\left(\frac{\rho_v}{\rho_l}\right)^{2/3}} \tag{2.4}$$

The slip-ratio in this equation is dependent on the density ratio:

$$S = \left(\frac{\rho_v}{\rho_l}\right)^{-1/3} \tag{2.5}$$

Zivi found that his correlation compared well with data he had taken on a steam/water system. It also worked well with data collected by Martinelli and Nelson [1948], Larson [1957], and Maurer [1960]. The correlation tended to form the lower bound of the experimental data, with the upper bound being given by the homogenous correlation. Zivi also realized that the two bounding curves approached each other as the pressure is increased. Additionally, he noticed that the determining factor when interpolating between the two limits is liquid entrainment. Realizing the importance of liquid entrainment, he stated that any physical model of two-phase flow should include it.

2.2.2 Smith Correlation

Another theoretical slip-ratio correlation was developed by Smith [1969]. His model assumes a liquid annular flow with a homogenous mixture phase of variable density in the center. Both phases have the same velocity head and are in thermal equilibrium. Using these assumptions, Smith derived a formula for the slip-ratio, S, in terms of the density ratio, quality, and entrainment ratio, K.

$$S = K + (1-K)\left[\frac{\left(\frac{\rho_v}{\rho_l}\right)^{-1} + K\left(\frac{1-x}{x}\right)}{1 + K\left(\frac{1-x}{x}\right)}\right]^{1/2} \tag{2.6}$$

Smith's correlation compared well with data he took on a steam/water system. He also compared the correlation at various values of K with data taken by Rouhani and Becker [1963], Haywood, Knights, Middleton, and Thom [1961], and Anderson and Mantzouranis [1960]. It was found that K=0.4 was the best value for fitting the experimental data to the correlation. Since the data taken by the aforementioned researchers was all taken on different experimental setups, the possibility of having a systematic error in the empirical determination of K was eliminated. Smith also found that the experimental data was generally within ±10% of his correlation. He also stated that his correlation was valid for all conditions of concurrent two-phase flow irrespective of flow regime, pressure, mass velocity, mass dryness fraction, and rate of change of enthalpy.

2.2.3 Rigot Correlation

Rigot merely assumed that the slip-ratio for his application was 2, giving rise to the following correlation.

$$\alpha = \frac{1}{1 + \left(\frac{1-x}{x}\right)\left(\frac{\rho_v}{\rho_l}\right)\cdot 2} \tag{2.7}$$

2.2.4 Ahrens-Thom Correlation

Ahrens [1983] developed an empirical value for the slip-ratio by using the steam/water data of Thom [1964]. The slip-ratio, S, is dependent on the density and viscosity ratios. The values for S are shown in Table 2.1. In this method, the slip-ratio is effectively only dependent on operating pressure, and is thus independent of quality.

Table 2.1 Slip Ratios Generalized from Thom's Steam/Water Data

$\left(\frac{\rho_v}{\rho_l}\right)\left(\frac{\mu_l}{\mu_v}\right)^{0.2}$	S
0.00116	6.45
0.0154	2.48
0.0375	1.92
0.0878	1.57
0.187	1.35
0.446	1.15
1.0	1.00

2.3 Lockhart-Martinelli Correlations

All of the correlations which fall into this category employ the parameter of Lockhart and Martinelli [1949]. This parameter is defined as:

$$X_{tt} = \left(\frac{1-x}{x}\right)^{0.9}\left(\frac{\rho_v}{\rho_l}\right)^{0.5}\left(\frac{\mu_l}{\mu_v}\right)^{0.1} \tag{2.8}$$

This parameter was developed as a means of correlating pressure drop for four different types of flow: turbulent vapor and liquid, viscous liquid and turbulent vapor, turbulent liquid and viscous vapor, and viscous liquid and vapor phases. They found that this parameter could also be used to correlate the void fraction in any of the four flows. Air-liquid mixtures were used in their experiments; the liquids used were benzene, kerosene, water, and various oils.

2.3.1 Baroczy Correlation

Baroczy [1965] proposed a void fraction correlation using the Lockhart-Martinelli parameter. His correlation was based on isothermal, two-phase, two component liquid fraction data for liquid mercury-nitrogen and water-air systems. He found that his data compared better when density and viscosity ratios were incorporated into his correlation in addition to the Lockhart-Martinelli parameter. The tabular representation of the Baroczy method is shown in Table 2.2.

Table 2.2 Baroczy Correlation

$\left(\frac{\rho_v}{\rho_l}\right)\left(\frac{\mu_l}{\mu_v}\right)^{0.2}$	X_{tt} 0.01	0.04	0.1	0.2	0.5	1	3	5	10	30	100
	Liquid Fraction (1-α)										
0.00002				0.0012	0.009	0.068	0.17	0.22	0.30	0.47	0.71
0.0001			0.0015	0.0054	0.030	0.104	0.23	0.29	0.38	0.57	0.79
0.0004		0.0022	0.0072	0.180	0.066	0.142	0.28	0.35	0.45	0.67	0.85
0.001	0.0018	0.0066	0.0170	0.0345	0.091	0.170	0.32	0.40	0.50	0.72	0.88
0.004	0.0043	0.0165	0.0370	0.0650	0.134	0.222	0.39	0.48	0.58	0.80	0.92
0.01	0.0050	0.0210	0.0475	0.0840	0.165	0.262	0.44	0.53	0.63	0.84	0.94
0.04	0.0056	0.0250	0.0590	0.1050	0.215	0.330	0.53	0.63	0.72	0.90	0.96
0.1	0.0058	0.0268	0.0640	0.1170	0.242	0.380	0.60	0.70	0.78	0.92	0.98
1	0.0060	0.0280	0.0720	0.1400	0.320	.500	0.75	0.85	0.90	0.94	0.99

Since Baroczy's correlation is a function of physical properties, it can be applied to fluids other than those which he tested. His correlation also compared well with the steam correlation of Martinelli and Nelson, as well as with the steam void fraction data of Isbin [1957] and Larson [1957].

When comparing his correlation with data taken by Staub and Zuber [1964], Baroczy noticed an apparent mass flux effect on void fraction. However, he did not account for this in his correlation.

2.3.2 Wallis and Domanski Correlations

Wallis [1969] developed a correlation for void fraction using the data of Lockhart and Martinelli. This correlation, given below, was based on data collected at low pressures.

$$\alpha = \left(1 + X_{tt}^{0.8}\right)^{-0.378} \tag{2.9}$$

Wallis noted that the accuracy of the correlation decreased as the frictional component of pressure drop decreases in proportion to other flow terms. This is because the Lockhart-Martinelli parameter balances frictional shear stress versus pressure drop.

In a later study by Domanski and Didion [1983], another correlation was proposed. They suggested that Wallis' correlation was good for values of $X_{tt} \leq 10$. For values of $X_{tt} > 10$, the following correlation was suggested.

$$\alpha = 0.823 - 0.157 \cdot \ln(X_{tt}) \qquad X_{tt} \leq 189 \qquad (2.10)$$

The upper bound on the above correlation is where the void fraction becomes negative, which is physically impossible. The data used by Domanski and Didion was collected using a heat pump.

2.4 Mass Flux Dependent Correlations

2.4.1 Hughmark Correlation

One of the earliest mass flux dependent correlations was developed by Hughmark [1962]. His correlation was based on the work of Bankoff [1960]. A bubble flow regime is assumed, with a radial gradient of bubbles across the channel. The bubble concentration decreases monotonically from the center of the tube to the tube wall. It is also assumed that the slip-ratio at any given radial location is 1, although the average vapor velocity is greater than the average liquid velocity because the vapor is concentrated in areas of higher velocity. Bankoff developed a correlation using these same assumptions, but it was only valid for a steam/water system; hence Hughmark developed a correlation which would also be applicable to air-liquid two-phase flow. Hughmark's correlation, as presented by Rice, is given by:

$$\alpha = \frac{K_H}{1 + \left(\frac{1-x}{x}\right)\frac{\rho_v}{\rho_l}} \qquad (2.11)$$

K_H is Hughmark's flow parameter, and is dependent on another parameter, Z, which is dependent on a viscosity averaged, α-weighted Reynolds number, the Froude number, and the liquid volume fraction. The relationship between K_H and Z, which is given below, is presented in Table 2.3.

Table 2.3 Hughmark Correlation Variables

Z	K_H
1.3	0.185
1.5	0.225
2	0.325
3	0.49
4	0.605
5	0.675
6	0.72
8	0.767
10	0.78
15	0.808
20	0.830
40	0.88
70	0.93
130	0.98

$$Z = \frac{Re_\alpha^{1/6} Fr^{1/8}}{y_L^{1/4}} \tag{2.12}$$

where

$$Re_\alpha = \frac{D_i \cdot G}{\mu_l + \alpha(\mu_v - \mu_l)} \tag{2.13}$$

$$Fr = \frac{V^2}{g_c D_i} = \frac{1}{g_c D_i}\left(\frac{Gx}{\beta \rho_v}\right)^2 \tag{2.14}$$

$$y_L = \frac{1}{1 + \left(\frac{x}{1-x}\right)\frac{\rho_l}{\rho_v}} = 1 - \beta \tag{2.15}$$

Combining the above terms gives the following expression for Z:

$$Z=\left[\frac{D_i \cdot G}{\mu_l+\alpha(\mu_v-\mu_l)}\right]^{1/6}\left[\frac{1}{g_c D_i}\left[\frac{Gx}{\rho_v \beta(1-\beta)}\right]^2\right]^{1/8} \tag{2.16}$$

Although Hughmark's correlation was developed for bubble-flow in vertical oil refinery pipelines, it also shows good agreement with horizontal flow data taken at higher pressures and with different flow regimes.

It should be noted that this correlation, although useful, is rather difficult to use due to its iterative nature.

2.4.2 Premoli Correlation

Premoli [1971] developed an empirical correlation based on experiments in which two-phase mixtures flowed upwardly in vertical adiabatic channels. A large number of conditions were tested involving mixture velocity, physical properties, and channel configurations. The correlation was developed by comparing slip-ratio and governing parameters. Premoli also optimized the correlation to minimize the errors in liquid density prediction. The correlation takes the slip-ratio form and is given by:

$$S=1+F_1\left[\frac{Y}{1+YF_2}-YF_2\right]^{1/2} \tag{2.17}$$

where

$$F_1=1.578\cdot Re_L^{0.19}\left(\frac{\rho_l}{\rho_v}\right)^{0.22} \tag{2.18}$$

$$F_2=0.0273\cdot We_L\, Re_L^{-0.51}\left(\frac{\rho_l}{\rho_v}\right)^{-0.08} \tag{2.19}$$

$$We_L=\frac{G^2 D_i}{\sigma \rho_l g_c} \tag{2.20}$$

$$Y=\frac{\beta}{1-\beta} \tag{2.21}$$

The mass flux dependence is provided by including the Reynolds number, Re_L, and Weber number, We_L.

Premoli's correlation showed 5% agreement with his experimental void fraction data.

2.4.3 Tandon Correlation

Another void fraction correlation was devised by Tandon [1985]. Tandon assumed an annular flow regime characterized by an axisymmetric liquid annulus and a vapor core without liquid entrainment. The liquid and vapor flows are also assumed to be steady, one dimensional, and turbulent. They also have constant properties corresponding to their saturated states. Additionally, it is assumed that there is no radial pressure gradient. Tandon's correlation takes the following form:

$$\alpha = 1 - 1.928 \cdot Re_l^{-0.315}[F(X_{tt})]^{-1} + 0.9293 \cdot Re_l^{-0.63}[F(X_{tt})]^{-2} \quad 50<Re_l<1125 \quad (2.22)$$

$$\alpha = 1 - 0.38 \cdot Re_l^{-0.088}[F(X_{tt})]^{-1} + 0.0361 \cdot Re_l^{-0.176}[F(X_{tt})]^{-2} \quad Re_l>1125 \quad (2.23)$$

where

$$F(X_{tt}) = 0.15\left[X_{tt}^{-1} + 2.85 \cdot X_{tt}^{-0.476}\right] \quad (2.24)$$

By incorporating both the Reynolds number, Re_L, and the Lockhart-Martinelli parameter, X_{tt}, Tandon included the effects of mass flux and wall shear stress, respectively.

Tandon's correlation predicted the experimental data of Isbin [1957] and Rouhani and Becker [1963] within ±15%.

2.4.4 Graham Correlation

A correlation for void fraction was also developed by Graham. This correlation was empirical in nature and the data used to formulate it was taken on the experimental setup used for the present study. The experimental data was correlated using the Froude rate parameter which is defined by Hurlburt and Newell [1997] as:

$$Ft = \left[\frac{\dot{m}_v V_v^2}{\dot{m}_l g_c D_i}\right]^{1/2} = \left[\frac{x^3 G^2}{\rho_v g_c D_i (1-x)}\right]^{1/2} \quad (2.25)$$

The Froude rate parameter is a ratio related to the kinetic energy of the vapor to the amount of energy required to pump the liquid from the bottom to the top of the tube. Graham's correlation takes the following form:

$$\alpha = 1 - \exp\left[-1 - 0.3 \cdot \ln(Ft) - 0.0328 \cdot \ln^2(Ft)\right] \qquad Ft>0.01032 \qquad (2.26)$$

$$\alpha = 0 \qquad Ft\leq 0.01032 \qquad (2.27)$$

Graham found that the above correlation fit his data within ±10%.

Chapter 3

Experimental Facility

The experimental apparatus used in these experiments was designed to allow in-tube refrigerant condensation in various test sections. Earlier versions of this apparatus have been described by Hinde [1992], Dobson [1994], Gaibel [1994], Kenney [1994], Ponchner [1995], Sweeney [1996], Graham [1998], and Dobson and Chato [1998]. Dobson provides an extremely detailed description of the entire system, whereas Graham provides a thorough description of the additions made to the system pertinent to the void fraction experiment. For these reasons, only a general description will be provided here.

The purpose of the facility is to provide refrigerant to the inlet of the test section at variety of different operating conditions. The parameters which are varied are mass flow rate, inlet temperature, and inlet quality of the refrigerant. A schematic of the facility is shown in Figure 3.1. The major portions which will be described herein are: the refrigerant loop, the water loop, the test sections, the equipment, and the data acquisition system.

3.1 The Test Facility

The refrigerant loop is constructed of 9.53 mm o.d. (3/8") smooth copper tubing and is fully insulated. The refrigerant is driven through the loop using a MicroPump^{TM} three-gear, variable speed pump. The pump is driven by a 0.25 kW three phase motor which is digitally controlled by an AC inverter. Since this pump does not require lubrication, experiments can be run with pure refrigerants. The mass flow rate of the refrigerant around the loop is controlled by varying the pump speed. Additionally, the flow rate can be altered by utilizing the bypass line around the pump, although this method is not very sensitive and is rarely used. The flow through the pump bypass is controlled by a needle valve.

The refrigerant flow rate is measured by one of two flow meters. For flow rates less than 0.90 kg/min, a Micro Motion D6^{TM} flow meter is used. For flows larger than this, a Max Machinery positive displacement flow meter is used. The uncertainties for these devices are ±0.1% and 0.31%, respectively. The flow meters are connected in parallel and valved such that flow can easily be directed towards either.

After the refrigerant passes through the flow meters, it enters the refrigerant heater section. This section is used to control the inlet temperature and quality of the refrigerant entering the test section. The heater section consists of five passes organized in a vertical, serpentine manner. There are four 180 Ω resistance heaters wrapped around each pass; thus providing up to 6.4 kW of

power. The heaters are secured to the surface with shrink tape, and are also insulated. The first nine heaters are always powered on and are controlled by a 0 to 240 V variable voltage transformer (Variac). Thus, a total of 2.88 kW is always available. If additional power is required, the other heater strips can be turned on using simple on/off switches, although these strips are not used often. The amount of power used is measured by two Ohio Semitronics watt-hour transducers whose uncertainty is 0.2%.

After flowing through the heaters, the refrigerant flows through an adiabatic section; this allows the flow to become fully developed before entering the test section. The test section is an insulated counterflow heat exchanger with two concentric tubes. Refrigerant flows through the inner tube and water flows through the outer tube. A schematic of the test section is shown in Figure 3.2. Pressure and temperature measurements are made within the test section as well.

In the heat exchanger, the water jacket is constructed from a transparent plastic tube. The annulus is actually built in sections since the thermocouples from the inner tube must be brought out of the section every 6 inches. The sections were held together using Weld-On^{TM} epoxy. The inner tube is held in place by nylon washers whose outer diameter is equal to the inner diameter of the outer tube. A schematic of the water loop is shown in Figure 3.3. The nylon washers have holes drilled in them to allow the water to flow through. They also provide better mixing of the water, and thus less temperature stratification. The inlet and outlet temperatures of the water are measured using type-T thermocouple probes. Dobson estimated the uncertainty of these thermocouples to be ±0.1%. The water flow rate through the water jacket is controlled by a needle valve attached to a rotameter. The actual flow rate of the water is measured by taking a timed sample in a graduated cylinder downstream of the test section. According to Dobson, the uncertainty of these measurements is less than 1.5%. Within the water annulus, the pressure had to be high enough to eliminate air bubbles. It was found that using a pressure of 70-140 kPa (10-20 psig) was adequate.

Three different types of copper test sections were used in this study. First, a smooth 6.04 mm i.d. tube was run. Following this tube were two enhanced tubes: a 8.93 mm i.d. helically grooved tube and a 8.89 mm i.d. axially grooved tube. A schematic of the grooved tubes in shown in Figure 3.4 and the dimensions of the tubes are given in Table 3.1.

Table 3.1 Dimensions of Tubes

Geometry	Base Diameter	Outer Diameter	Cross Sectional Area
Smooth	6.04 mm	7.94 mm	28.65 mm^2
0° Axial Grooves	8.89 mm	9.53 mm	60.90 mm^2
18° Helical Grooves	8.93 mm	9.53 mm	60.64 mm^2

Temperature measurements are taken by type-T thermocouples located at five equally spaced stations on the tube. Four thermocouples are at each station, placed at 0°, 60°, 180°, and 240° around the tube. The technique used to mount the thermocouples is outlined in Polaski [1993]. The thermocouples are held in place by grooved copper couplings. These couplings are soldered to the tube, and then the thermocouples are soldered to the tube. Lastly, the thermocouples are covered with Delta Bond™ thermal epoxy. This epoxy strengthens the bond with the tube and protects the thermocouple from the water flowing over it.

Upon exiting the test section, the refrigerant flows through an after condenser. The after condenser is manufactured by Refrigerant Research and has a capacity of 7 kW. The purpose of the after condenser is to return the refrigerant to a sub-cooled liquid state. A sub-cooled liquid state is required because the pump and flow meters do not operate correctly when vapor is present.

Following the after condenser is a receiver submerged in a temperature controlled water tank. The receiver/water tank combination is used to control the overall pressure and temperature of the system. The performance of the system is dependent on how much refrigerant is sent through the receiver. This is controlled by a series of ball valves.

After the refrigerant goes through the receiver, it passes through one more after condenser and a filter/drier. The after condenser ensures that there is no vapor in the flow and the filter/drier removes any water and impurities that may have formed in the tube. Finally, the flow returns to the pump.

3.2 Measurement Devices

Absolute pressure measurements are made at four locations around the refrigerant loop by strain-gage type pressure transducers. The two most critical transducers are located at the test section inlet. Both are manufactured by BEC. One has a range of 0-2100 kPa and the other has a 0-3500 kPa range. Dobson estimated the uncertainty on these transducers to be ±7 kPa. The primary purpose of these transducers is to verify agreement between the measured saturation temperature and the saturation temperature based on pressure. Transducers are also located at the test section outlet, after condenser outlet, and heater inlet. All three of these transducers are made by Setra and have a range of 0-6890 kPa with an estimated uncertainty of ±35 kPa. These transducers are used primarily for leak detection, although the transducer located at the heater inlet is used during data reduction. In addition to the five absolute pressure transducers, there is also a Sensotec differential pressure transducer which measures the pressure drop across the test section. This transducer has a 0-35 kPa range with an uncertainty of ±0.5 kPa.

In addition to the temperature measurements made on the test section, thermocouples are also placed around the entire refrigerant loop. Thermocouple probes are located at the heater inlet, adiabatic section inlet, test section outlet, and after condenser inlet and outlet. The temperature at the heater inlet is used to find the refrigerant enthalpy at that point. The probes at the adiabatic section inlet and test section outlet are used to find enthalpies during single phase tests. All of these thermocouples are type-T as well.

3.3 Data Acquisition System

The data from the system is collected on a Power Macintosh computer with a National Instruments NB-MIO-16 board installed. All temperature, pressure, and flow rate data is taken and then transmitted to the computer. The thermocouple voltages are collected using two Campbell Scientific AM64™ multiplexers and a Campbell Scientific 21X™ datalogger. Each multiplexer is capable of reading 64 analog signals at once, and the datalogger records the data from the multiplexers every 10 seconds. The datalogger is connected to the computer through the serial port. The pressure and flow rate measurements are sent from a voltage board to the NB-MIO-16 in the computer. The data is displayed and saved on the computer using National Instruments LabView 4.0 software.

In addition to the data collected on the computer, the void fraction of the system was determined. This can not be recorded automatically since it requires refrigerant to be pulled out the system during operation. Precise details of how the void fraction measurement system was built are given by Graham. For this reason, only an overview will be given here.

In order for refrigerant too be pulled from the test section during operation, ball valves are at both the inlet and outlet of the test section. These valves are mechanically connected, thus allowing them to be simultaneously be shut, trapping the moving refrigerant in the test section. The system also has a bypass line for the refrigerant to flow through once the ball valves are shut. This line must be manually opened and shut. Once the refrigerant is trapped, it is drained out of the system into a Refrigeration Research 1917™ receiver. The valve stem and connector piece which allow the receiver to be attached to the system were specially designed and are shown in Figures 3.5 and 3.6, respectively. The receiver tank used has an internal valve which allows it to be opened and shut. It also has two ports, one of which has a pressure gauge attached.

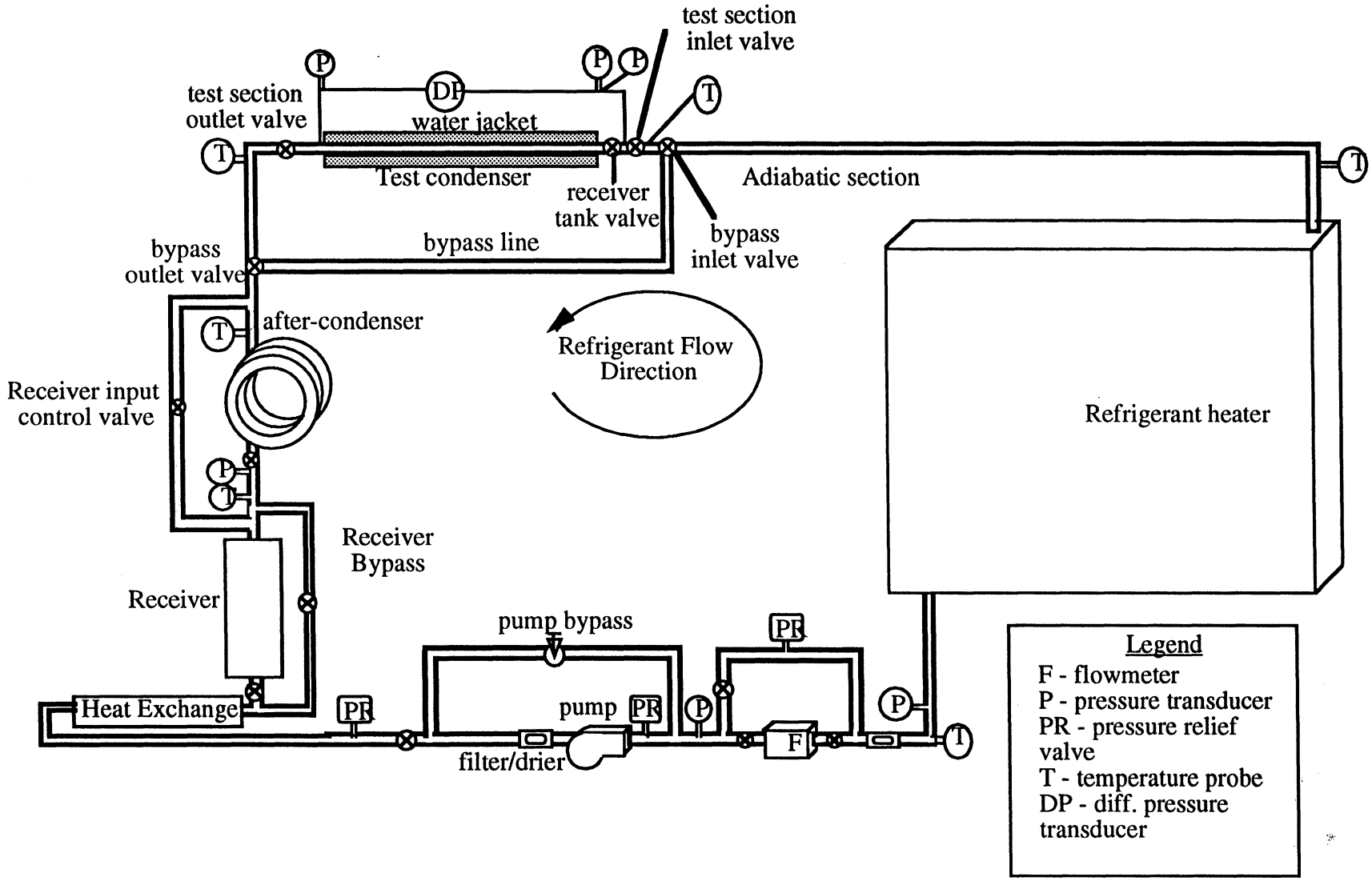

Figure 3.1 Test condenser loop

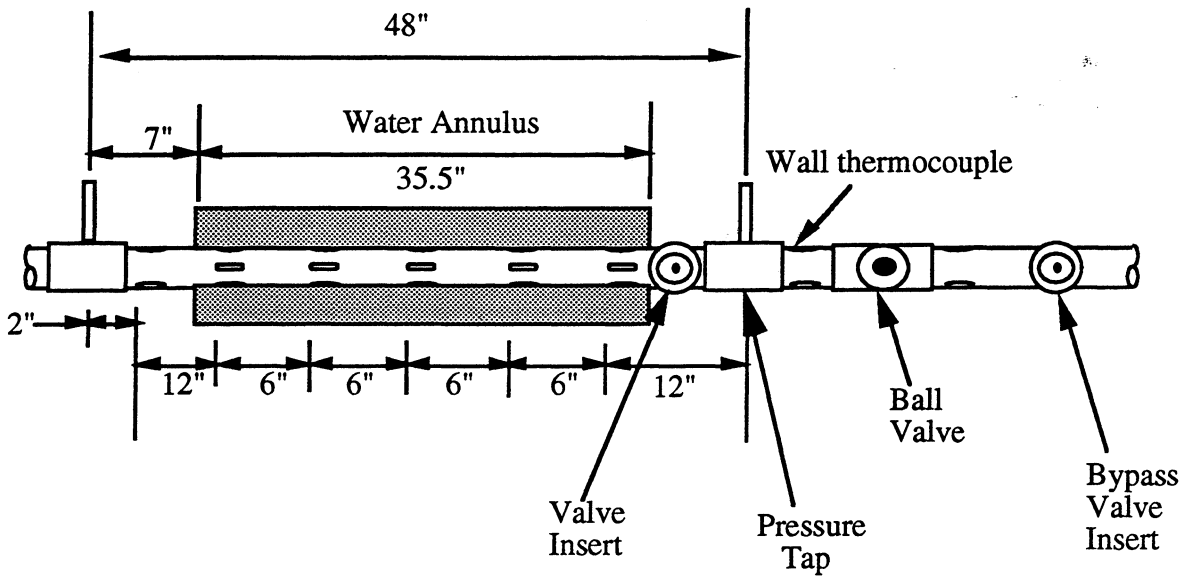

Figure 3.2 Test section schematic

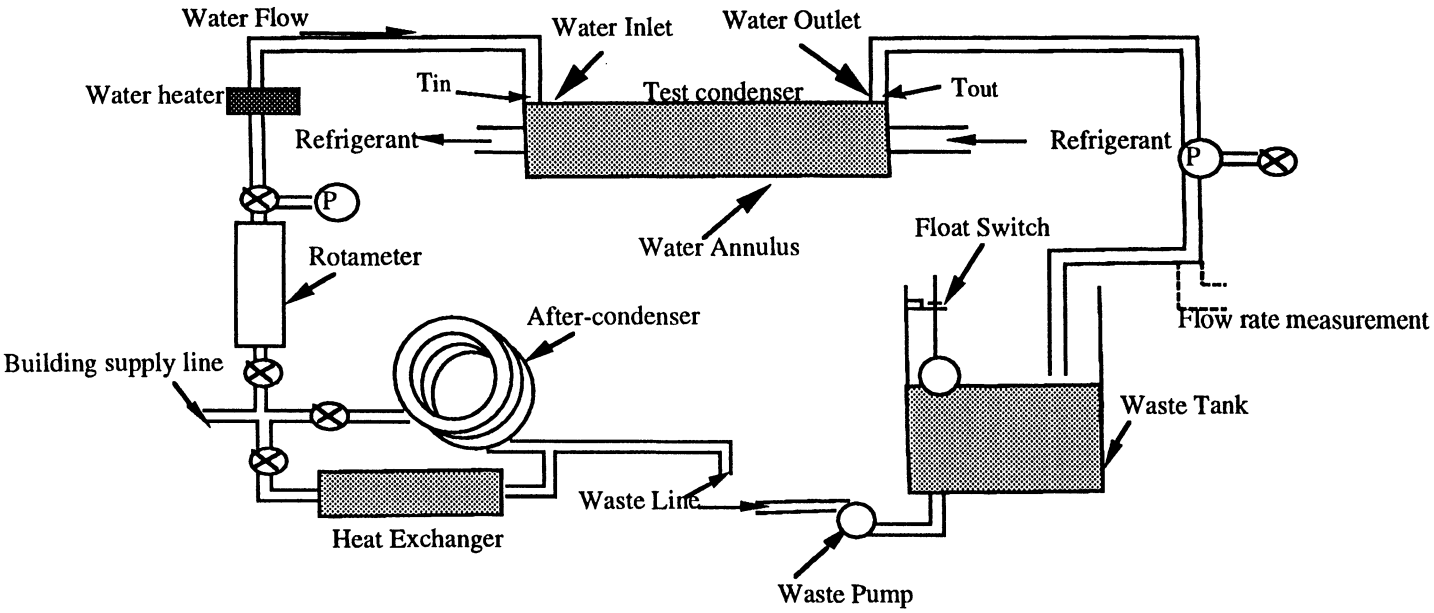

Figure 3.3 Schematic of the water loop

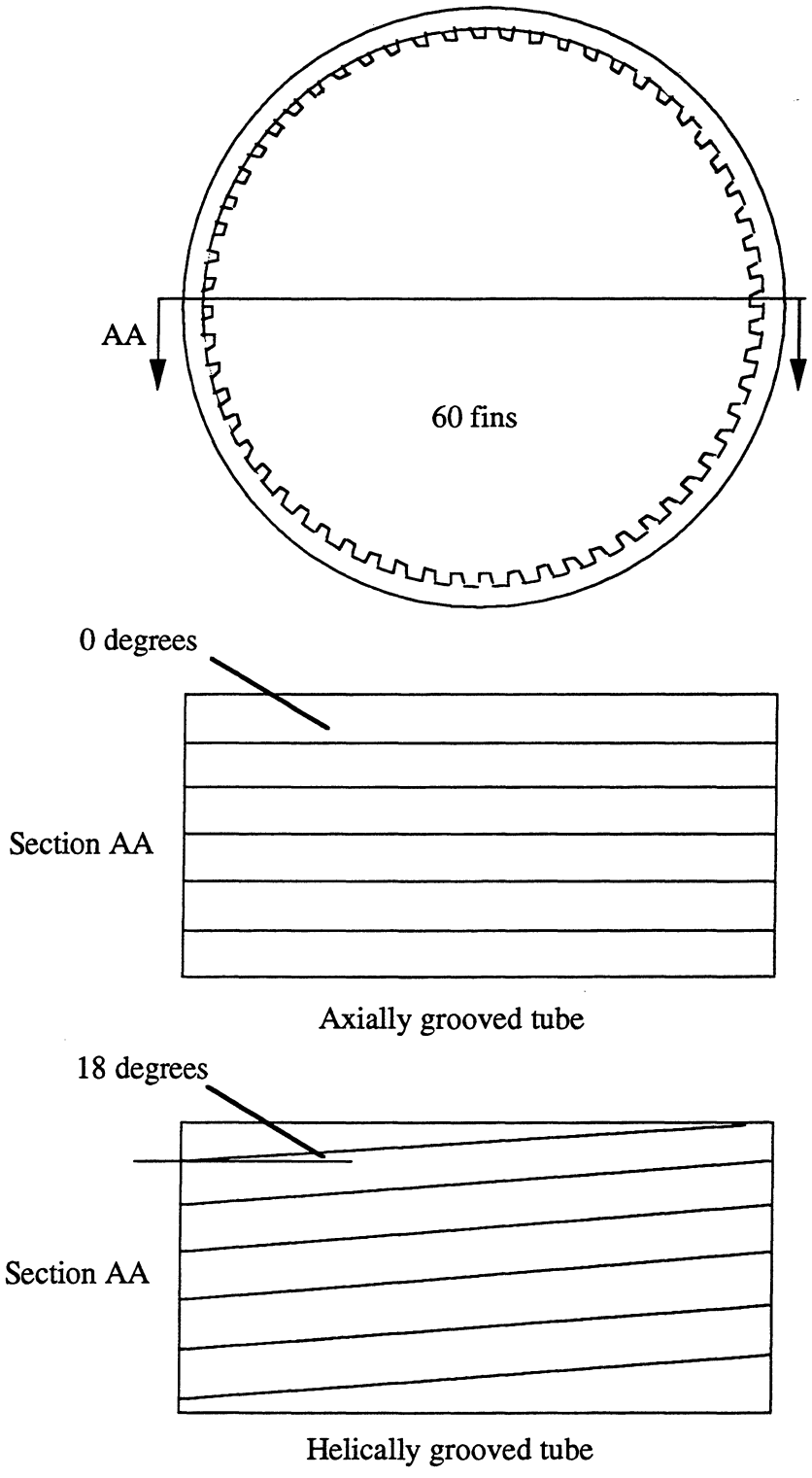

Figure 3.4 Enhanced tube cross sections

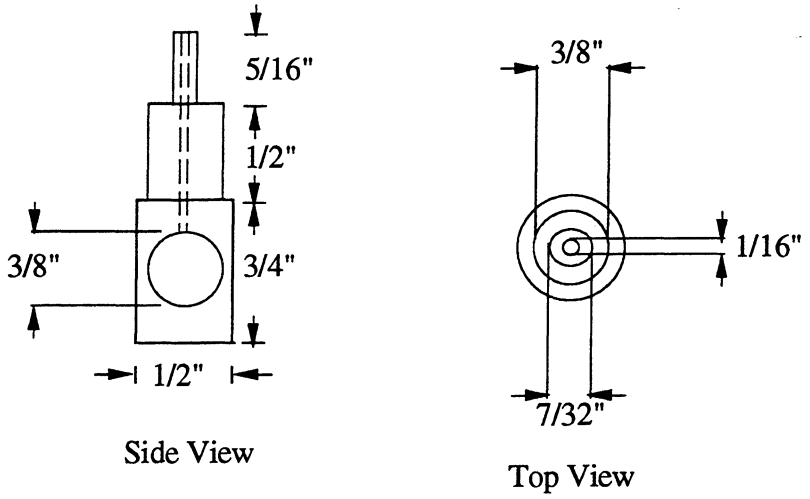

Figure 3.5 Void fraction tap

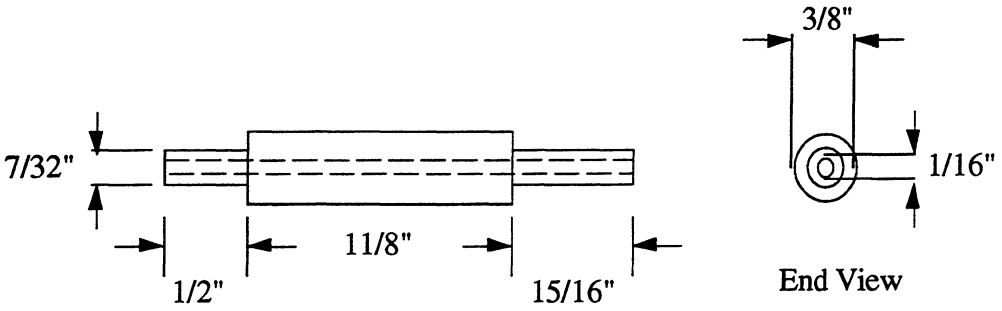

Figure 3.6 Valve insert

Chapter 4

Experimental Procedures

The operational procedures involving the test condenser loop are the same as those given in Hinde [1992], Dobson [1994], Ponchner [1995], and Sweeney [1996]. For this reason, only the details regarding test section volumes and void fraction will be given here.

Before running any tests on the condenser, the test section's volume must be determined. This measurement is extremely crucial for calculating the void fraction. The volume of the test section is found using ideal gas relations. First, an evacuated receiver tank is pressurized to approximately 800 kPa with R134a, R22, or nitrogen. The tank is then weighed before being attached to the evacuated test section at the void fraction tap. The test section's valves must be closed on both ends and the pressure tap valves must be closed as well. At this point the receiver tank valve and the test section void fraction tap are opened, allowing the gas to flow into the test section. After sufficient time has passed to allow the system to equilibrate, the pressure and temperature in the test section are recorded so that the specific volume of the gas in the test section can be calculated using the ideal gas law. Then, the void fraction tap and receiver tank valve are closed and the tank is removed and weighed. By knowing the amount of mass that was transferred to the test section and the specific volume of the gas, the test section volume can be found. This method provides results with an estimated uncertainty of ±10%. At least five trials with each gas were run in order to assure consistency. The initial pressure in the tank was systematically lowered with each trial as well in order to have a larger matrix.

Once the test section volume is determined, the system can be operated. The test matrix for this study was slightly smaller than that run by Graham [1998] since it was found that the most interesting points occurred at lower qualities and mass fluxes. At the higher quality points and mass fluxes, trends tended to be less visible. Mass fluxes of 75 and 300 kg/m^2-s and qualities of 0.1, 0.3, and 0.5 were run for the 6.04 mm i.d. smooth tube. For the 8.89 mm i.d. axial and 8.93 mm i.d. helical tubes, mass fluxes of 75, 150, 300, and 450 kg/m^2-s with qualities of 0.1, 0.3, and 0.5 were run. The test section inlet saturation temperature was generally within half a degree of 35 ^{o}C.

R134a and R410A were the refrigerants which were tested. Since R410A is a mixture of 50% R32 and 50% R125, a gas chromatograph was used to test the data samples in order to assure that there was not preferential distilling of one component. This was done to make sure that the composition of refrigerant in the system remained constant.

Before a point is taken, an evacuated, weighed receiver tank is attached to the test section via the void fraction tap. Once steady state is reached for a given point (e.g. mass flux = 75

kg/m^2-s, quality = 0.1, and saturation temperature = 35 ^oC), the pressure taps are closed and then the test section is isolated by simultaneously closing the ball valves at the inlet and outlet. Immediately after this, the bypass line is opened so that the system can continue to flow. The Variac is turned down so that the refrigerant does not get too hot since the bypass does not condense refrigerant as the test section does. The receiver tank valve and the void fraction tap are opened. The majority of refrigerant from the test section condenses into the tank because it is cooled in a bucket of ice. After the system has equilibrated, the test section pressure and temperature are recorded so that the mass of vapor left in the test section can be estimated using the ideal gas law or other property relations. Then the void fraction tap and the receiver tank are closed. The receiver tank is dried and weighed again.

Once the test section volume and the mass of refrigerant in the section at a given condition are known, the void fraction can be calculated. However, before finding the void fraction a parameter called "static" quality or "x_s," is defined. Static quality is the quality in a non-flowing tube section or in a component that has been isolated from the refrigerant flowing in a test loop. This term is convenient for analysis and is an alternate way of presenting void fraction. The relation between static quality and void fraction is given below:

$$x_s = [((1-\alpha)/\alpha)*(v_v/v_l) + 1]^{-1} \qquad (4.1)$$

where α = void fraction (the vapor cross sectional area to the total cross sectional area)

v_v = specific volume of the vapor phase
v_l = specific volume of the liquid phase
x_s = ratio of the mass of vapor to the total mass in a static test section volume

It should be recognized that the static quality is different than the quality of the refrigerant in a flowing loop. The local quality is defined as the ratio of vapor mass flow rate to the total refrigerant mass flow rate, whereas the static quality is defined as the mass of vapor in a closed component to the total mass of refrigerant in the closed component. The difference between quality and static quality is a measure of the average velocity difference between the liquid and vapor phases.

Chapter 5

Smooth Tube Results

In this chapter, the void fraction results from a 6.04 mm i.d. tube are presented and discussed. The 6.04 mm i.d. tube will be used as a reference case upon which the 8.93 mm i.d. helically grooved tube and 8.89 mm i.d. axially grooved tube will be compared in Chapters 6 and 7. After the data has been presented, it will be compared with the 11 correlations listed in Chapter 2. This will help in determining if a new correlation is needed or if one of the existing ones will suffice.

5.1 Void Fraction Results

The void fraction data obtained in this study can be compared and presented using four different parameters: quality, mass flux, refrigerant, and tube geometry. The effects of varying each of these parameters on void fraction will be discussed, and, when possible, explained.

5.1.1 Effect of Quality on Void Fraction during Condensation

Throughout all of the tests run during the course of this study, there has been a consistent trend involving quality. In Figures 5.1 and 5.2, the void fraction is plotted against the average quality for R134a and R410A, respectively. From these plots, it can be seen that void fraction increases with average quality.

This trend is expected since void fraction is defined as the ratio of vapor volume to total volume in a tube. Since higher qualities naturally have more vapor, it is expected that they would have higher void fractions as well.

5.1.2 Effect of Mass Flux on Void Fraction during Condensation

It can also be seen from Figures 5.1 and 5.2 that mass flux has an effect on void fraction. Void fraction tends to increase with mass flux. The magnitude of the increase is dependent on the average quality as well; e.g. the increase in void fraction from a mass flux of 75 kg/m^2-s to 300 kg/m^2-s is larger for an inlet quality of 10% than for 50%.

One possible explanation for the mass flux effect deals with the different flow regimes encountered at different conditions. Taitel and Dukler [1976] proposed a flow regime map which included five flow regimes: stratified smooth, stratified-wavy, annular, intermittent (plug and

slug), and dispersed bubble. The parameters used to determine flow regime are the Lockhart-Martinelli parameter, X_{tt}, and a modified Froude number, F_{td}, shown below.

$$F_{td} = \sqrt{\frac{\rho_v}{\rho_l - \rho_v}} \frac{Gx/\rho_v}{\sqrt{Dg_c \cos(\delta)}} \tag{5.1}$$

Figure 5.3 shows the various data points separated by mass flux on a Taitel-Dukler flow regime map. On this map, it is clear that most of the points lie in the annular region. However, most of the low mass flux points lie in the stratified wavy region. Figure 5.4 shows the same points, but they are separated by inlet quality. Here it should be noted that the low quality points are located in the stratified wavy region and are also near the intermittent flow regime region. These observations could be the reason for the largest mass flux dependence to be illustrated when comparing low mass fluxes at low qualities to higher mass fluxes.

For a more detailed explanation of the Taitel-Dukler flow regime map, see Dobson [1994] or Wattelet [1994].

5.1.3 Effect of Refrigerant on Void Fraction during Condensation

The data collected in this study also indicated that the refrigerant used also has an effect on the void fraction. Figures 5.5 and 5.6 show void fraction versus average quality for 75 kg/m^2-s and 300 kg/m^2-s, respectively. It is apparent that R134a consistently has a higher void fraction than R410A. R134a's higher void fraction is expected since it has a lower saturation pressure than R410A. R410A's higher saturation pressure causes it to have higher vapor densities, thus causing the vapor in the test section to flow more slowly than R134a vapor at the same conditions.

5.1.4 Effect of Tube Geometry on Void Fraction during Condensation

Comparing the 6.04 mm i.d. smooth tube data with that obtained by Graham for a 7.04 mm i.d. smooth tube leads to the conclusion that diameter has little effect on void fraction over the range tested. This can be seen in Figures 5.7 and 5.8. The larger tube seems to have a slightly lower void fraction at a given point.

5.1.5 Special Tests

While attempting to understand what caused the mass flux effect which is observed in the condenser loop, several special tests were run on the 6.04 mm i.d. smooth tube. These tests were also prompted by a mass flux independence during evaporation being observed by Wilson [1998] and Yashar [1998]. The question was raised whether the direction of heat transfer had an effect on void fraction.

First, tests were run with R134a in which the water in the condenser was turned off, essentially making the test section adiabatic. The results of this test are shown in Figure 5.9. The adiabatic points seem to follow the same trend as the standard test points. Although the adiabatic points have a higher void fraction, for a given inlet quality, they also have a higher average quality.

In addition to the tests run with R134a, several were run with R410A in the 6.04 mm i.d. smooth tube. Adiabatic tests were run with R410A, as well as several "evaporation" tests. This was accomplished by heating the water flowing through the test condenser to a temperature greater than that of the system (typically near 40 ^{o}C). Just as with the R134a trials, these tests showed the same trends as the standard points. This is shown in Figure 5.13.

These tests show that the direction of heat transfer does not appear to significantly affect void fraction.

5.2 Data Comparison

In this section, the data collected for the 6.04 mm i.d. smooth tube will be compared with the correlations reviewed in Chapter 2. The average errors are reported in addition to other trends which are observed. If a correlation seems to work well with the smooth tube, then it will also be compared with the enhanced tubes. However, if it does not, then it will not be reviewed for the enhanced tubes. This is done in order to establish a reference case.

5.2.1 Slip-Ratio Correlations

The experimental data is compared to the homogenous, Zivi [1964], Smith [1969], Rigot [1973], and Ahrens-Thom [1983] correlations in Figures 5.11 through 5.15, respectively. These correlations are defined in sections 2.1 and 2.2.

The homogenous correlation has tendency to over-predict the majority of data points which were taken. The data points taken at 75 kg/m^2-s and 300 kg/m^2-s also are clearly separated as well, with the points taken at 300 kg/m^2-s comparing reasonably well. The overall average prediction error of this correlation is 20.4%.

Unlike the homogenous correlation, the Zivi correlation tends to under-predict the void fraction. However, there is still an evident separation between the different mass fluxes, although Zivi's correlation compares better with the data taken at 75 kg/m^2-s. The average error for this correlation is 19.6%.

The Smith correlation is slightly different from the preceding two in that it generally over-predicts the data taken at 75 kg/m^2-s and under-predicts the data taken at 300 kg/m^2-s. Once again, there is a clear separation between the mass fluxes, this time represented by the 45^o line. The average error associated with this correlation is 16.3%.

Rigot's results are similar to those of Smith. This is rather surprising given the complex nature of Smith's slip ratio and the rather simple assumption of Rigot. It generally under-predicts points at 300 kg/m^2-s and over-predicts the points at 75 kg/m^2-s. The separate mass fluxes are also clearly separated again. An average error of 18.6% is calculated for this correlation.

The last slip ratio correlation to be discussed is that of Ahrens and Thom. Its results are remarkably similar to Rigot's and Smith's; this, too, is surprising since yet another method was used to determine the slip ratio. Once again, mass fluxes of 75 kg/m^2-s are generally over-predicted while the mass fluxes of 300 kg/m^2-s are generally under-predicted. The different mass fluxes are also separated. The average error for the Ahrens-Thom correlation is 17.6%

It should be noted that none of these correlations were expected to work since they do not include a mass flux dependence, although they all had average errors near 20%. It should also be noted that all of the correlations tend to work better for points that were taken at higher inlet qualities, and hence for points with higher void fractions. This is probably because the correlations are generally forced to have a void fraction of 1 at a quality of 100%. Mass flux effects are also generally most evident with low inlet qualities. Finally, it can be seen that none of these correlations were preferential to either R134a or R410A.

5.2.2 Lockhart-Martinelli Correlations

In this section, the data will be compared with the two Lockhart-Martinelli correlations which were investigated in section 2.3. The comparisons of the Baroczy [1965] and Wallis [1969] correlations are shown in Figures 5.16 and 5.17, respectively.

The Baroczy correlation shows good agreement with most of the points taken at 75 kg/m^2-s, but it under-predicts those taken at 300 kg/m^2-s. Additionally, there is a clear separation between the two mass fluxes. The average overall prediction error for this correlation is 15.9%.

Wallis' correlation differs significantly from that of Baroczy. It predicts the points taken at 300 kg/m^2-s extremely well (average error of 4.4%), but it over-predicts the points at

75 kg/m^2-s. The mass flux separation is not as obvious, but it still exists. The average error associated with this correlation is 15.3%.

Once again, it is not expected that either of these correlations should predict this study's data very well since a mass flux dependence is not included. However, the average error for these correlations was near 15%, making them somewhat better than the slip ratio correlations. This may be because the Lockhart-Martinelli parameter is based on vapor shearing liquid in the annular flow regime, and this could be a more accurate representation of what is physically occurring. The Lockhart-Martinelli correlations also showed better agreement at higher void fractions, although the improvement was not as large as for the slip ratio correlations. It should also be noted that neither correlation performed much differently for either of the refrigerants.

5.2.3 Mass Flux Dependent Correlations

The mass flux dependent correlations which will be compared to the experimental data are those proposed by Hughmark [1962], Premoli [1971], Tandon [1985], and Graham [1998]. These are all discussed in section 2.4. The comparisons are shown in Figures 5.18 through 5.21, respectively.

Hughmark's correlation spreads the data out significantly. With the exception of several points, most of the data is under-predicted, although the 75 kg/m^2-s points are represented fairly well. Surprisingly, the separate mass fluxes tend to follow their own trends, although the trends are not as well defined as in the aforementioned correlations. The overall average error for this correlation is 17.2%, which is higher than both the Baroczy and Wallis correlations.

The Premoli correlation performs slightly better than that of Hughmark. The data taken at 75 kg/m^2-s is mostly over-predicted, and that taken at 75 kg/m^2-s is under-predicted. A mass flux separation is still observed as well. The average error for this correlation is 14.4%.

The best correlation by an outside investigator is that given by Tandon. Tandon's correlation collapses the data decently, although mass flux separation can still be seen. Most of the 300 kg/m^2-s points are under-predicted, although the average prediction error on these points is only 7.2%. The 75 kg/m^2-s points are mostly over-predicted. The overall average error for this correlation is 13.6%.

Graham's [1998] correlation, which was developed in a companion study, is by far the best correlation. It collapses the data excellently, and no mass flux separation can be seen. The only problem with this correlation is that it tends to under-predict the data. However, this same trend is demonstrated by his own data in Figure 5.22. In both cases, there seems to be a systematic offset. For this reason, a format similar to Graham's will be used to correlate the data

from this study. The average prediction error for this correlation is 10.2%, which is by far the lowest. For points taken at inlet qualities higher than 10%, the average error drops to nearly 7%.

The mass flux dependent correlations provided rather unexpected results. It was expected that they would collapse the data, although only Graham's correlation did. This may be because the Froude Rate ties the fluid kinetic energy (mass flux) to gravity directly, whereas the others have no gravitational dependence. However, overall these correlations displayed the lowest average errors. In this respect, they did perform better than the other correlations.

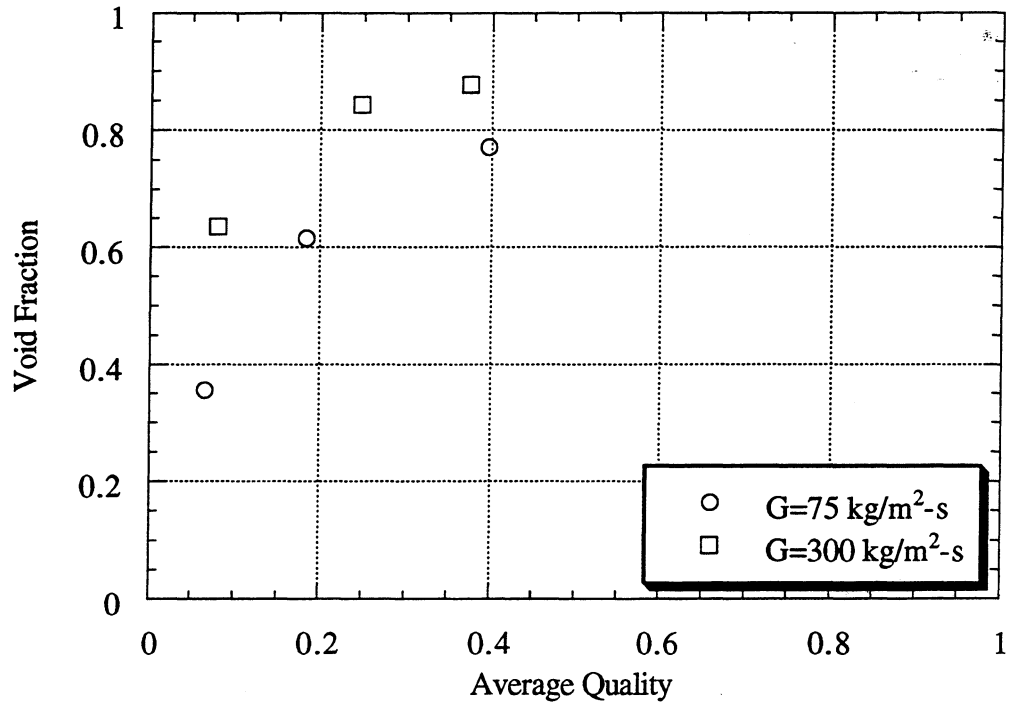

Figure 5.1 Void fraction vs. average quality for R134a in the 6.04 mm i.d. smooth tube

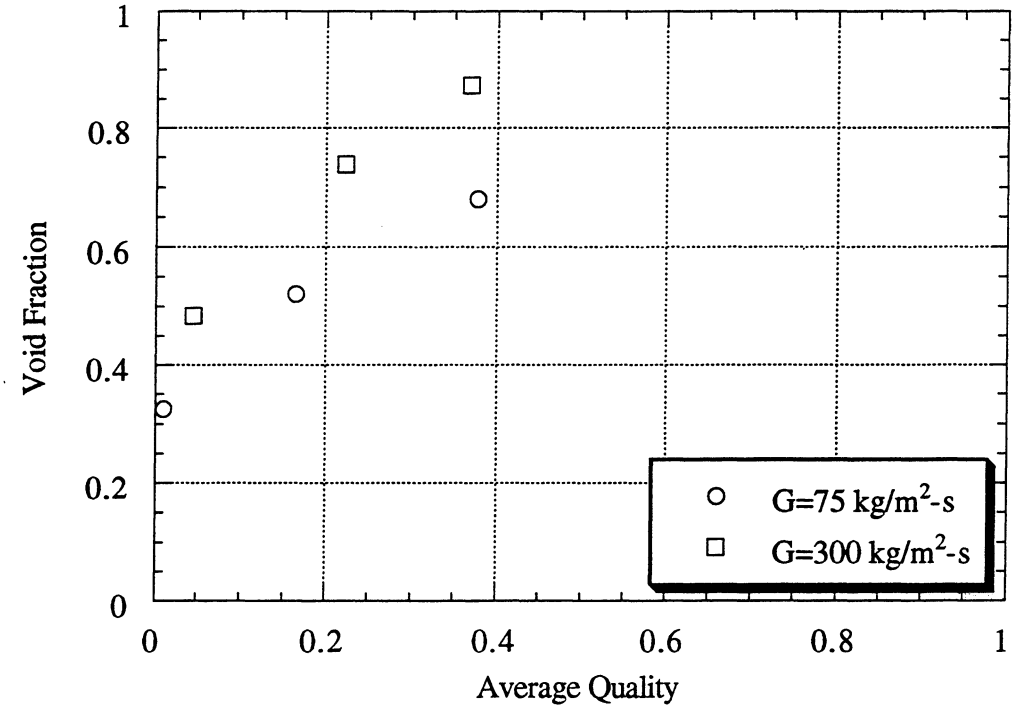

Figure 5.2 Void fraction vs. average quality for R410A in the 6.04 mm i.d. smooth tube

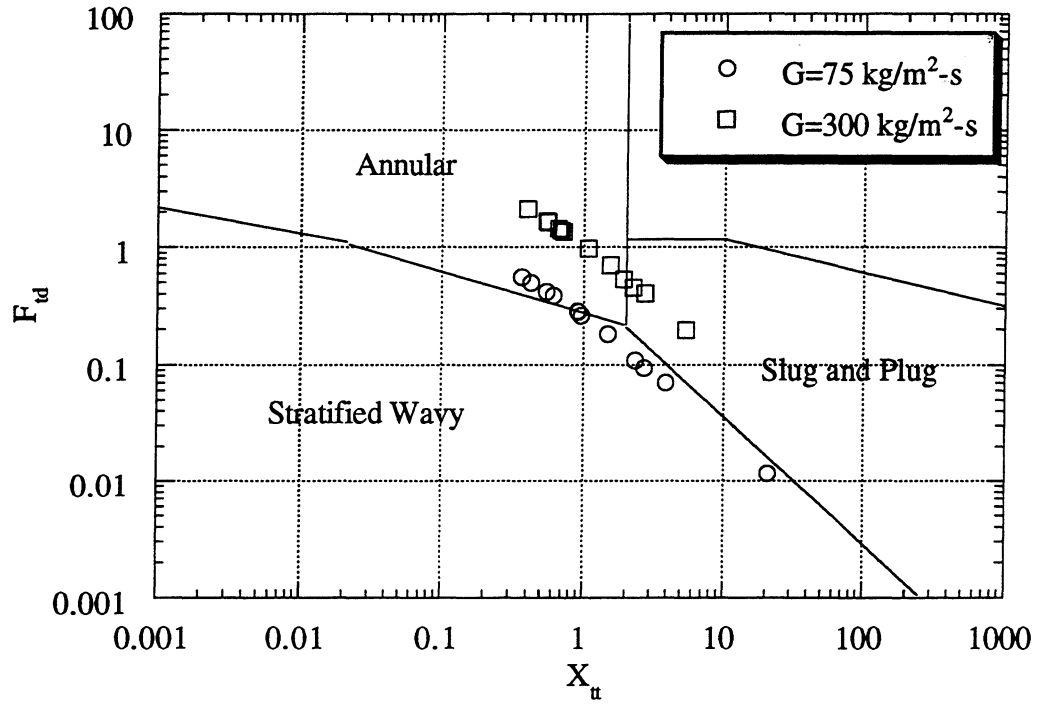

Figure 5.3 Void fraction data for both refrigerants in the 6.04 mm i.d. smooth tube separated by mass flux shown on a Taitel-Dukler flow regime map

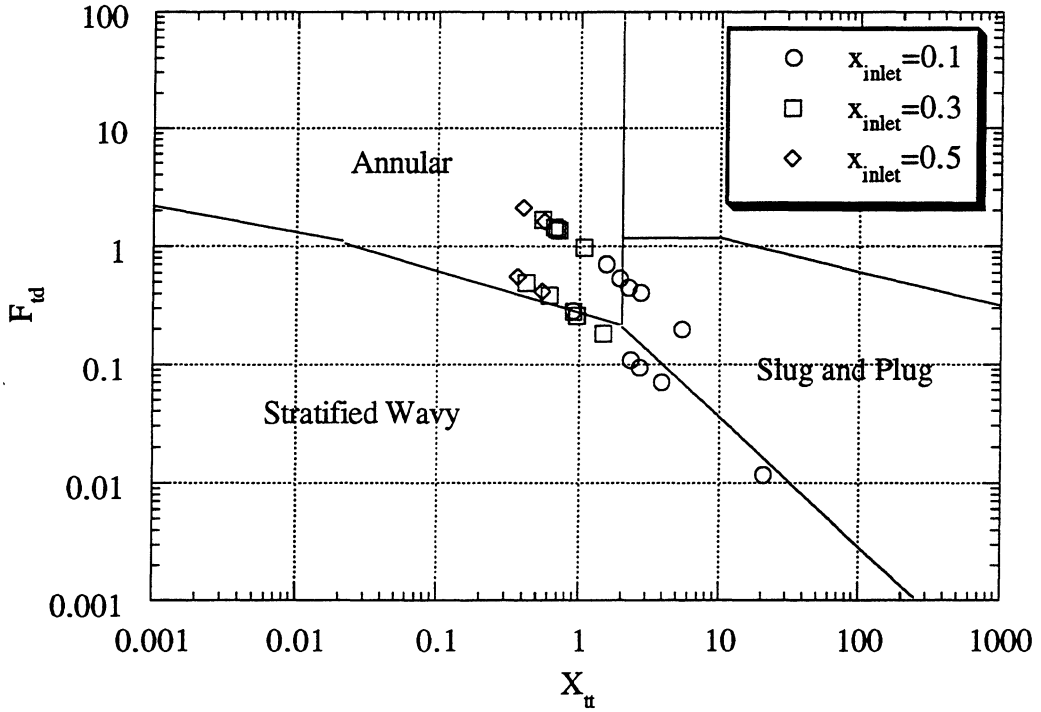

Figure 5.4 Void fraction data for both refrigerants in the 6.04 mm i.d. smooth tube separated by inlet quality shown on a Taitel-Dukler flow regime map

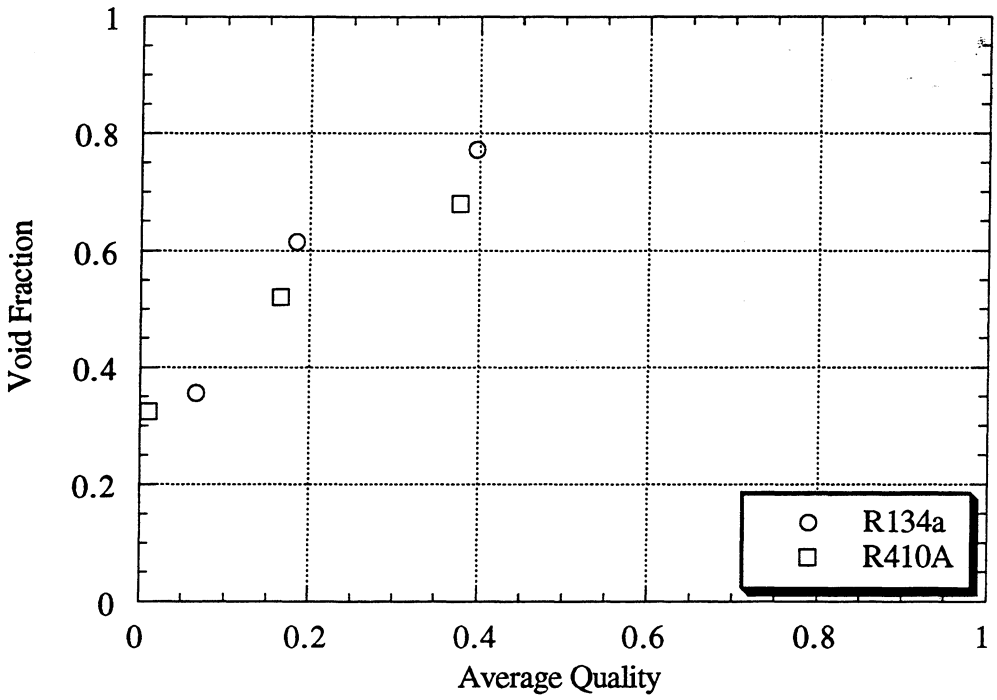

Figure 5.5 Void fraction vs. average quality in the 6.04 mm i.d. smooth tube for G=75 kg/m^2-s

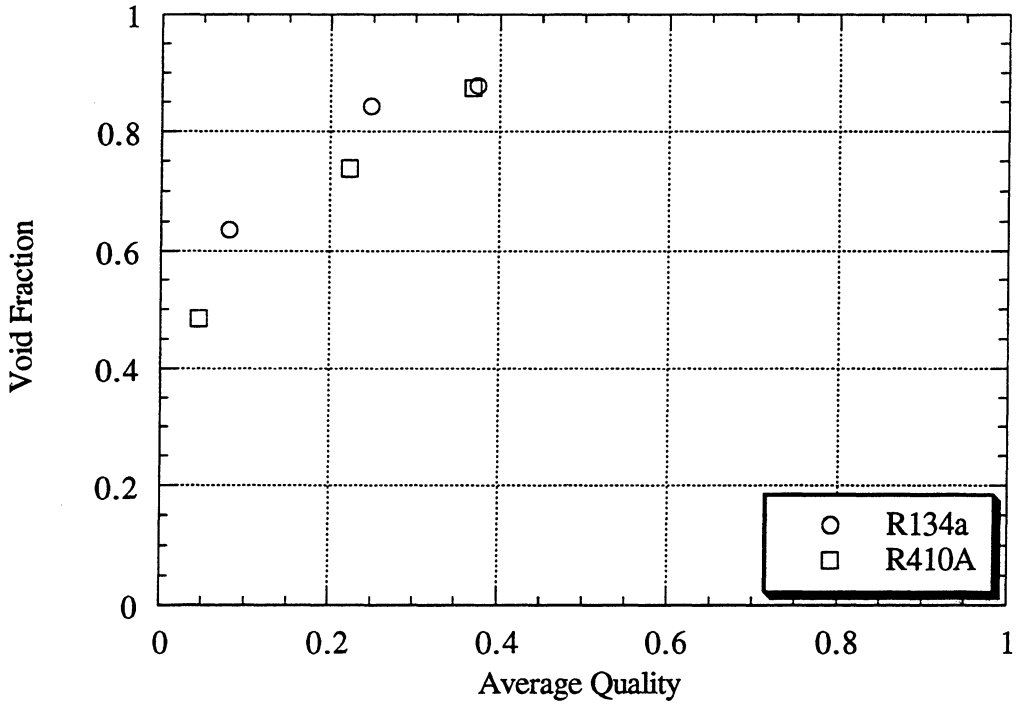

Figure 5.6 Void fraction vs. average quality in the 6.04 mm i.d. smooth tube for G=300 kg/m^2-s

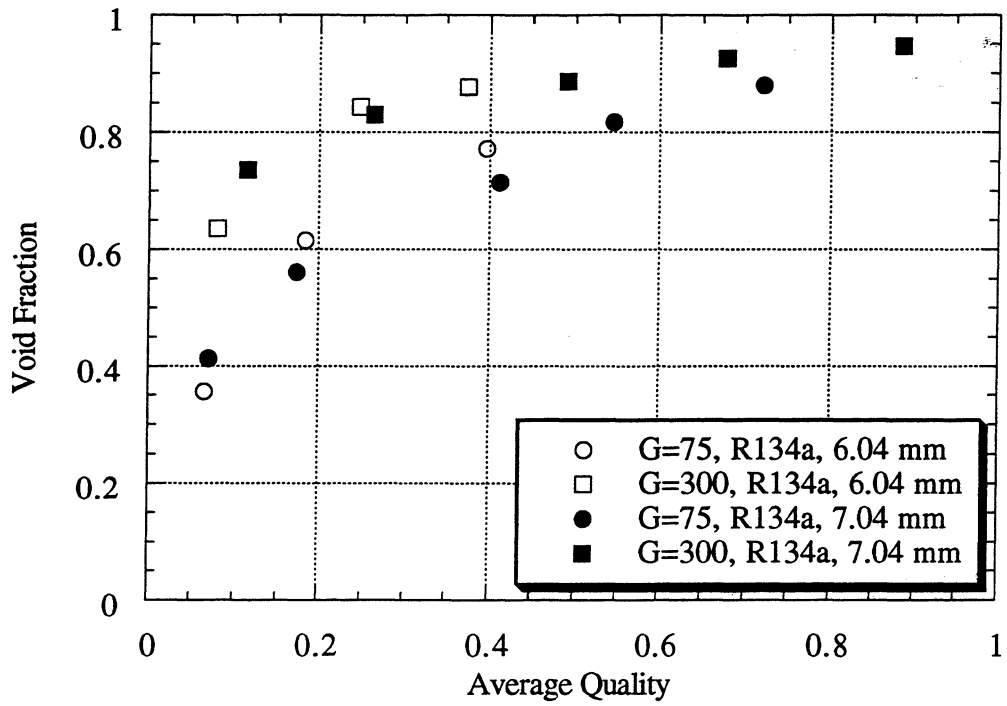

Figure 5.7 Void fraction vs. average quality for R134a in both the 6.04 and 7.04 mm i.d. smooth tubes (G is in kg/m^2-s)

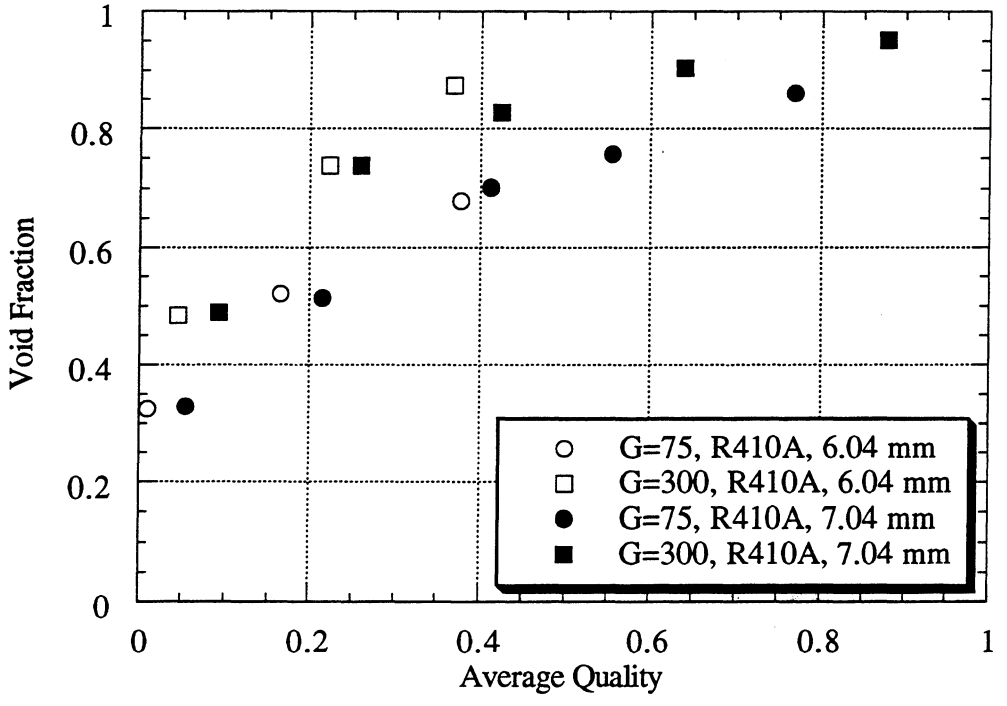

Figure 5.8 Void fraction vs. average quality for R410A in both the 6.04 and 7.04 mm i.d. smooth tubes (G is in kg/m^2-s)

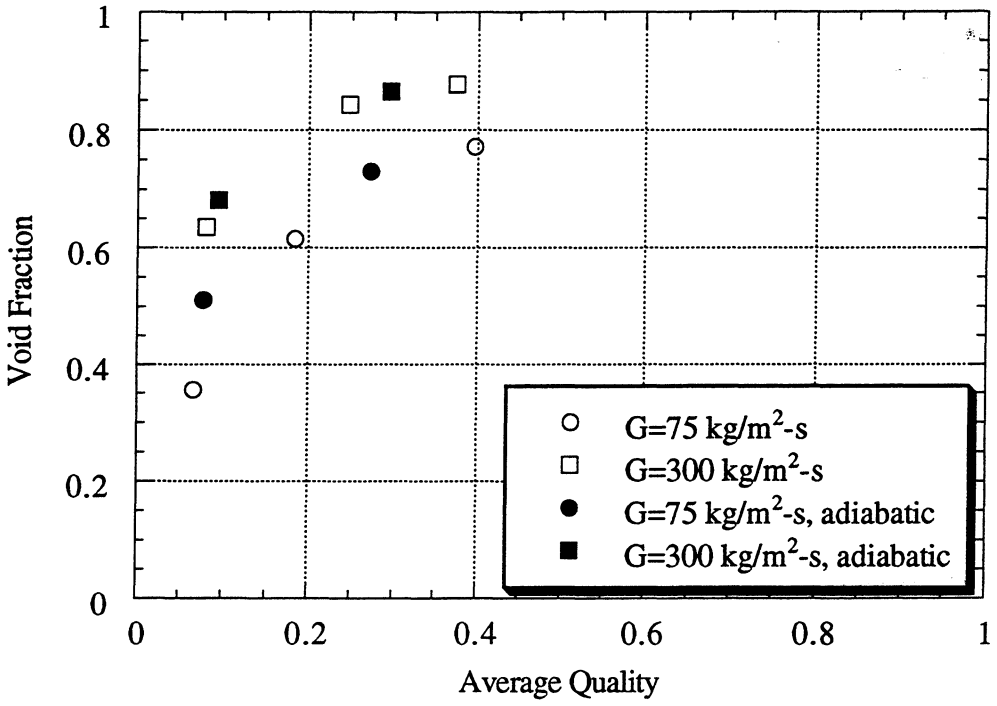

Figure 5.9 Void fraction vs. average quality for the adiabatic tests with R134a in the 6.04 mm i.d. smooth tube

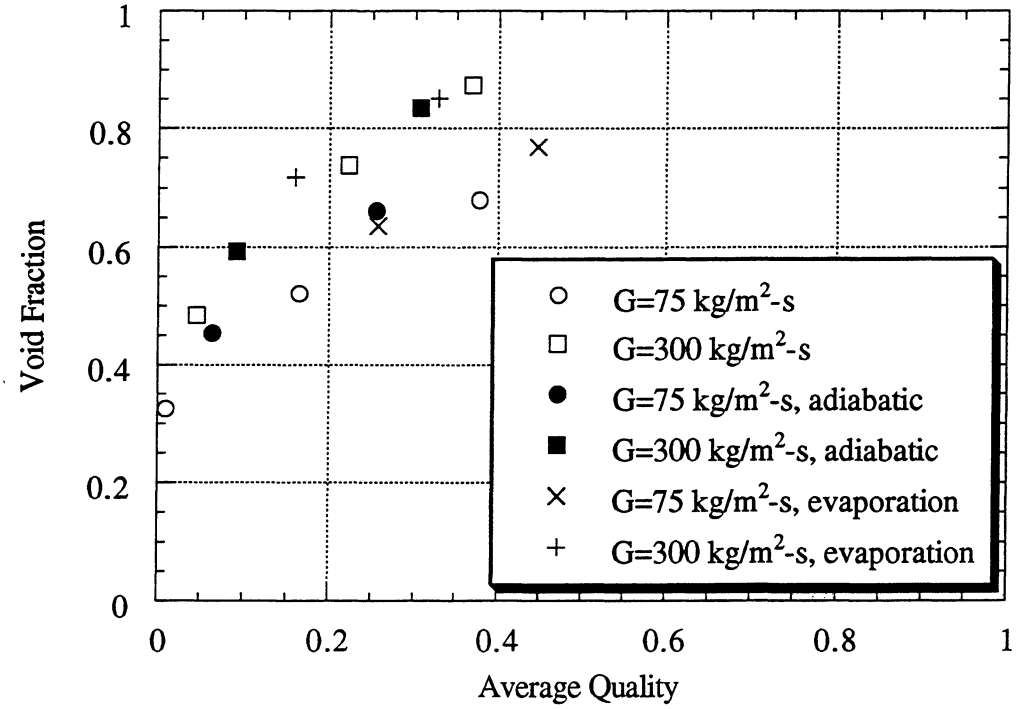

Figure 5.10 Void fraction vs. average quality for the adiabatic and evaporation tests with R410A in the 6.04 mm i.d. smooth tube

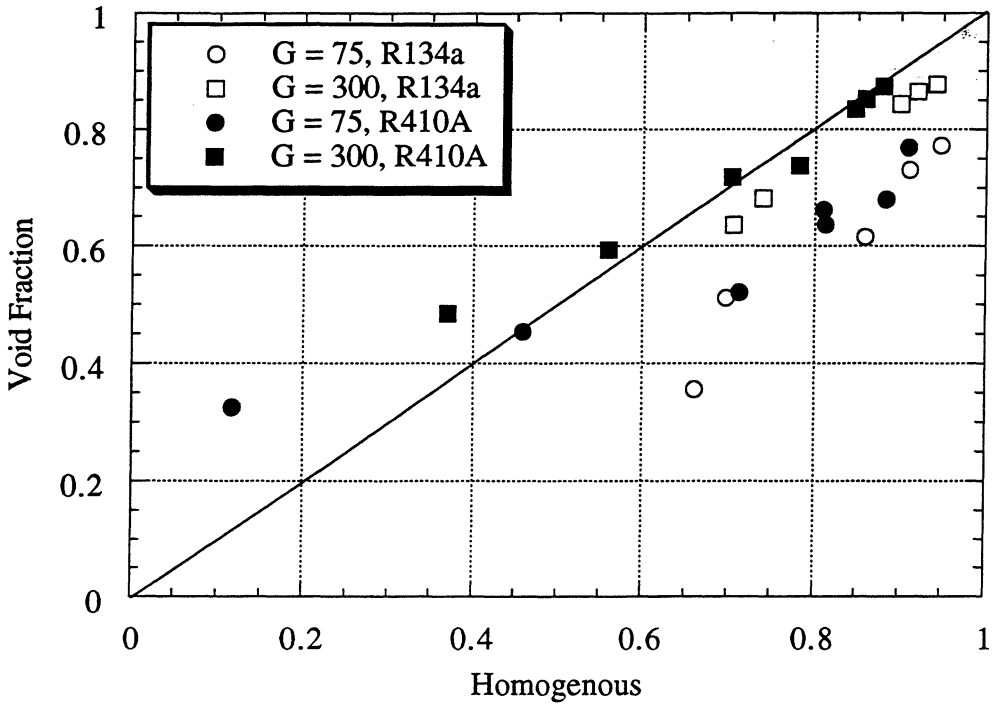

Figure 5.11 Actual void fraction vs. homogenous prediction for the 6.04 mm i.d. smooth tube (G is in kg/m^2-s)

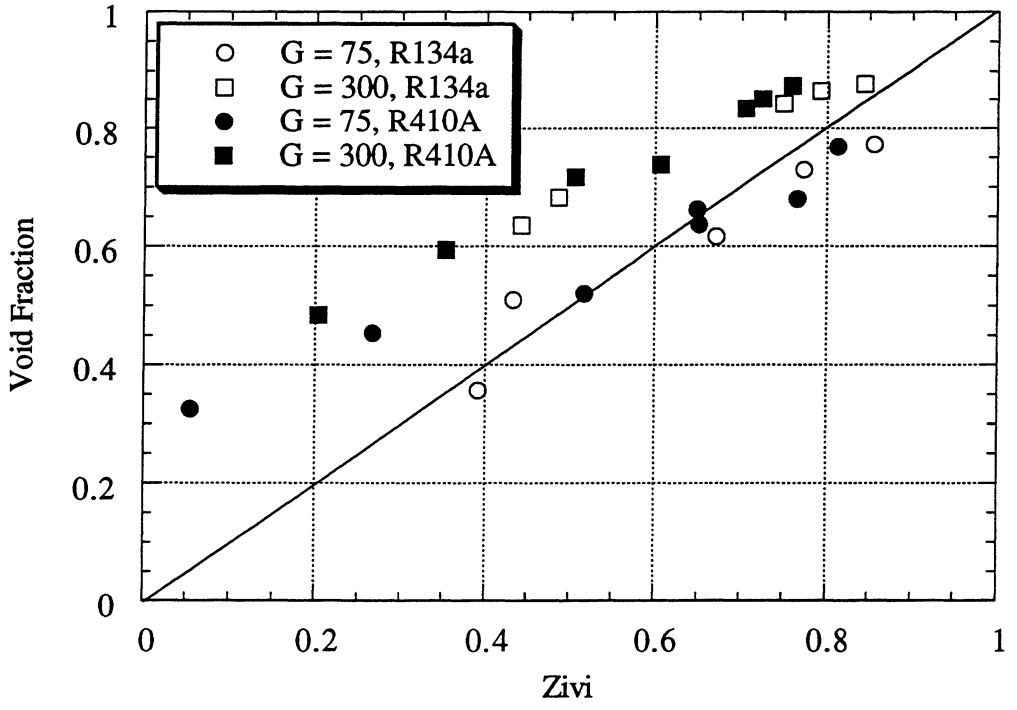

Figure 5.12 Actual void fraction vs. Zivi prediction for the 6.04 mm i.d. smooth tube (G is in kg/m^2-s)

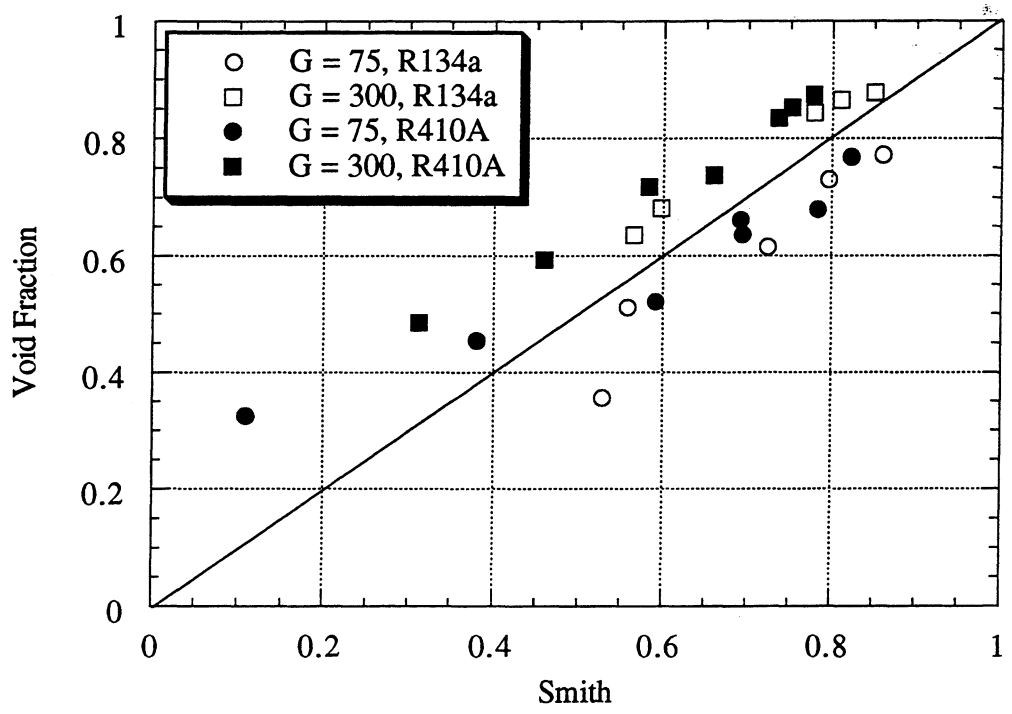

Figure 5.13 Actual void fraction vs. Smith prediction for the 6.04 mm i.d. smooth tube (G is in kg/m^2-s)

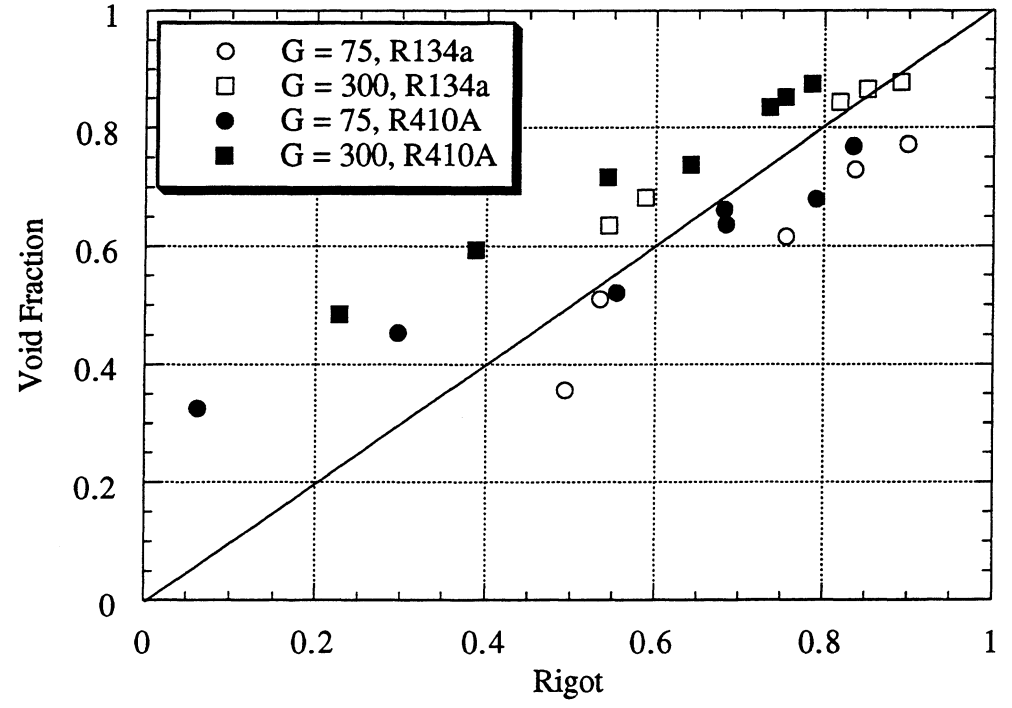

Figure 5.14 Actual void fraction vs. Rigot prediction for the 6.04 mm i.d. smooth tube (G is in kg/m^2-s)

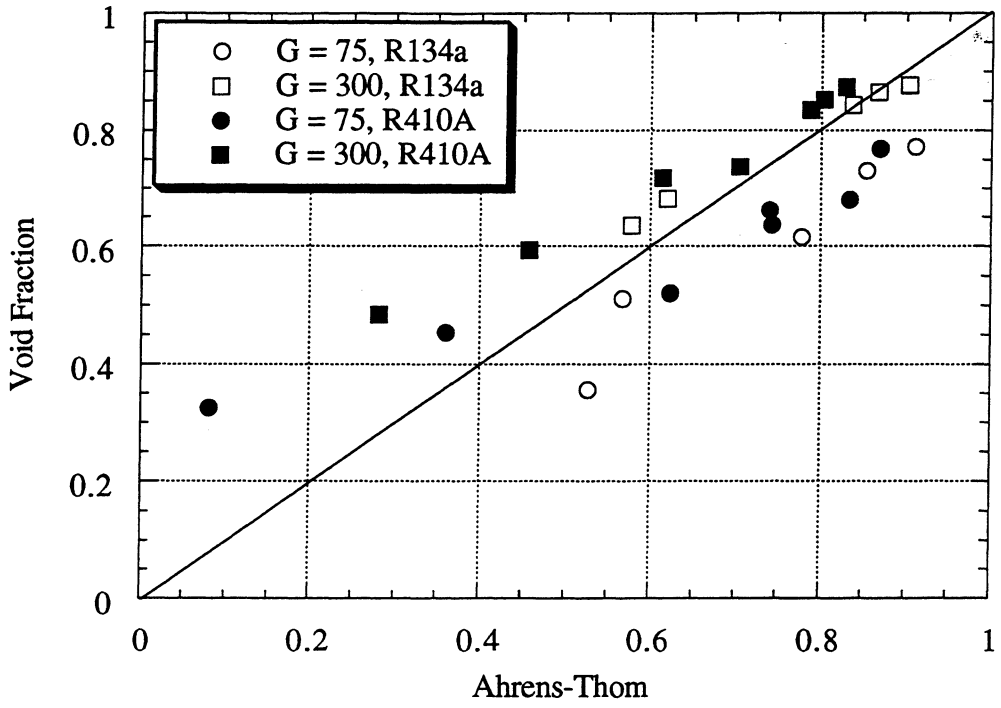

Figure 5.15 Actual void fraction vs. Ahrens-Thom prediction for the 6.04 mm i.d. smooth tube (G is in kg/m^2-s)

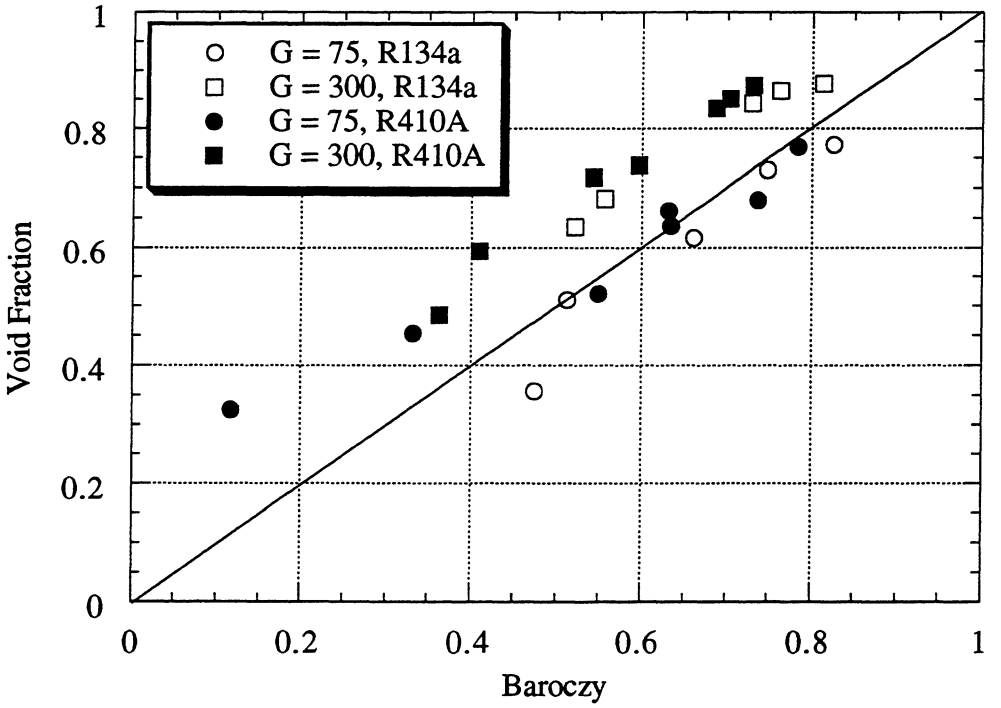

Figure 5.16 Actual void fraction vs. Baroczy prediction for the 6.04 mm i.d. smooth tube (G is in kg/m^2-s)

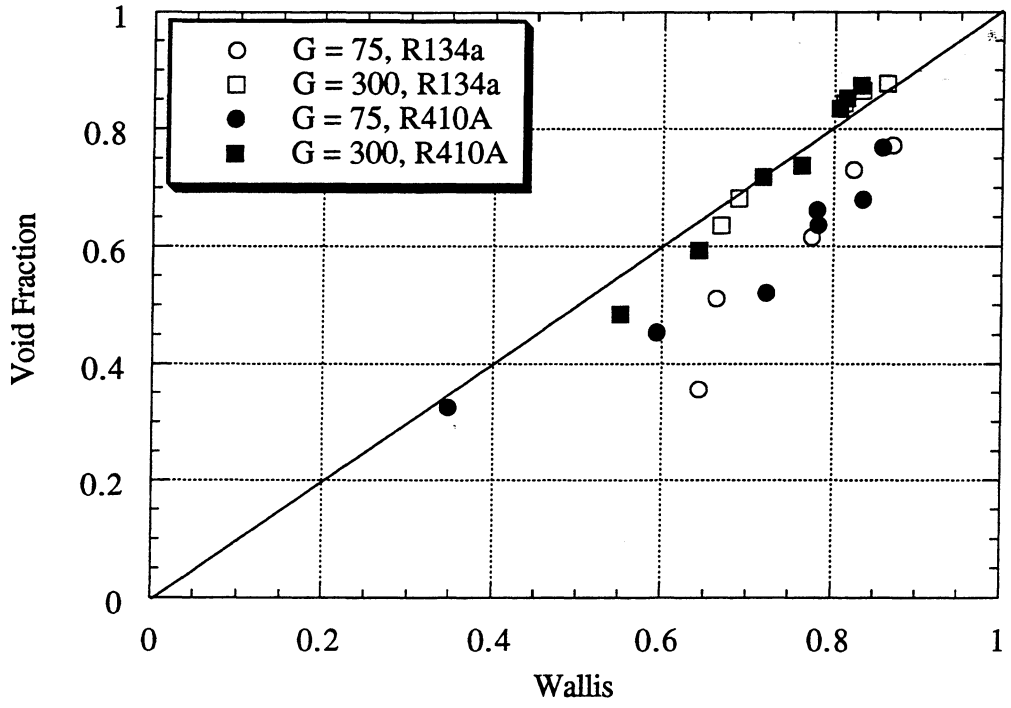

Figure 5.17 Actual void fraction vs. Wallis prediction for the 6.04 mm i.d. smooth tube (G is in kg/m^2-s)

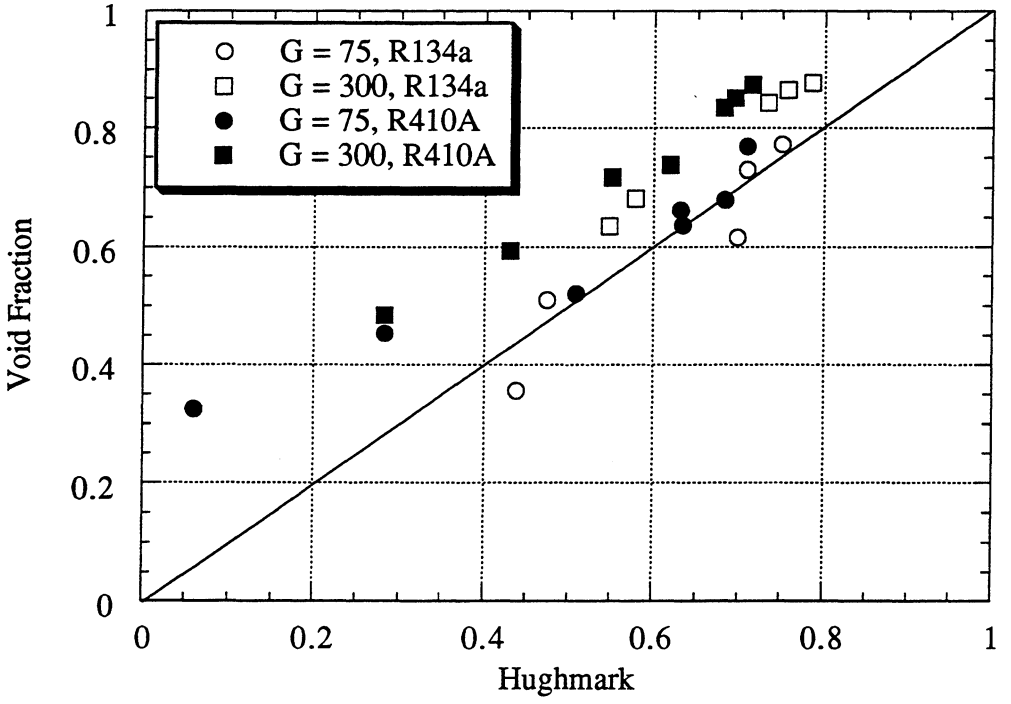

Figure 5.18 Actual void fraction vs. Hughmark prediction for the 6.04 mm i.d. smooth tube (G is in kg/m^2-s)

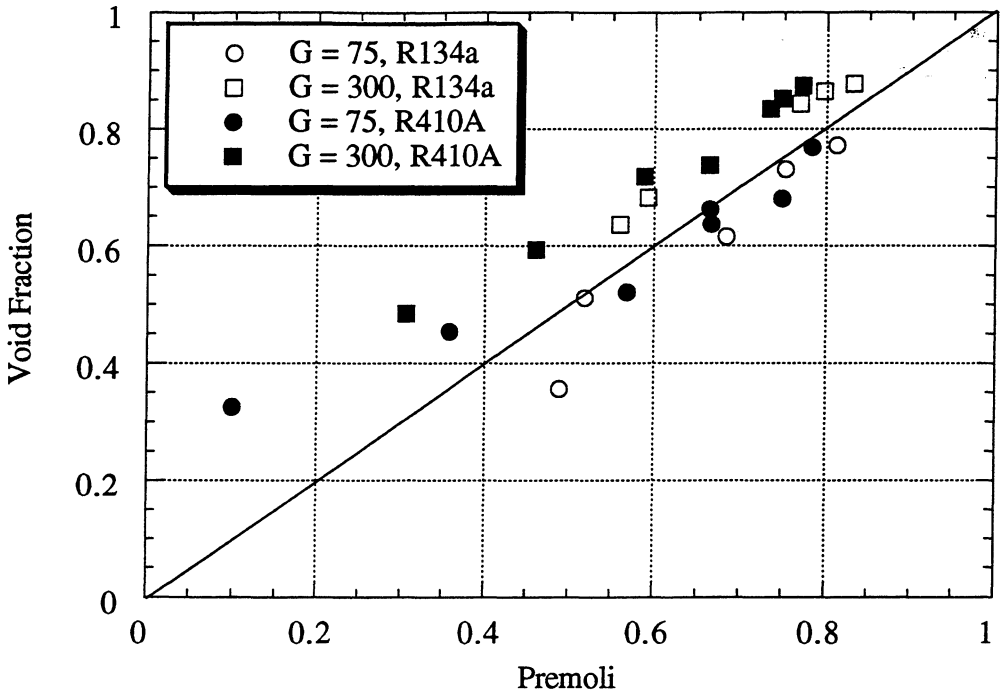

Figure 5.19 Actual void fraction vs. Premoli prediction for the 6.04 mm i.d. smooth tube (G is in kg/m^2-s)

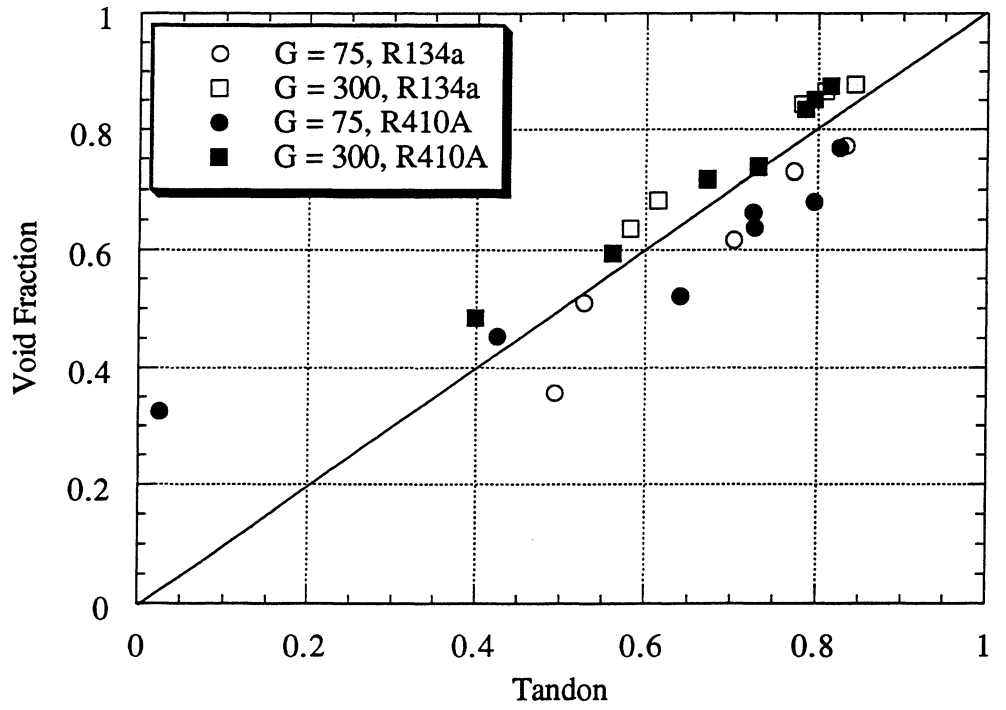

Figure 5.20 Actual void fraction vs. Tandon prediction for the 6.04 mm i.d. smooth tube (G is in kg/m^2-s)

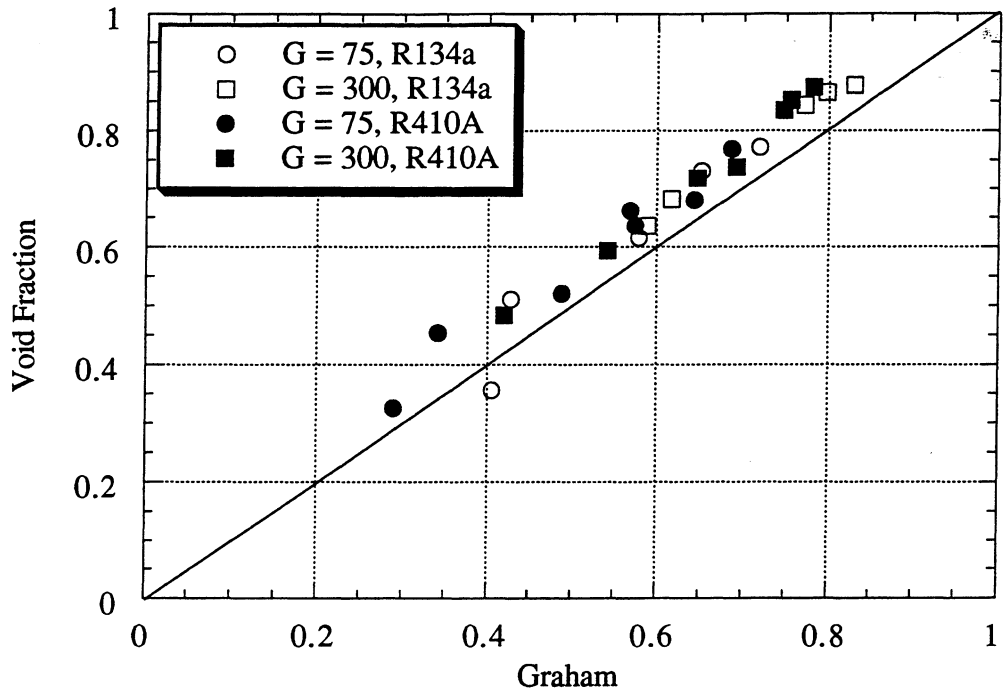

Figure 5.21 Actual void fraction vs. Graham prediction for the 6.04 mm i.d. smooth tube (G is in kg/m^2-s)

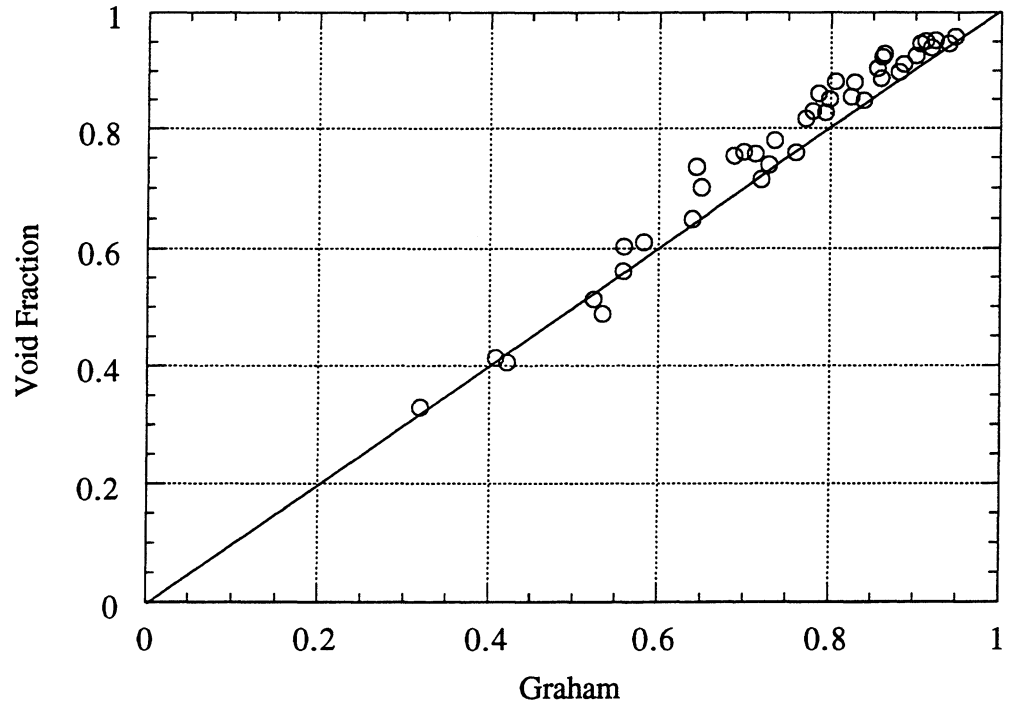

Figure 5.22 Actual void fraction vs. Graham prediction for the 7.04 mm i.d. smooth tube

Chapter 6

Helically Grooved Tube Results

In this chapter, the void fraction results from the 8.93 mm i.d helically grooved are presented and discussed. The results will be compared with those obtained for the 6.04 mm i.d. smooth tube, and a brief discussion pertaining to the correlations presented in Chapter 2 will follow.

6.1 Void Fraction Results

Many of the trends observed in the smooth tube analysis are also demonstrated by the helical tube. Three parameters will be used to compare this data: mass flux, refrigerant, and tube geometry.

6.1.1 Effect of Mass Flux on Void Fraction during Condensation

In Figures 6.1 and 6.2, void fraction is plotted against average quality for both R134a and R410A at the four mass fluxes tested. Once again, it is very apparent that there is a definite mass flux dependence being exhibited by the void fraction. For any given inlet quality, 75 kg/m^2-s has the lowest void fraction, followed by 150 kg/m^2-s, 300 kg/m^2-s, and finally by 450 kg/m^2-s.

In addition, there is a larger mass flux dependence at the points of lower quality and mass flux than at those of higher quality. Similar to the smooth tube, this is explained by the flow regime. In the Taitel-Dukler map shown in Figure 6.3, it can be seen that the points for a low mass flux are generally in the stratified flow regime. In Figure 6.4, it can be seen that the low quality points are near to the intermittent flow regime. Most of the other points fall into the annular flow regime. It seems that the closer the points are to the stratified and intermittent flow regimes, the more mass flux dependence they exhibit.

It should be noted that for the 300 kg/m^2-s and 450 kg/m^2-s cases, not all inlet qualities could be tested due to the size of the tube. Since the tube's cross sectional area is significantly larger than that of the smooth tube, it takes much more heat to raise the quality. This, in turn, makes it difficult to reach higher quality points while also maintaining an inlet temperature of 35 ^{o}C.

6.1.2 Effect of Refrigerant on Void Fraction during Condensation

Figures 6.5 through 6.7 show void fraction versus average quality for 75 kg/m^2-s, 150 kg/m^2-s, and 300 kg/m^2-s. From these plots, it can be seen that R134a generally has a higher void fraction than R410A. Interestingly, the difference is not as large as for the smooth tube. There is one point taken at 300 kg/m^2-s which does not fit the trend, but this is most likely a bad data point.

The reason for the trend is the same as for the smooth tube; the R410A has higher vapor densities, and hence the vapor flows more slowly.

6.1.3 Effect of Tube Geometry on Void Fraction during Condensation

The effect of having microfins with an 18° helix angle is seen in Figures 6.8 and 6.9. The general trend seems to be that the helically grooved tube has lower void fractions than the smooth tube at most points. This may be caused by the helical tube data being "pushed" closer to the stratified flow regime than similar data taken for the smooth tube. This is shown in Figure 6.10. Another possibility is that the boundaries of the flow map are affected by microfins. Also, fins tends to slow the stream-direction velocity of the liquid, thus increasing the average film thickness.

Unfortunately, data was not taken for two helically grooved tubes with different diameters. For this reason, it is not possible to assess the effects of diameter on helically grooved tubes.

6.2 Data Comparison

Since none of the outside investigators' correlations reviewed in Chapter 2 compared well with the smooth tube, they will not be reviewed for the axial tube. Only the Graham [1998] correlation will be compared in detail since it was the lone correlation to collapse the data of the smooth tube well. However, the graphical comparisons of the other correlations are all shown in Appendix B, which also includes a table of the average prediction error associated with each correlation.

6.2.1 Graham Correlation

Figure 6.11 shows how Graham's correlation compares with the actual data from the 8.93 mm i.d. helical tube. The data collapses exceptionally well for both refrigerants and all mass fluxes, but the correlation does tend to over predict some of the lower void fraction points. The average prediction error for this correlation is 13.2%. However, when excluding points taken at inlet qualities of 10%, the average error drops below 5%.

Due to the excellent ability of this correlation to collapse the data, a correlation of similar form will be used to predict the experimental data.

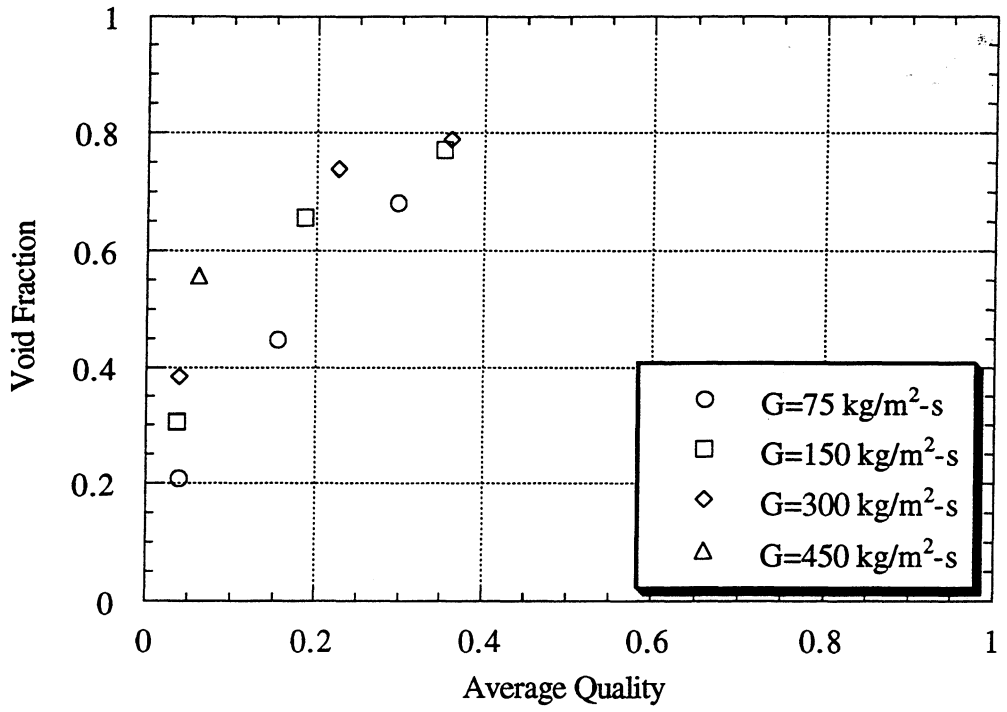

Figure 6.1 Void fraction vs. average quality for R134a in the 8.93 mm helical tube

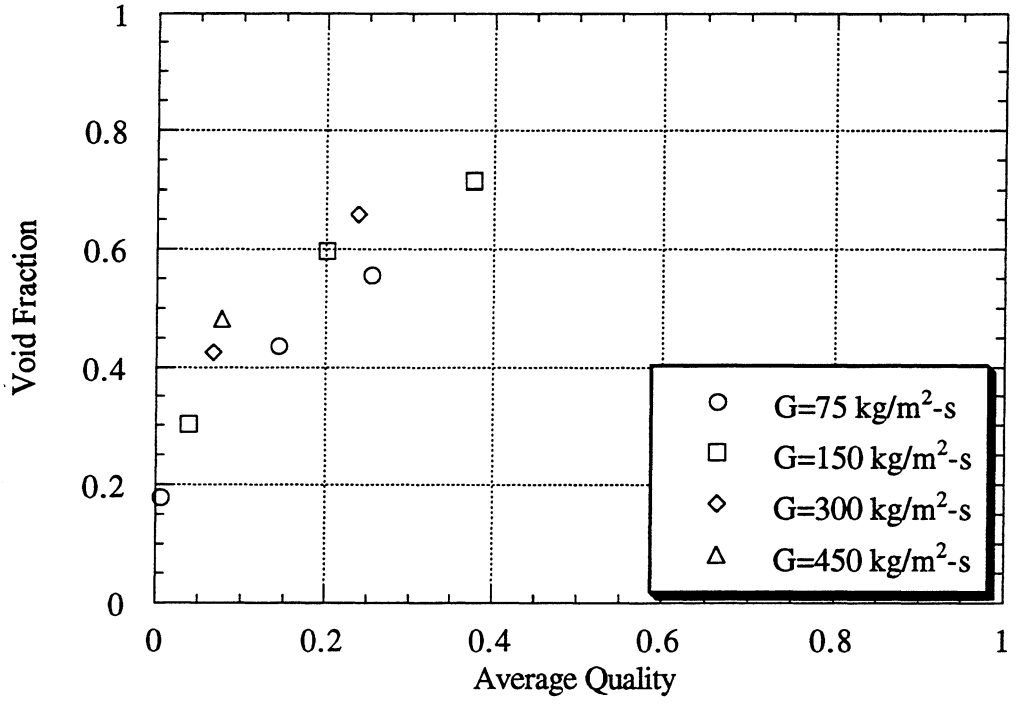

Figure 6.2 Void fraction vs. average quality for R410A in the 8.93 mm helical tube

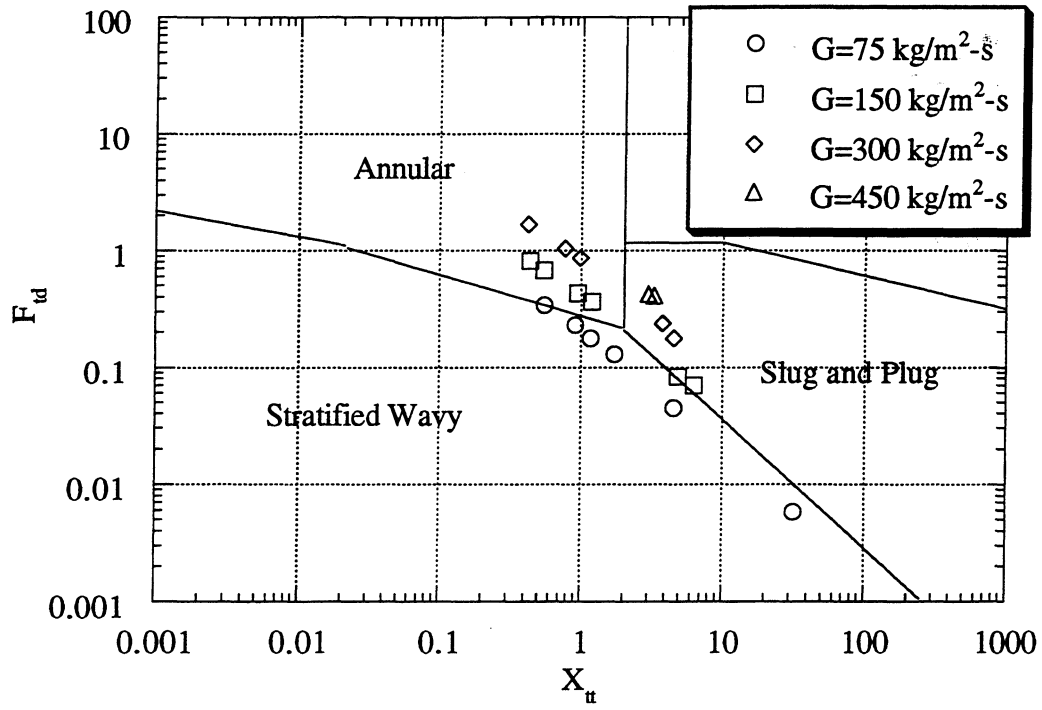

Figure 6.3 Void fraction data for both refrigerants in the 8.93 mm i.d. helical tube separated by mass flux shown on a Taitel-Dukler flow map

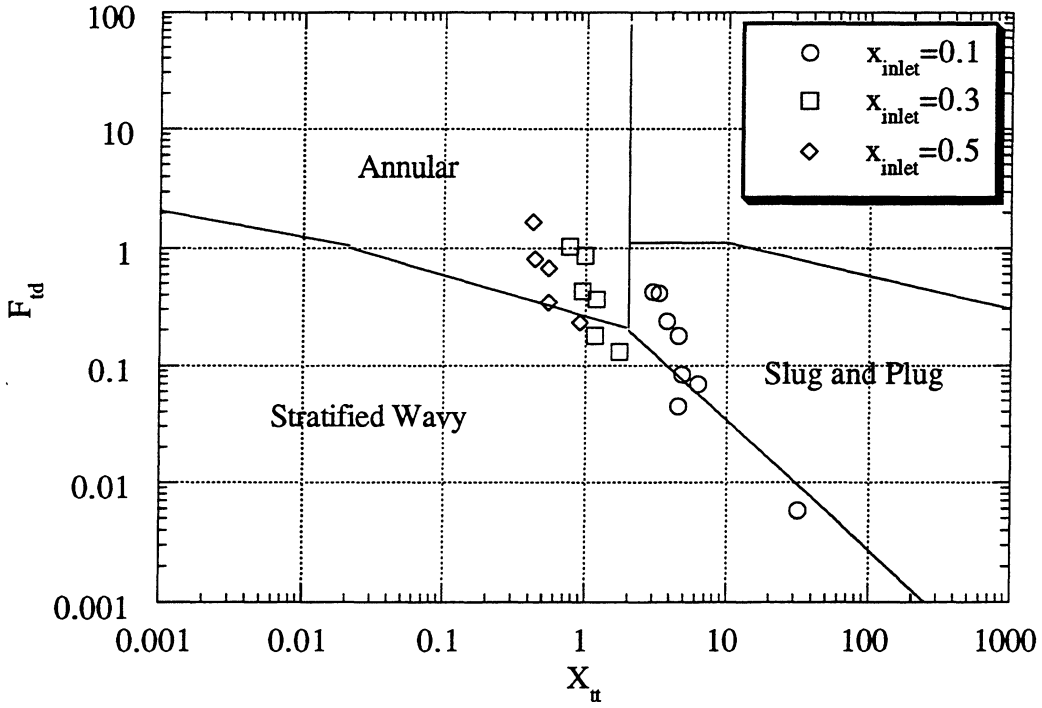

Figure 6.4 Void fraction data for both refrigerants in the 8.93 mm i.d. helical tube separated by inlet quality shown on a Taitel-Dukler flow map

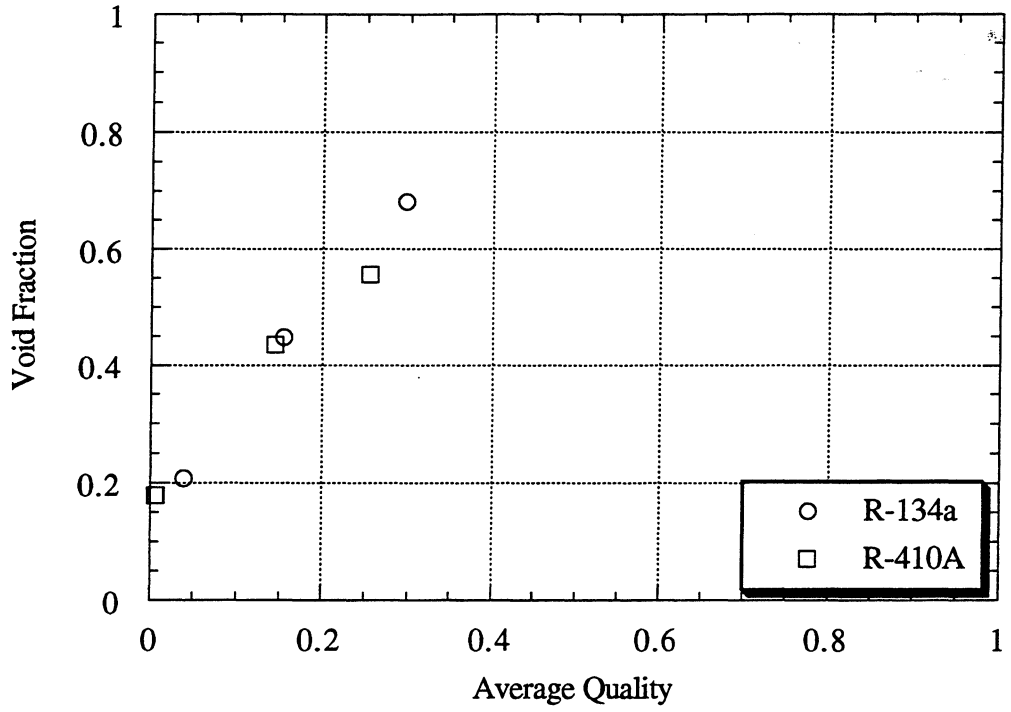

Figure 6.5 Void fraction vs. average quality in the 8.93 mm i.d. helical tube for G=75 kg/m^2-s

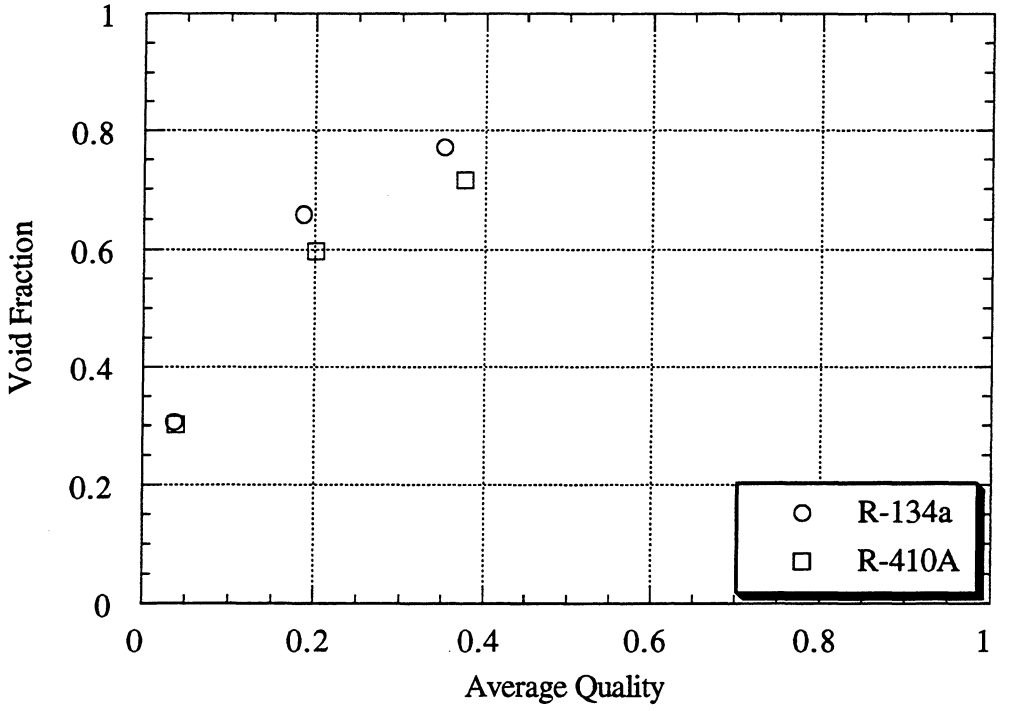

Figure 6.6 Void fraction vs. average quality in the 8.93 mm i.d. helical tube for G=150 kg/m^2-s

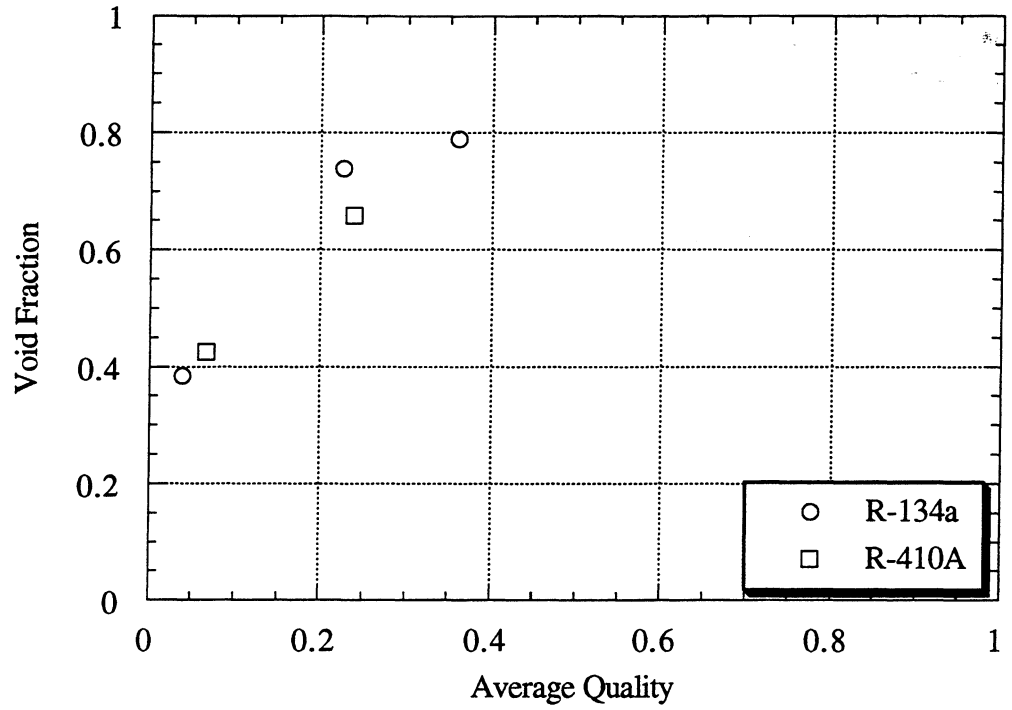

Figure 6.7 Void fraction vs. average quality in the 8.93 mm i.d. helical tube for G=300 kg/m^2-s

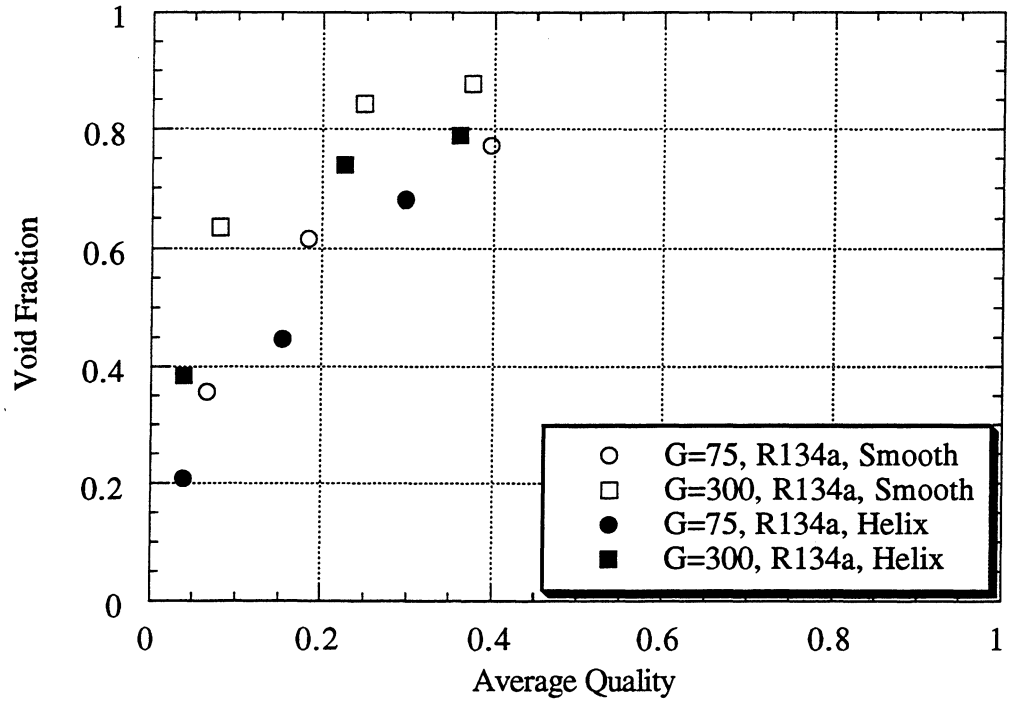

Figure 6.8 Void fraction vs. average quality for R134a in both the 6.04 mm i.d. smooth tube and the 8.93 mm i.d. helical tube (G is in kg/m^2-s)

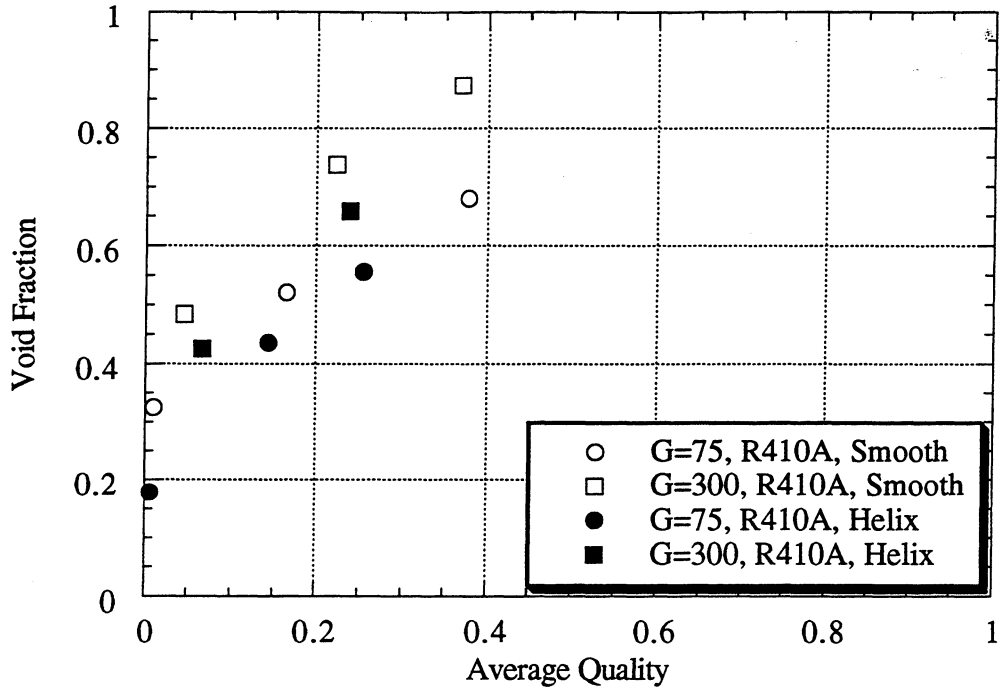

Figure 6.9 Void fraction vs. average quality for R410A in both the 6.04 mm i.d. smooth tube and the 8.93 mm i.d. helical tube (G is in kg/m^2-s)

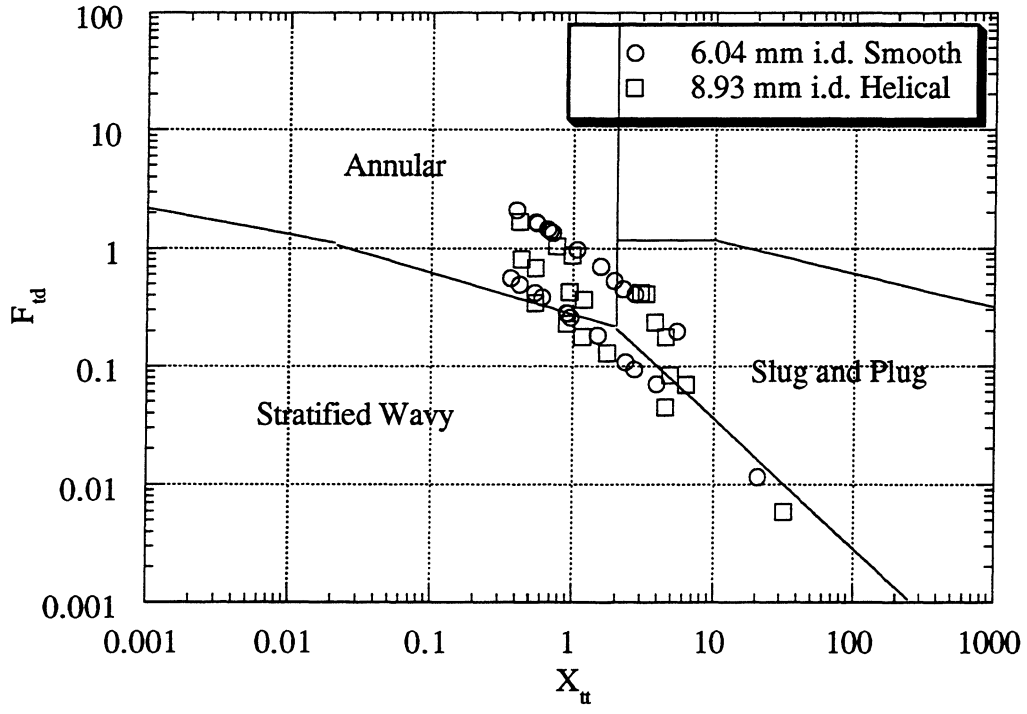

Figure 6.10 Void fraction data for both refrigerants in the 6.04 mm i.d. smooth tube and the 8.93 mm i.d. helical tube on a Taitel-Dukler flow map

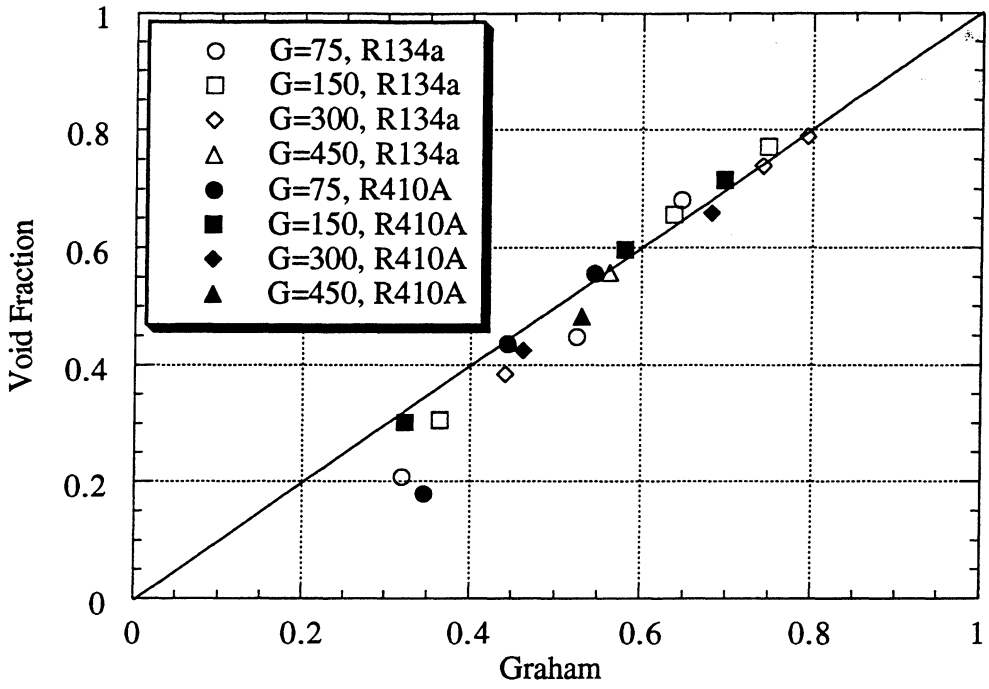

Figure 6.11 Actual void fraction vs. Graham prediction for the 8.93 mm i.d. helical tube (G is in kg/m^2-s)

Chapter 7

Axially Grooved Tube Results

The results obtained for the 8.89 mm i.d. axially grooved tube are presented and discussed in this chapter. The results will be compared with those obtained for the 6.04 mm i.d. smooth tube as well as with those of the 8.93 mm i.d. helically grooved tube. A brief discussion pertaining to the correlations from Chapter 2 will also be included.

7.1 Void Fraction Results

The axial tube demonstrates many of the same trends which are observed in the smooth and helical tubes. The parameters which will be used to analyze this data are mass flux, refrigerant, and tube geometry.

7.1.1 Effect of Mass Flux on Void Fraction during Condensation

The effect of mass flux on void fraction during condensation is illustrated in Figures 7.1 and 7.2. Similar to the smooth and helical tubes, void fraction tends to increase with mass flux, with larger increases being observed at lower average qualities. The void fraction at 75 kg/m^2-s is lowest, followed by 150, 300, and 450 kg/m^2-s.

The explanation for the mass flux dependence exhibited is once again given by the Taitel-Dukler flow map. The axial tube data is separated by mass flux in Figure 7.3. Here it can be seen that the low mass flux points generally lie in the stratified flow regime. In Figure 7.4, the data is separated by inlet quality, and it can be seen that most of the low inlet quality points lie in the intermittent slug and plug flow regime. The remaining points lie in the annular flow regime. It seems that the further points are from the annular regime, the more mass flux dependence they exhibit.

As with the helical tube, it should be noted that some of the higher inlet qualities at high mass fluxes were not obtained for this section due to the tremendous amount of heat required to reach the inlet quality.

7.1.2 Effect of Refrigerant on Void Fraction during Condensation

In Figures 7.5 through 7.7, void fraction is plotted against average quality for mass fluxes of 75, 150, and 300 kg/m^2-s. In these plots, it is apparent that R134a consistently has a higher void fraction than R410A.

This trend is due to the higher saturation pressure of R410A which causes the R410A vapor to flow more slowly than R134a vapor.

7.1.3 Effect of Tube Geometry on Void Fraction during Condensation

The effect of axial grooves can be seen in Figures 7.8 and 7.9 where void fraction is plotted against average quality for both R134a and R410A in the 6.04 mm i.d. smooth tube and the 8.89 mm i.d. axial tube. It is apparent that void fractions for the axial tube are consistently lower than those of the smooth tube. This may be explained by the Taitel-Dukler flow map shown in Figure 7.10. Here, it seems that the axial tube data lies closer to the stratified flow regime. It is also possible that the axial grooves shift the boundaries within the flow map.

In Figures 7.11 and 7.12, void fraction is plotted against average quality for both refrigerants in the 8.93 mm i.d. helical tube and the 8.89 mm i.d. axial tube. Although the trend is not as noticeable as with the smooth tube data, it appears that the axial tube has slightly higher void fractions than the helical tube. The data for these two tubes is plotted on a Taitel-Dukler flow map in Figure 7.13, but there are no apparent trends.

Unfortunately, diameter effects in axial tubes were unable to be observed since only the 8.89 mm i.d. tube was tested.

7.2 Data Comparison

As with the helical tube, only the Graham [1998] correlation will be discussed in this section since the predictions of outside investigators deviated significantly from the smooth tube data, which is being used as a reference case. However, the graphical comparisons of the other correlations are displayed in Appendix C. The average error of each of these correlations is given in Table C.1.

7.2.1 Graham Correlation

In Figure 7.14, Graham's correlation is compared to the 8.89 mm i.d. axial tube data. It can be seen that this correlation collapses the data exceptionally well for all mass fluxes and

refrigerants, although it does underpredict some of the high void fraction points. The average prediction error was 4.38%.

A format similar to Graham's will be used to correlate this data since it works very well.

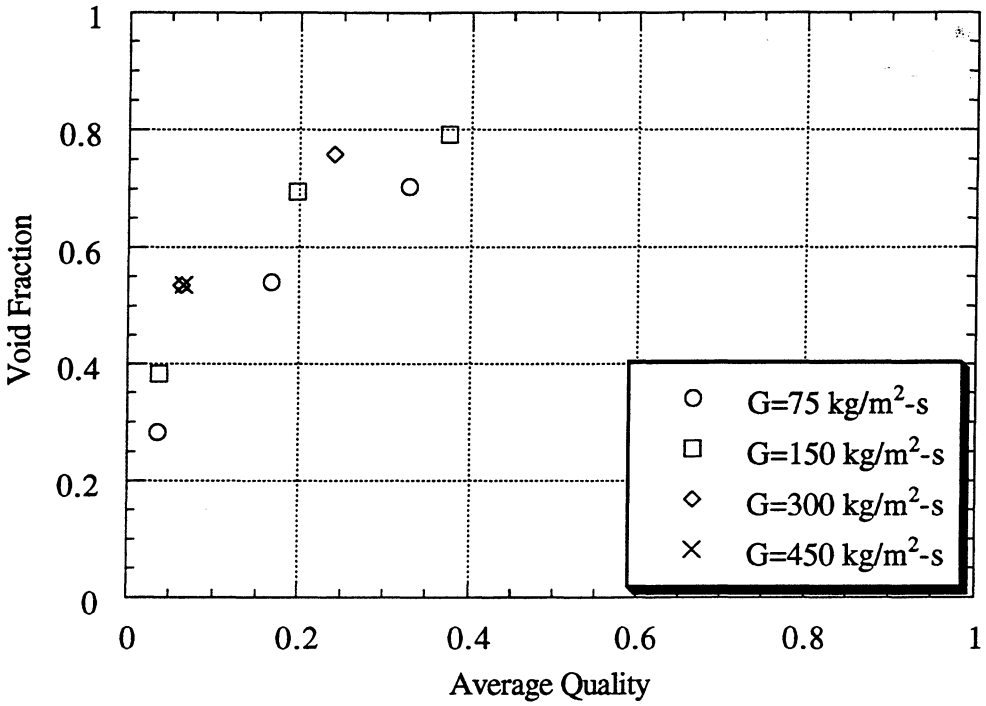

Figure 7.1 Void fraction vs. average quality for R134a in the 8.89 mm i.d. axial tube

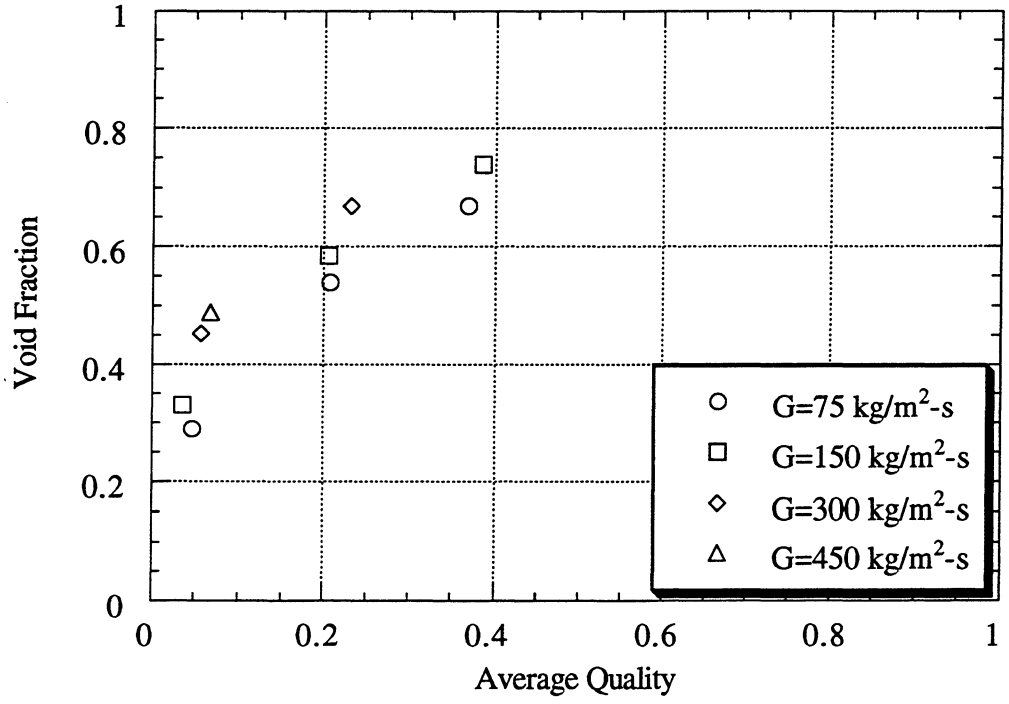

Figure 7.2 Void fraction vs. average quality for R410A in the 8.89 mm i.d. axial tube

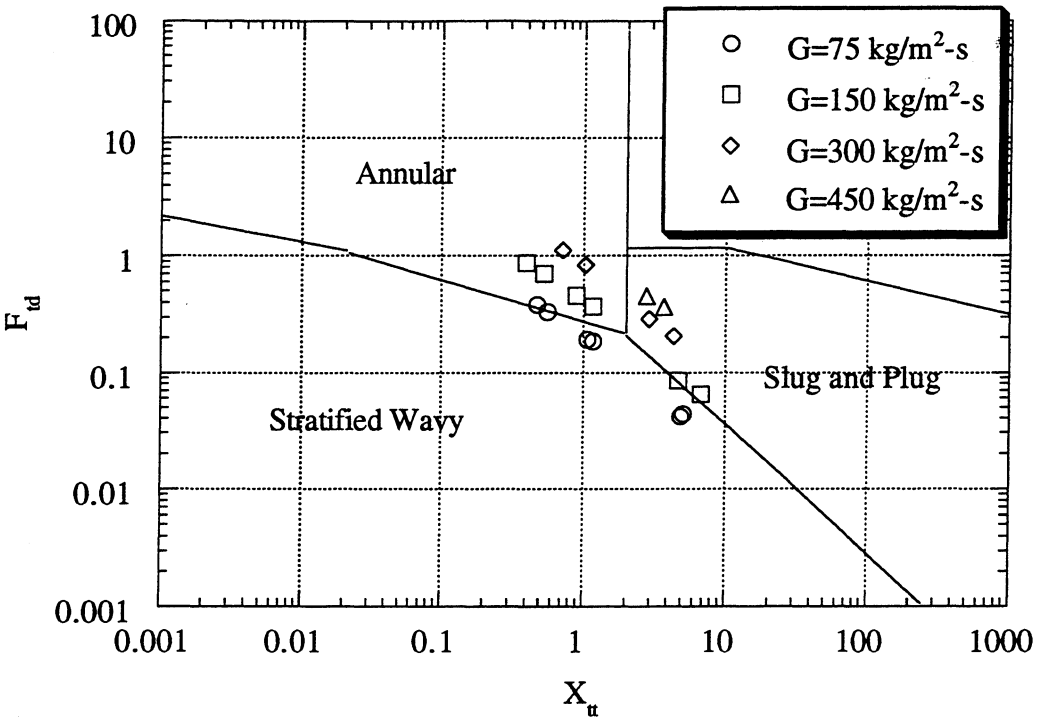

Figure 7.3 Void fraction data for both refrigerants in the 8.89 mm i.d. axial tube separated by mass flux shown on a Taitel-Dukler flow regime map

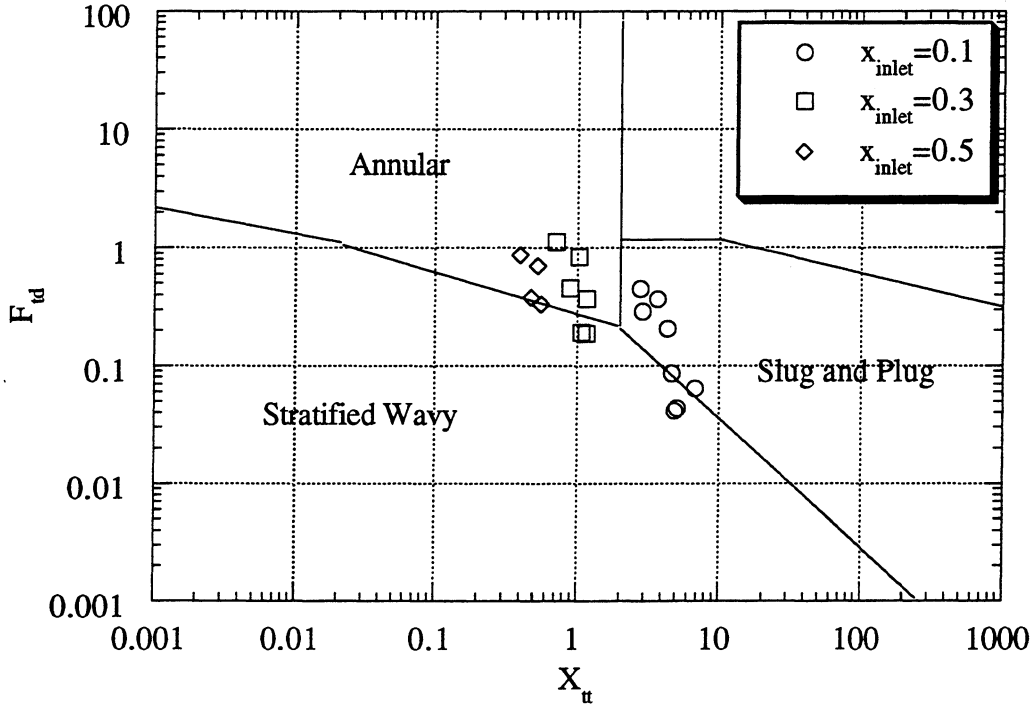

Figure 7.4 Void fraction data for both refrigerants in the 8.89 mm i.d. axial tube separated by inlet quality shown on a Taitel-Dukler flow regime map

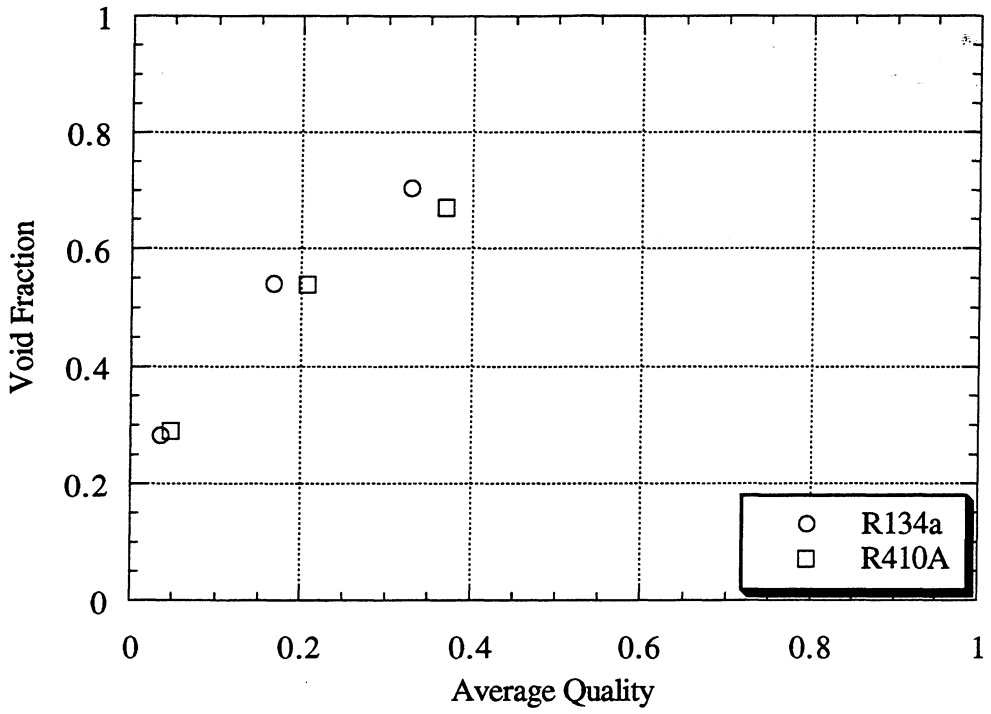

Figure 7.5 Void fraction vs. average quality in the 8.89 mm i.d axial tube for G=75 kg/m^2-s

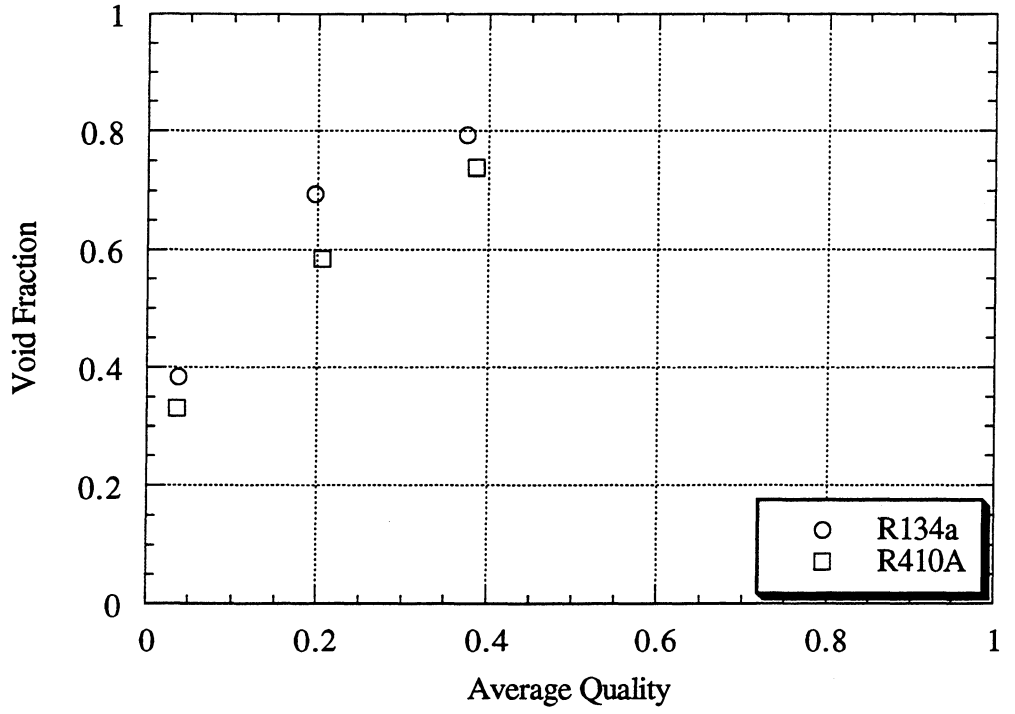

Figure 7.6 Void fraction vs. average quality in the 8.89 mm i.d axial tube for G=150 kg/m^2-s

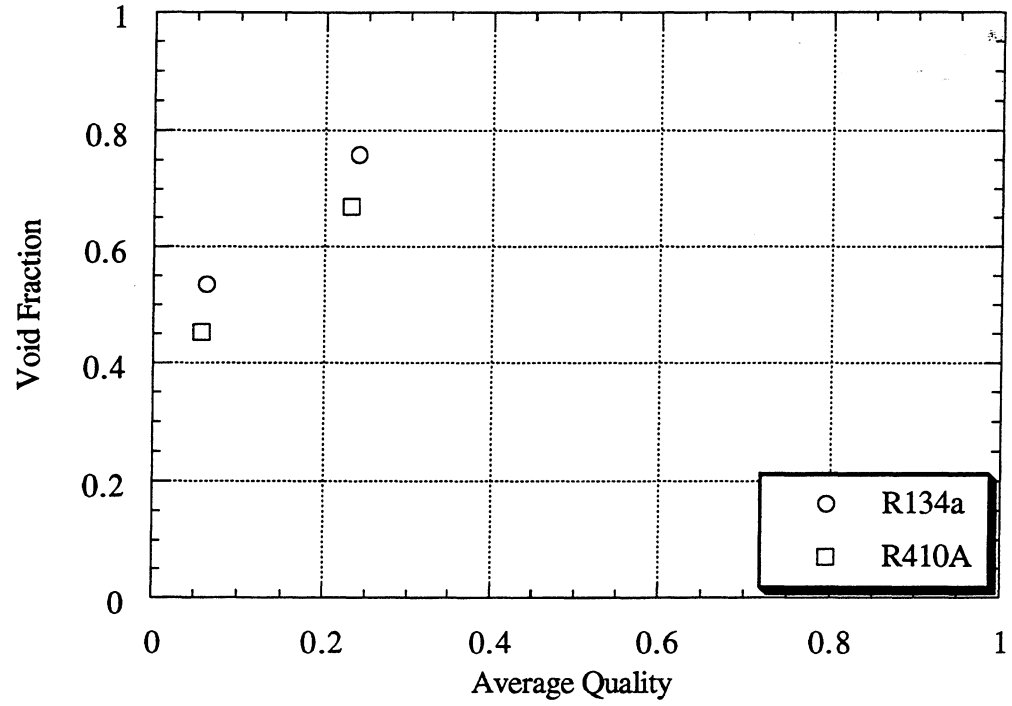

Figure 7.7 Void fraction vs. average quality in the 8.89 mm i.d axial tube for G=300 kg/m^2-s

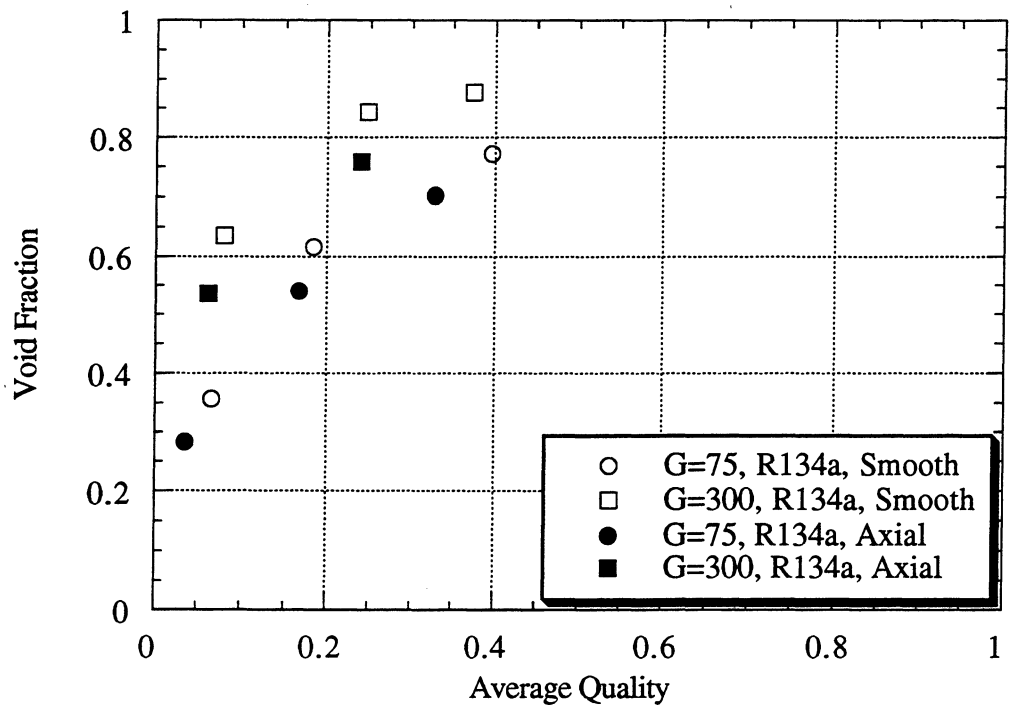

Figure 7.8 Void fraction vs. average quality for R134a in both the 6.04 mm i.d. smooth tube and the 8.89 mm i.d. axial tube (G is in kg/m^2-s)

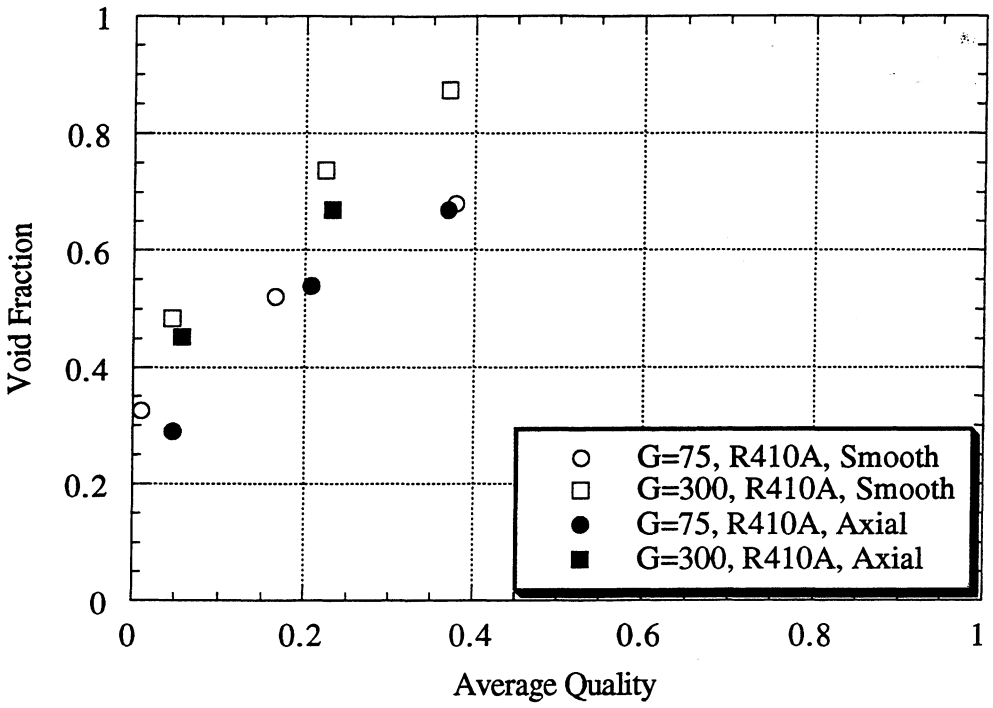

Figure 7.9 Void fraction vs. average quality for R410A in both the 6.04 mm i.d. smooth tube and the 8.89 mm i.d. axial tube (G is in kg/m^2-s)

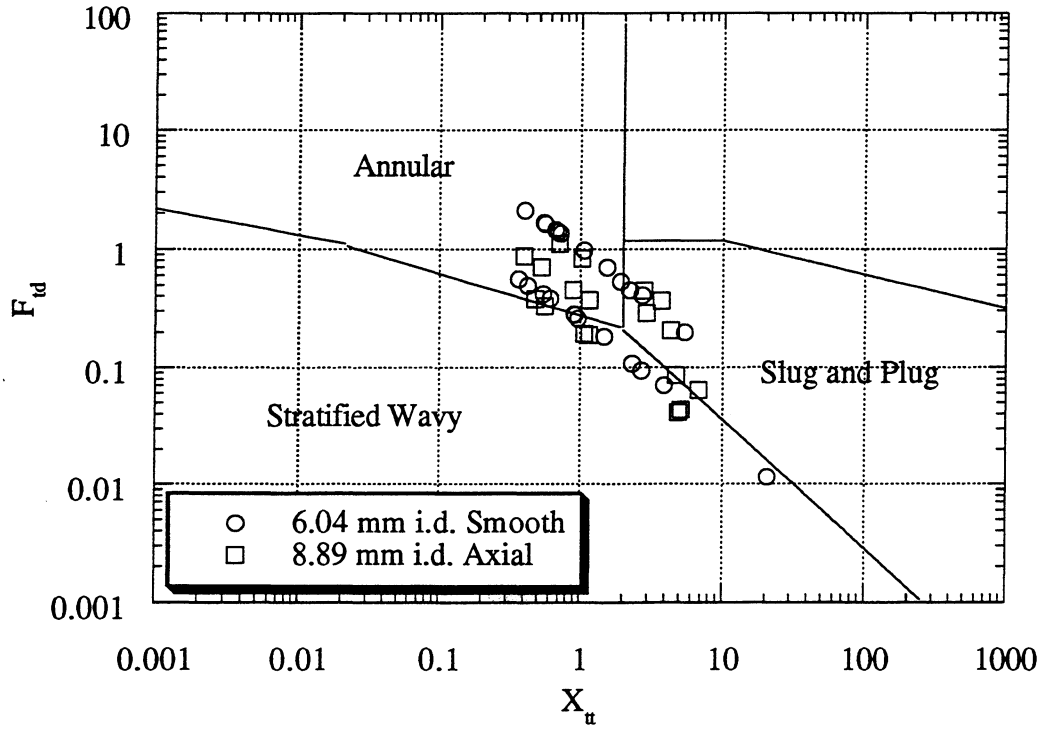

Figure 7.10 Void fraction data for both refrigerants in the 6.04 mm i.d. smooth tube and the 8.89 mm i.d. axial tube shown on a Taitel-Dukler flow regime map

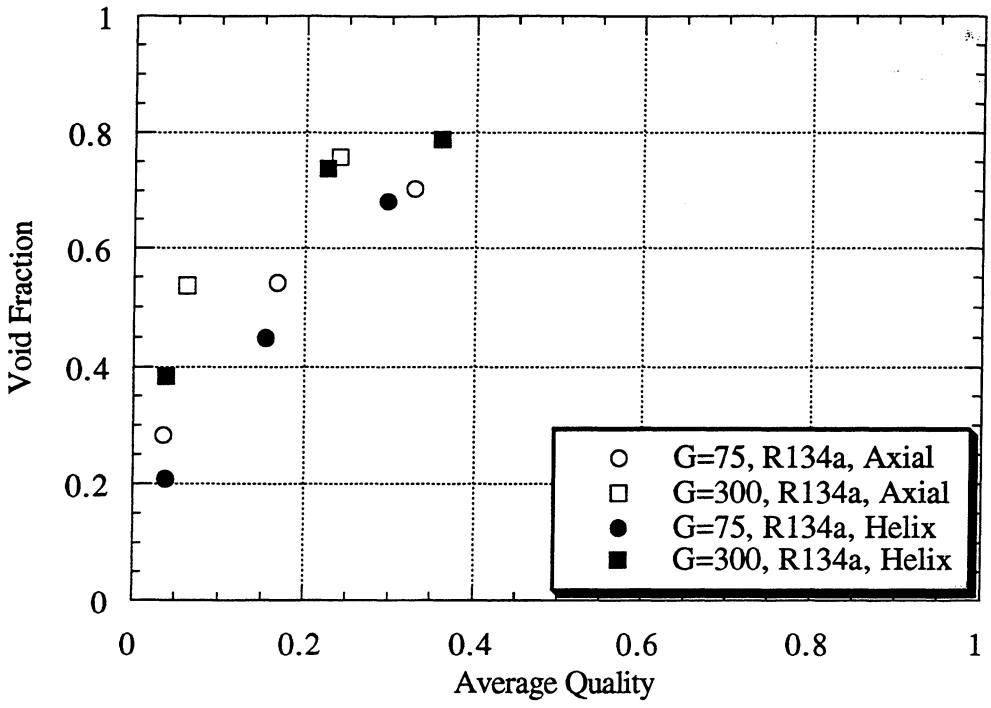

Figure 7.11 Void fraction vs. average quality for R134a in both the 8.93 mm i.d. helical tube and the 8.89 mm i.d. axial tube (G is in kg/m^2-s)

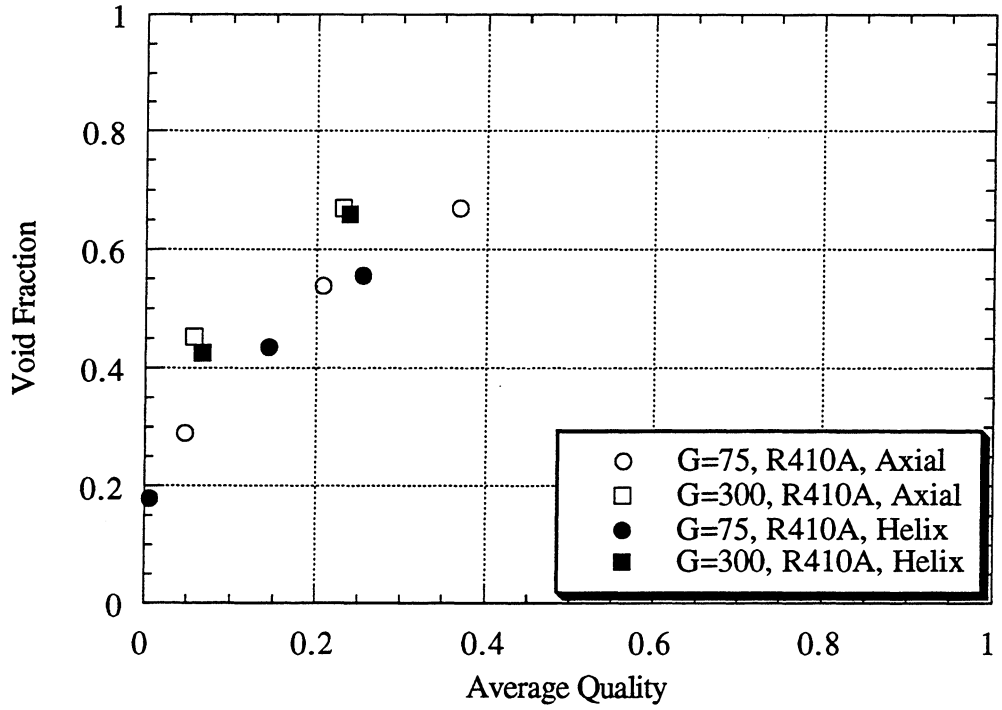

Figure 7.12 Void fraction vs. average quality for R410A in both the 8.93 mm i.d. helical tube and the 8.89 mm i.d. axial tube (G is in kg/m^2-s)

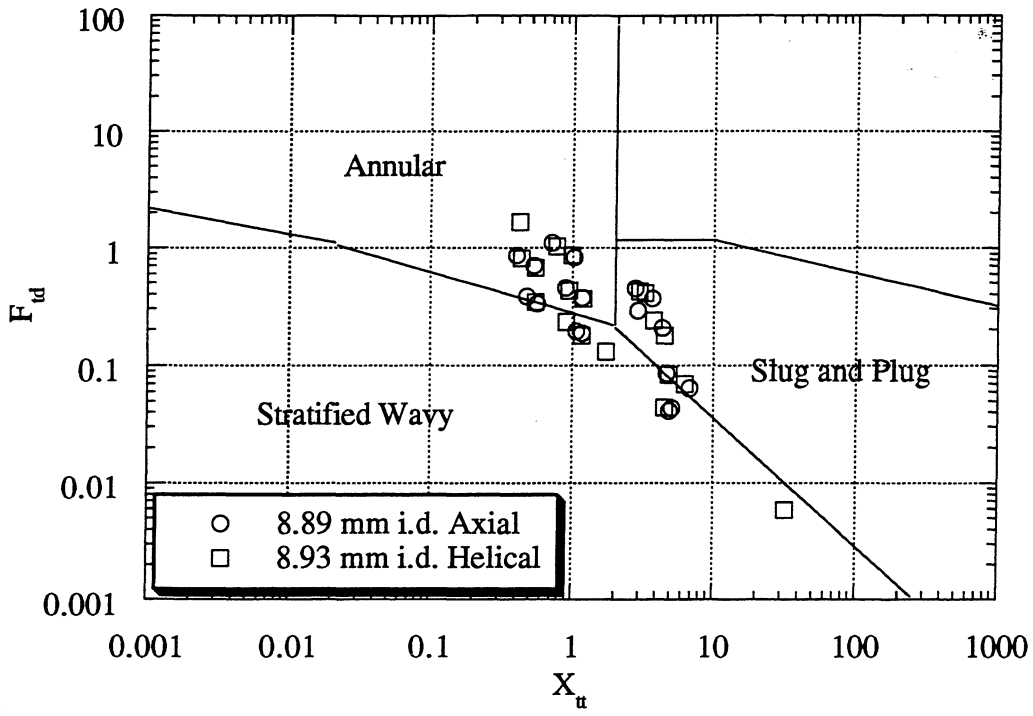

Figure 7.13 Void fraction data for both refrigerants in the 8.93 mm i.d. helical tube and the 8.89 mm i.d. axial tube shown on a Taitel-Dukler flow regime map

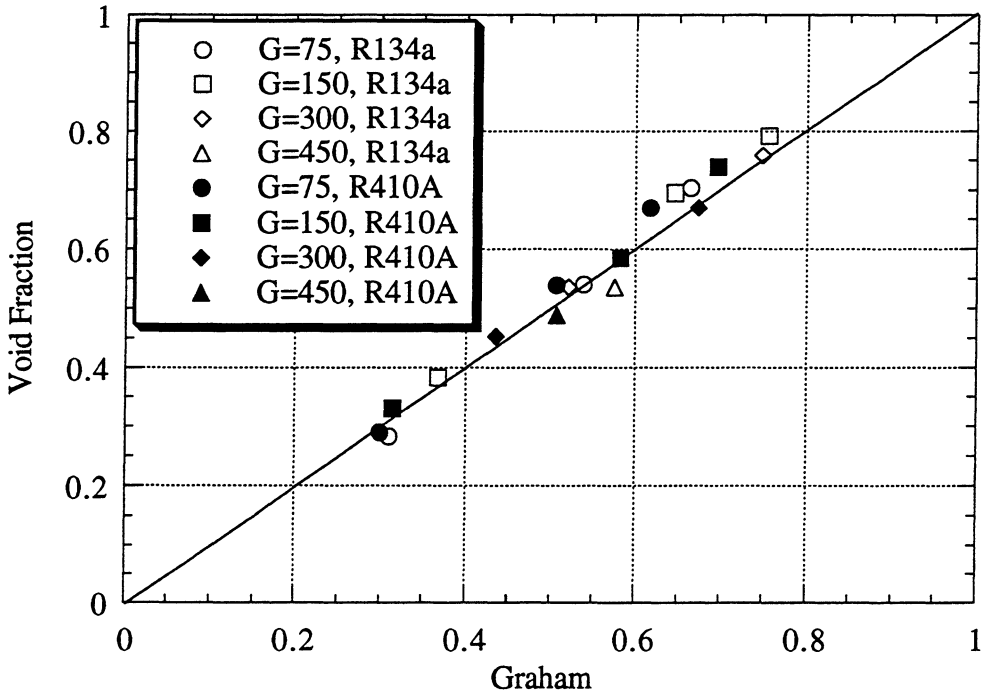

Figure 7.14 Actual void fraction vs. Graham prediction for the 8.89 mm i.d. axial tube (G is in kg/m^2-s)

Chapter 8

Correlation of Data

In this chapter, several possible correlating parameters will be discussed. In addition, the experimental data will be correlated. First, a smooth tube correlation will be formulated using the data taken on the 6.04 mm i.d. tube in this study and the data taken on the 7.04 mm i.d. tube in Graham's [1998] companion study. The enhanced tube correlations will be based on the smooth tube correlation. The smooth tube data will also be compared to the data of Sacks [1974].

8.1 Potential Correlation Parameters

Since the Taitel-Dukler flow regime map has been used extensively in the analyses of data, it seems appropriate that the Lockhart-Martinelli parameter and Taitel-Dukler Froude number be considered as correlating parameters. The Froude Rate parameter of Hurlburt and Newell [1997] will also be discussed since it has previously proven to correlate the data very well.

8.1.1 The Lockhart-Martinelli Parameter

The Lockhart-Martinelli parameter, which is defined in Chapter 2, was initially developed for pressure drop correlations, but has also been used to correlate void fraction. Figure 8.1 shows all of the smooth tube void fraction data plotted against the Lockhart-Martinelli parameter. It appears that this parameter does not collapse the smooth tube data from this study. In Figure 8.2, a portion of the data is separated by mass flux and refrigerant. Here, the data is clearly separated into lines of different mass flux, although the parameter is impartial to which refrigerant is used. For this reason, this parameter will not be used to correlate the data.

8.1.2 The Taitel-Dukler Froude Number

Taitel and Dukler created what can be described as a "modified" Froude number when creating their flow regime map. This parameter is defined in Chapter 5. In Figure 8.3, all of the smooth tube void fraction data is plotted against this parameter. This parameter also does not collapse the data. In Figure 8.4, a portion of data separated by mass flux and refrigerant is shown. Once again, lines of separate mass flux can be seen. Thus, this parameter will not be used to correlate the data.

8.1.3 The Froude Rate Parameter

The Froude Rate parameter, which is defined in Chapter 2, was developed while studying the transition between stratified and annular flow. Graham used this parameter to correlate his void fraction data. The smooth tube void fraction data is plotted against this parameter in Figure 8.5. As can be seen, when plotted on a logarithmic scale, the data collapses very well. In Figure 8.6, a portion of the data which is separated by mass flux and refrigerant is plotted against this parameter. Here, there are no lines of mass flux or refrigerant separation. For this reason, the Froude Rate parameter will be used to correlate the void fraction data from this study.

8.2 Correlating the Data

The existing void fraction data will be correlated using the Froude Rate parameter. First, the smooth tube data will be correlated. A variation of the smooth tube correlation will be used to correlate the helical and axial tube data.

8.2.1 Smooth Tube Correlation

A least squares analysis was used to correlate the data from the 6.04 and 7.04 mm i.d. smooth tubes. The curvature of the data on a semi-logarithmic plot suggests a correlation of the following form:

$$\alpha = R - \exp\left[\sum_{n=0}^{n_0} a_n (\ln Ft)^n\right] \tag{8.1}$$

For the data collected in both this study and in Graham's companion study, it was found that a value of $n_0=3$ gave the best curve fit for the smooth tube data. One point was excluded in the analysis since it is so far from the rest. The expression for void fraction as a function of Froude Rate is given below:

$$\alpha = 1.045 - \exp\left[-1 - 0.342 \cdot \ln(Ft) - 0.0268 \cdot \ln^2(Ft) + 0.00597 \cdot \ln^3(Ft)\right]$$

$$0.044 \le Ft \le 454 \tag{8.2}$$

It should be noted that the void fractions at the extreme limits are 0.357 and 0.980; this accommodates all of the data obtained in this study. Figure 8.7 shows the actual versus predicted void fraction for the above correlation. The majority of the data falls within ±10% and the standard deviation is 4.19. The average prediction error is 3.73%. The prediction error for each individual point is given in Tables A.1 through A.4. The greatest errors are associated with the points which have low Froude Rates.

It should be noted that points with extremely low Froude Rates generally have a low mass flux as well as a low average quality. In this situation, it is reasonable to assume that the slip-ratio is near unity. For this reason, it is suggested that the homogenous void fraction model may work in the region not bound by the correlation given here; i.e. Ft<0.044. Figure 8.8 shows what the homogenous model looks like on a Froude Rate basis in this region. For all mass fluxes and refrigerants, it can be seen that the curve leads to the general area where this study's correlation begins.

In the late 1970's, Paul Sacks collected a large amount of void fraction data using R11, R12, and R22 in a 9.6 mm i.d. smooth tube test condenser. This data is plotted against the predicted void fraction in Figures 8.9 through 8.11. As can be seen, the correlation accurately predicts the void fraction within 10% for most data points. The average errors are 4.80%, 6.88%, and 7.37% for R11, R12, and R22, respectively. Once again, the points which exhibit the greatest error are those whose Froude Rate is very low.

8.2.2 Helical Tube Correlation

As has been mentioned previously, the smooth tube correlation will be used to correlate the helical tube data. This can be done because it seems that the data taken on the 8.93 mm i.d. helical tube shows a systematic offset from the data taken on the two smooth tubes (Figures 6.8 and 6.9). In Figure 8.12, the helical tube void fraction data is plotted against Froude Rate, showing that it too is collapsed by this parameter. Thus, the helical correlation will take the following form:

$$\alpha_{helical} = a + (1-a)\cdot\alpha_{smooth} \tag{8.3}$$

Using a least squares analysis, it is found that a = -0.124 provides excellent correlation. For the helical case, the correlation works for void fractions of 0.277 to 0.977. The actual versus predicted void fraction is shown in Figure 8.13. It can be seen that most of the data falls within ±10% with the exception of one bad point. The average error for this correlation is 5.95% with a standard deviation of 7.50. The average deviation for the individual points is given in Table A.5.

8.2.3 Axial Tube Correlation

The axial tube data will also be correlated using the smooth tube correlation. Similar to the helical tube, the axial tube tends to have a systematic offset from the smooth tube data. This is shown in Figures 7.8 and 7.9. Additionally, the axial tube data is collapsed excellently by the Froude Rate in Figure 8.14. Thus, the correlation for the axial tube takes the following form.

$$\alpha_{axial} = b + (1 - b) \cdot \alpha_{smooth} \tag{8.4}$$

Using a least squares analysis, it is found that excellent agreement is obtained from b = -0.0687. This allows the correlation to work for void fractions ranging from 0.313 to 0.979. Two data points actually fall below this value, but they are quite close. In Figure 8.15, the actual versus predicted void fraction is shown for this correlation. It can be seen that the data falls within ±10%. This correlation has an average error of 5.11% with a standard deviation of 3.83. The average deviation for the individual points is given in Table A.6.

8.3 Application of the Correlations

The correlations for the three tubes can all be used to predict the amount of refrigerant charge required in a single tube, horizontally mounted condenser during operation if the inlet and outlet qualities are known. Although the correlations are a function of the Froude Rate parameter, this parameter is a function of the quality. It is assumed that the mass flux and tube diameter are constant for a particular application. Thus, the correlations can be numerically integrated in increments over the range of qualities in order to determine the amount of refrigerant charge required for operation.

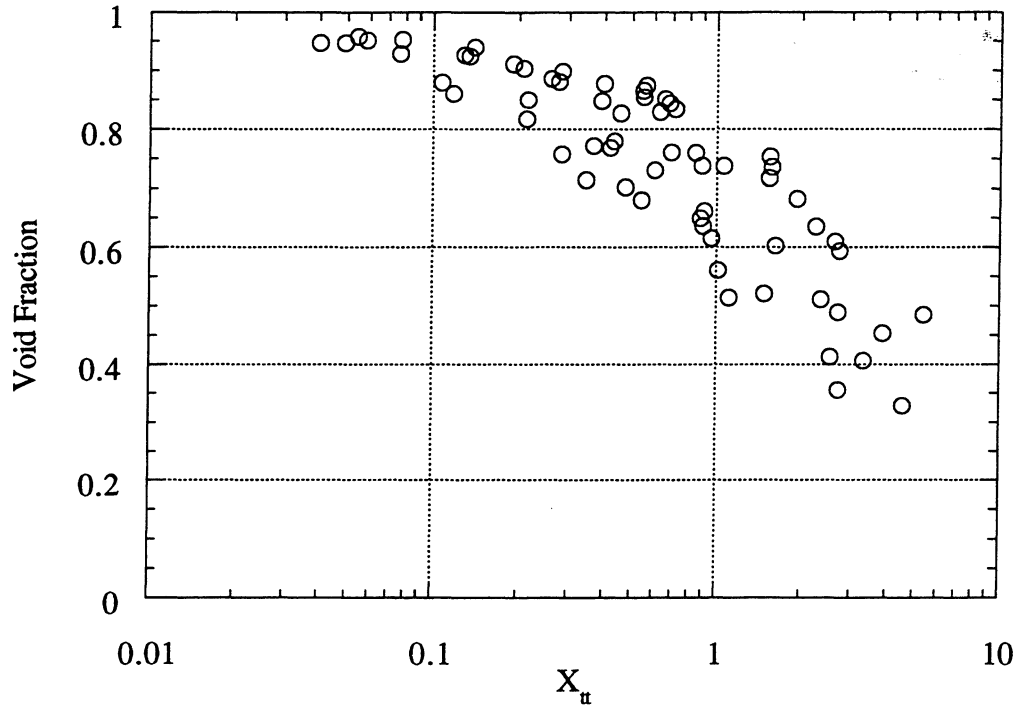

Figure 8.1 Void fraction vs. the Lockhart-Martinelli parameter for both refrigerants in the 6.04 and 7.04 mm i.d. smooth tubes

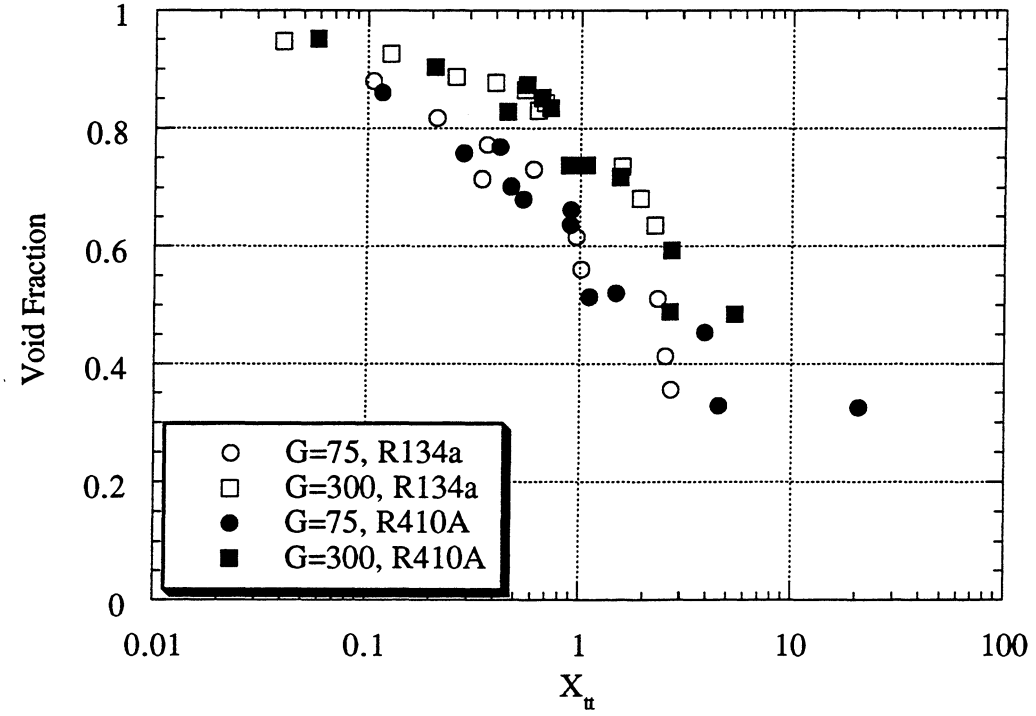

Figure 8.2 Void fraction vs. the Lockhart-Martinelli parameter for both the 6.04 and 7.04 mm i.d. smooth tubes with mass flux and refrigerant separation (G is in kg/m^2-s)

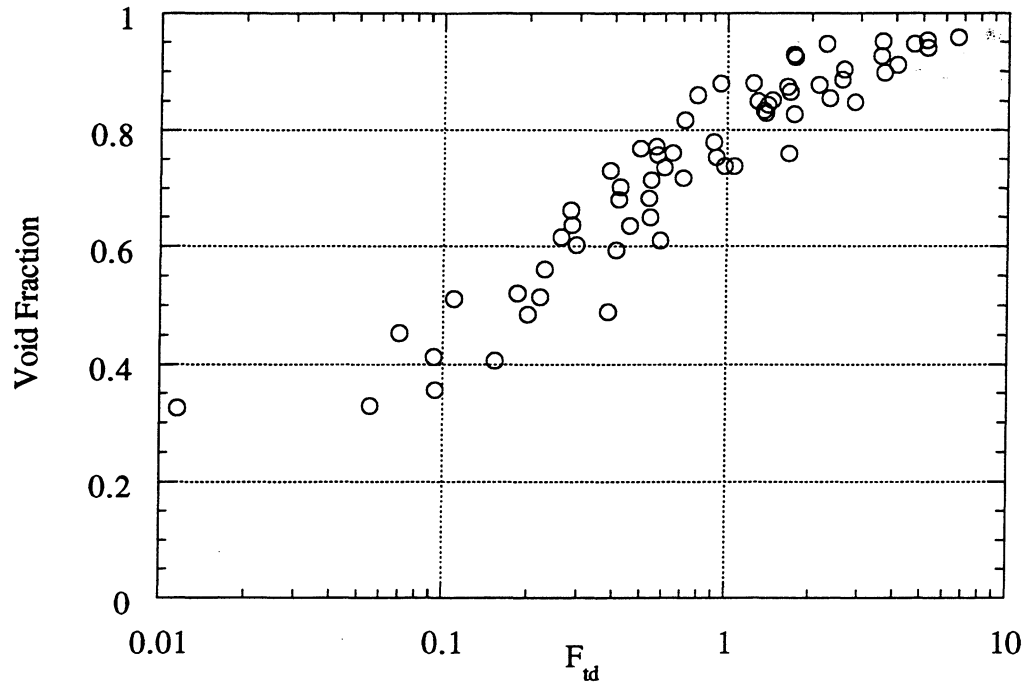

Figure 8.3 Void fraction vs. the Taitel-Dukler Froude number for both refrigerants in the 6.04 and 7.04 mm i.d. smooth tubes

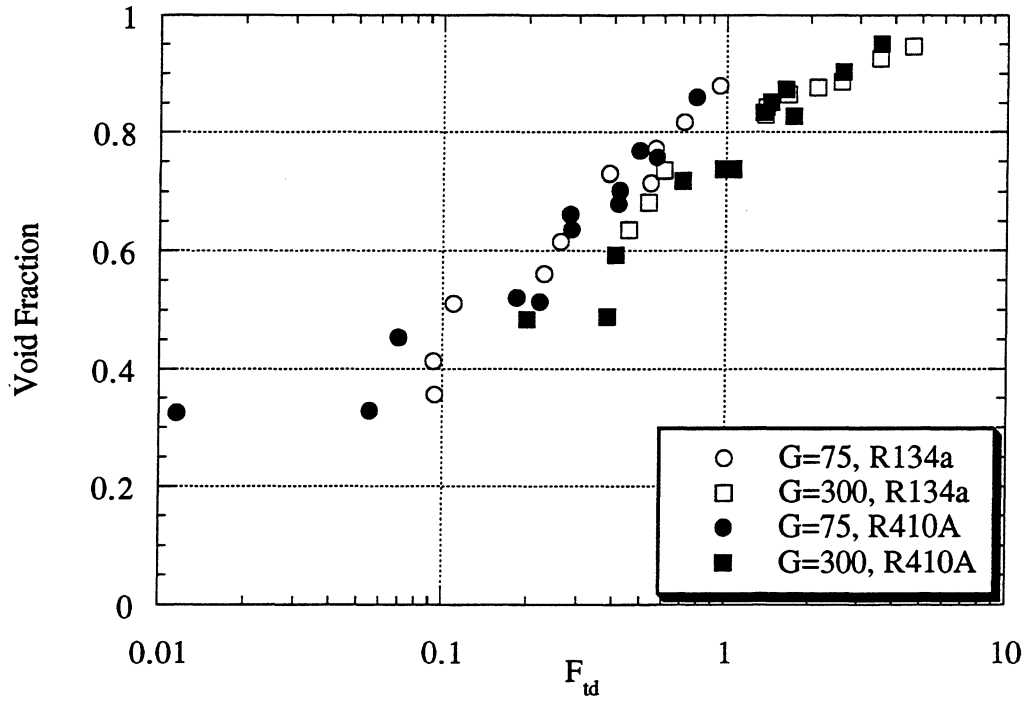

Figure 8.4 Void fraction vs. the Taitel-Dukler Froude number for both the 6.04 and 7.04 mm i.d. smooth tubes with mass flux and refrigerant separation (G is in kg/m^2-s)

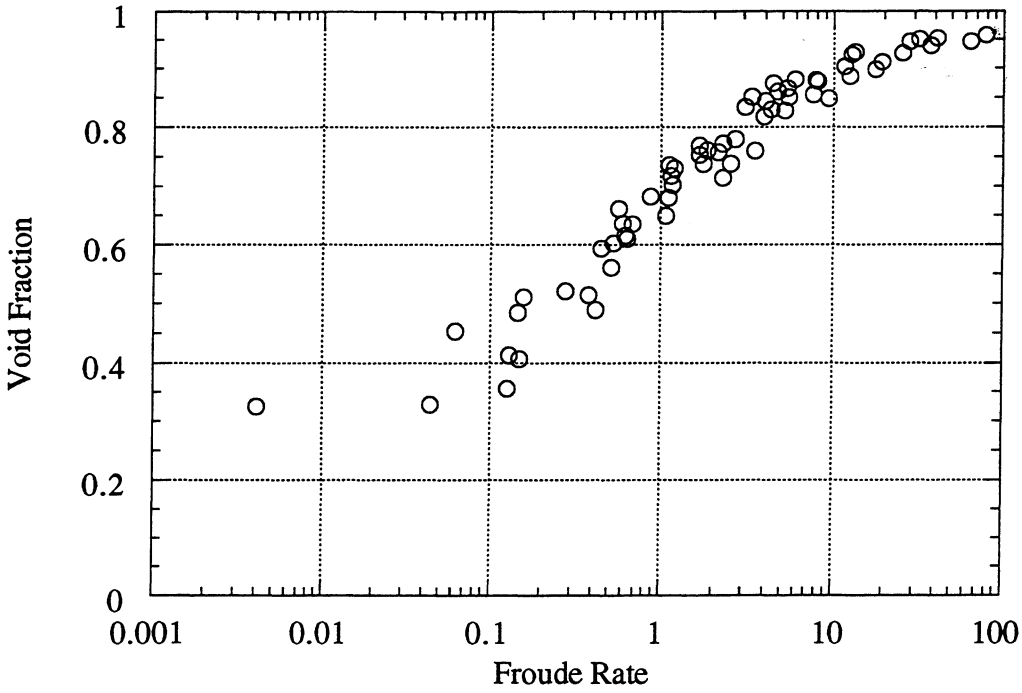

Figure 8.5 Void fraction vs. the Froude Rate for both refrigerants in the 6.04 and 7.04 mm i.d. smooth tubes

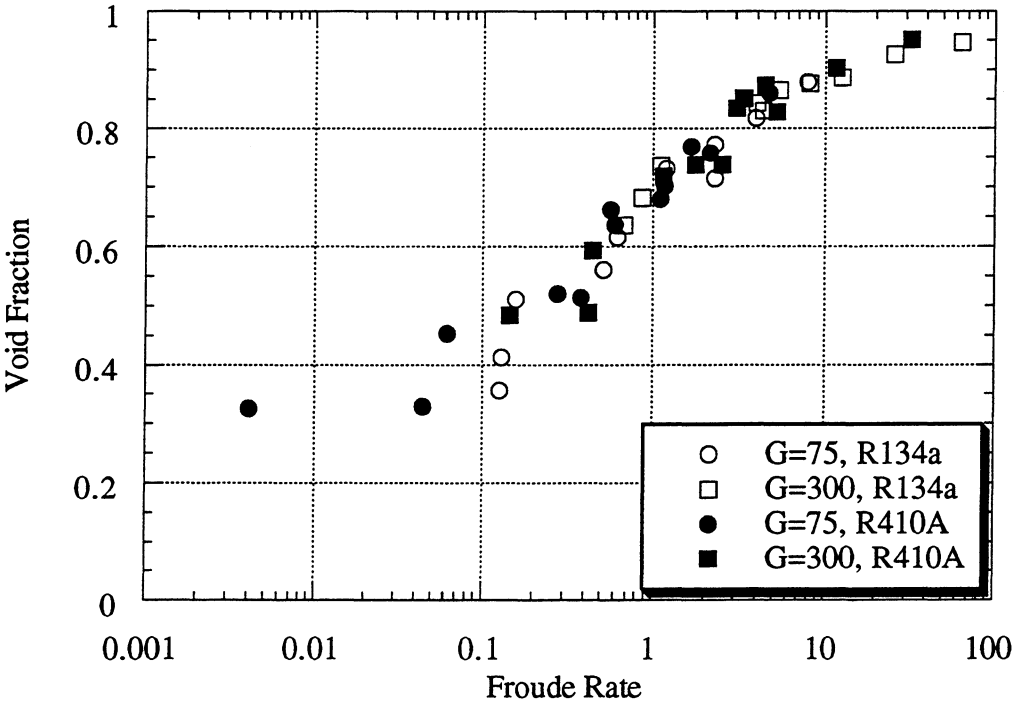

Figure 8.6 Void fraction vs. the Froude Rate for both the 6.04 and 7.04 mm i.d. smooth tubes with mass flux and refrigerant separation (G is in kg/m^2-s)

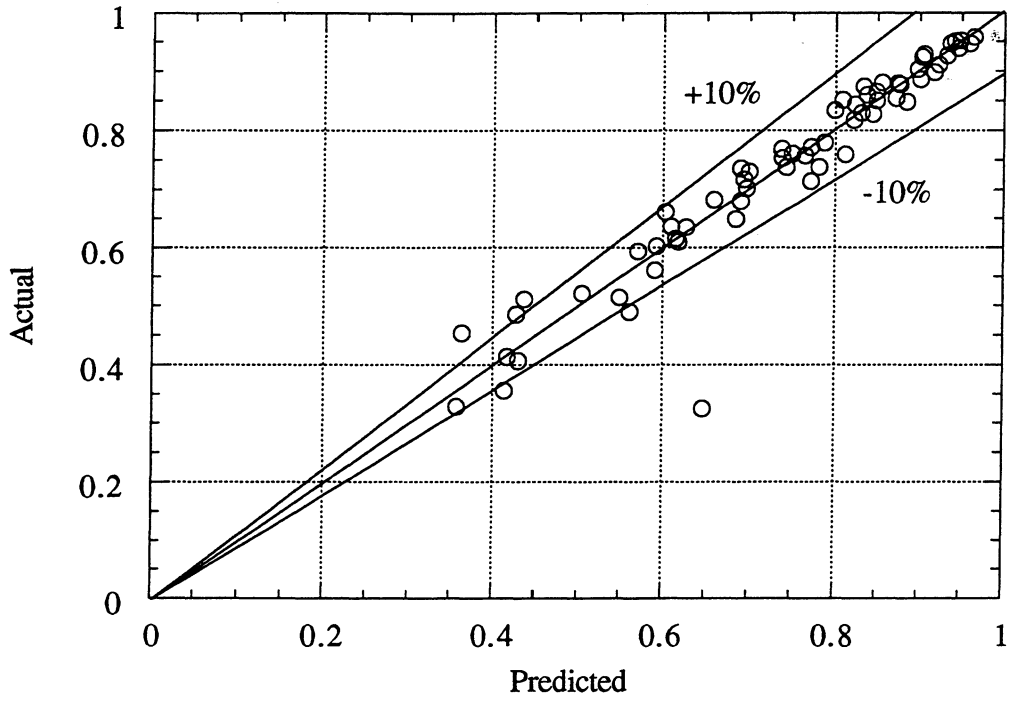

Figure 8.7 Actual void fraction vs. the prediction of the smooth tube correlation, Eq. (8.2), for both the 6.04 and 7.04 mm i.d. smooth tubes

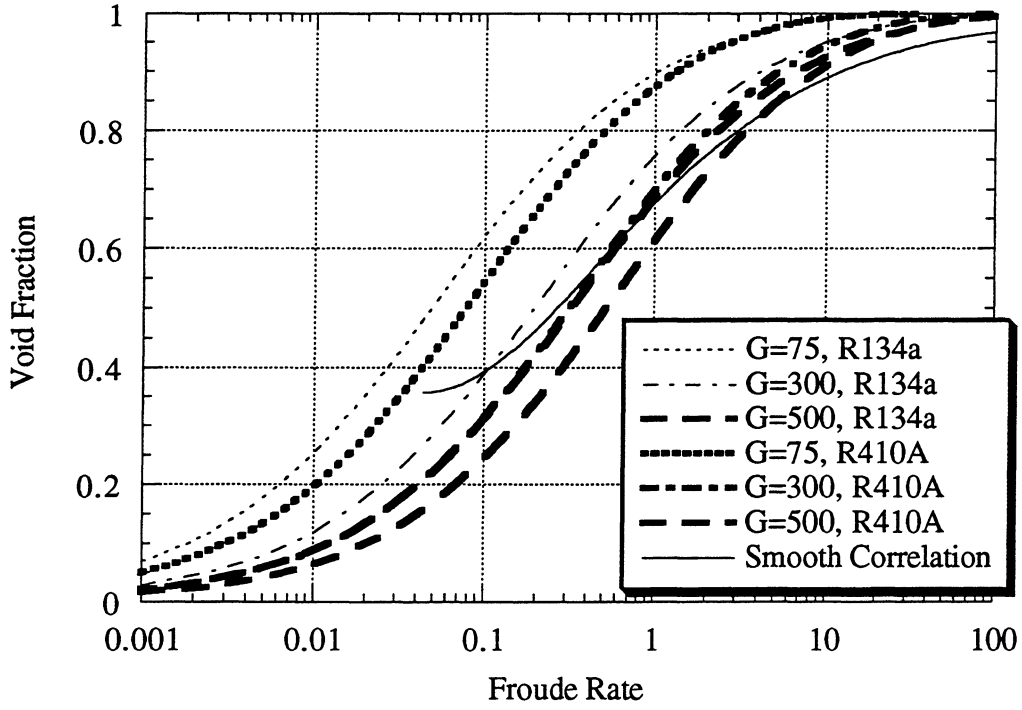

Figure 8.8 Void fraction vs. Froude Rate for the smooth tube correlation and several homogenous correlation curves

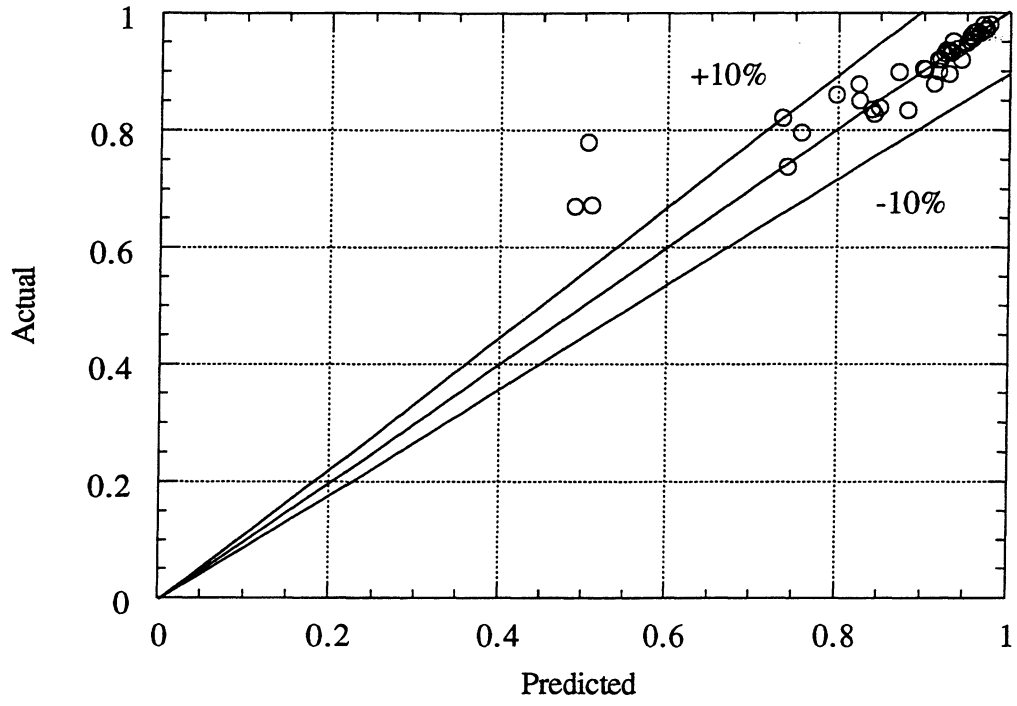

Figure 8.9 Sacks' R11 data vs. the prediction of the smooth tube correlation, Eq. (8.2)

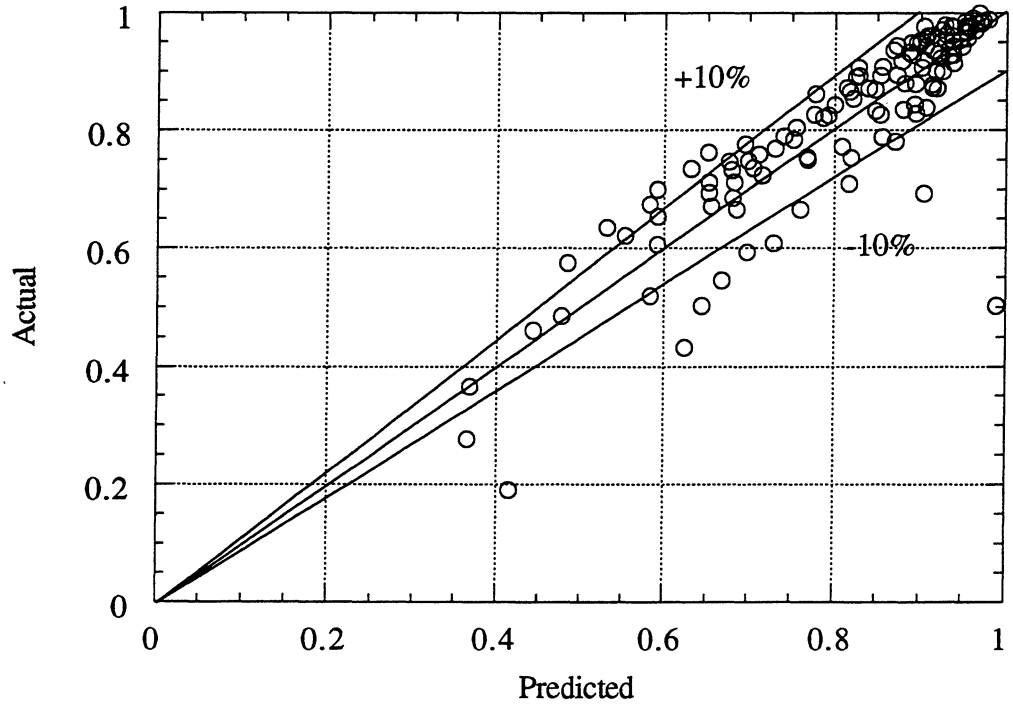

Figure 8.10 Sacks' R12 data vs. the prediction of the smooth tube correlation, Eq. (8.2)

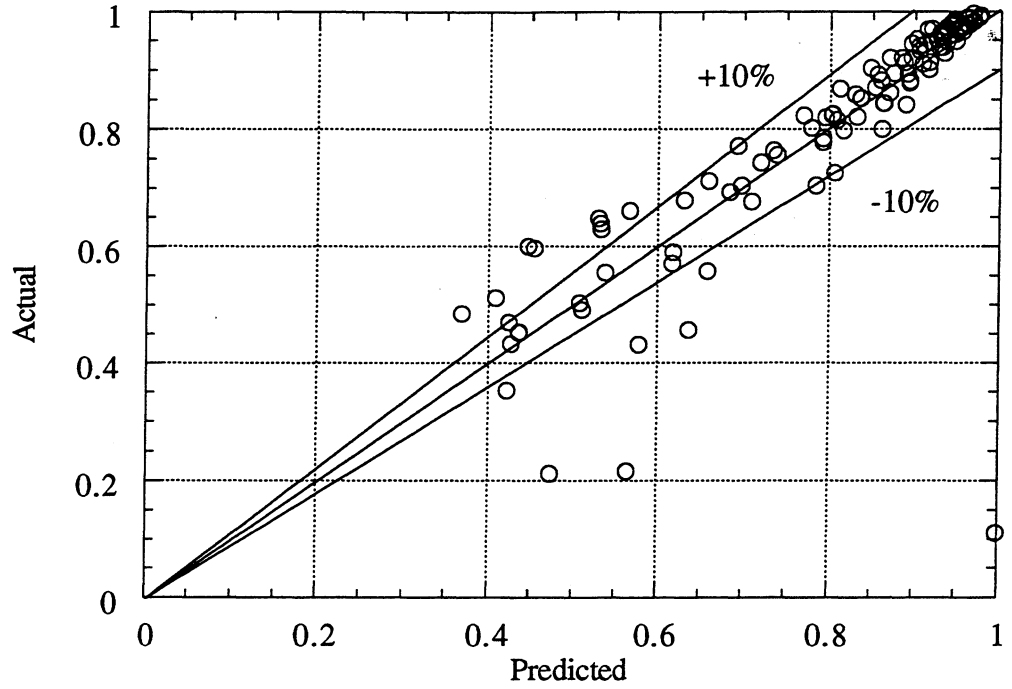

Figure 8.11 Sacks' R22 data vs. the prediction of the smooth tube correlation, Eq. (8.2)

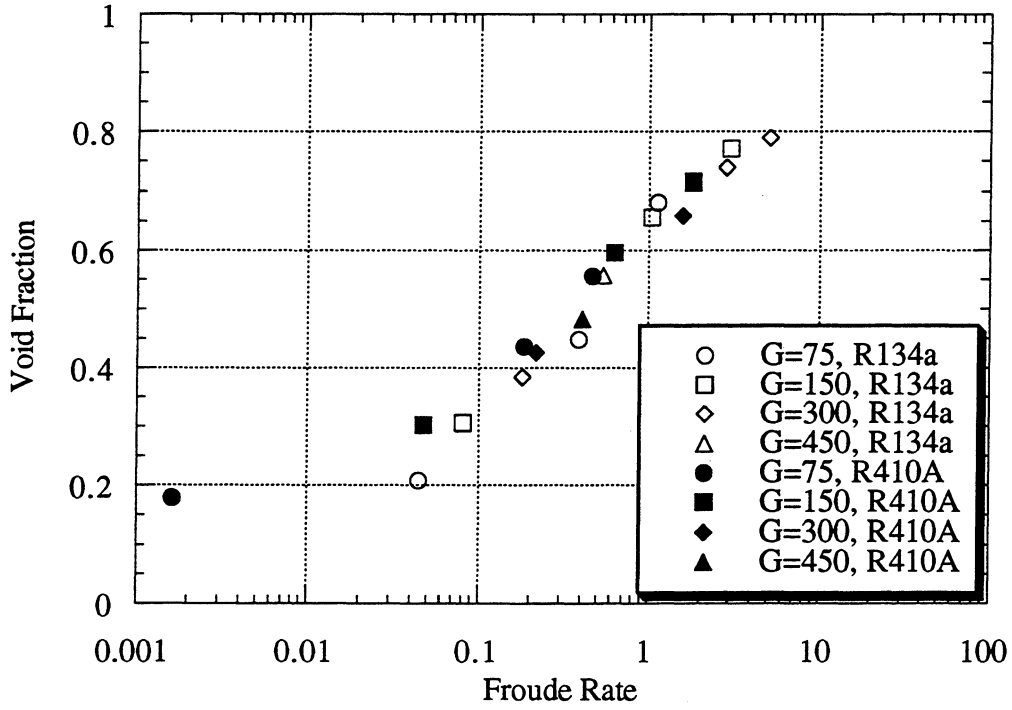

Figure 8.12 Void fraction vs. Froude Rate for the 8.93 mm i.d. helical tube (G is in kg/m^2-s)

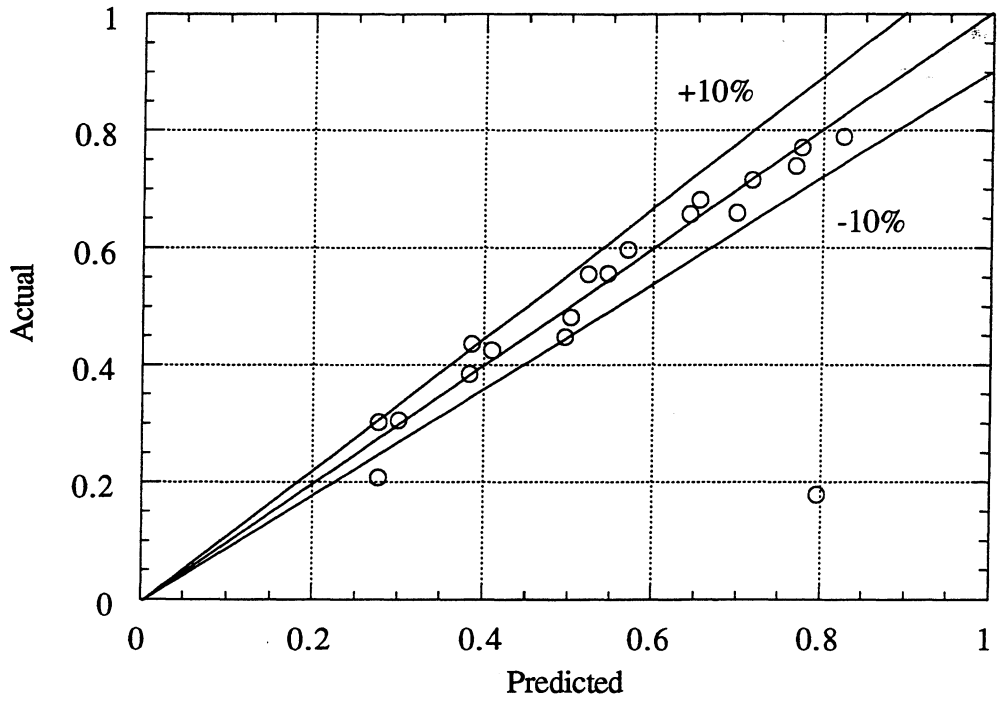

Figure 8.13 Actual void fraction vs. the prediction of the helical tube correlation, Eq. (8.3), for the 8.93 mm i.d. helical tube

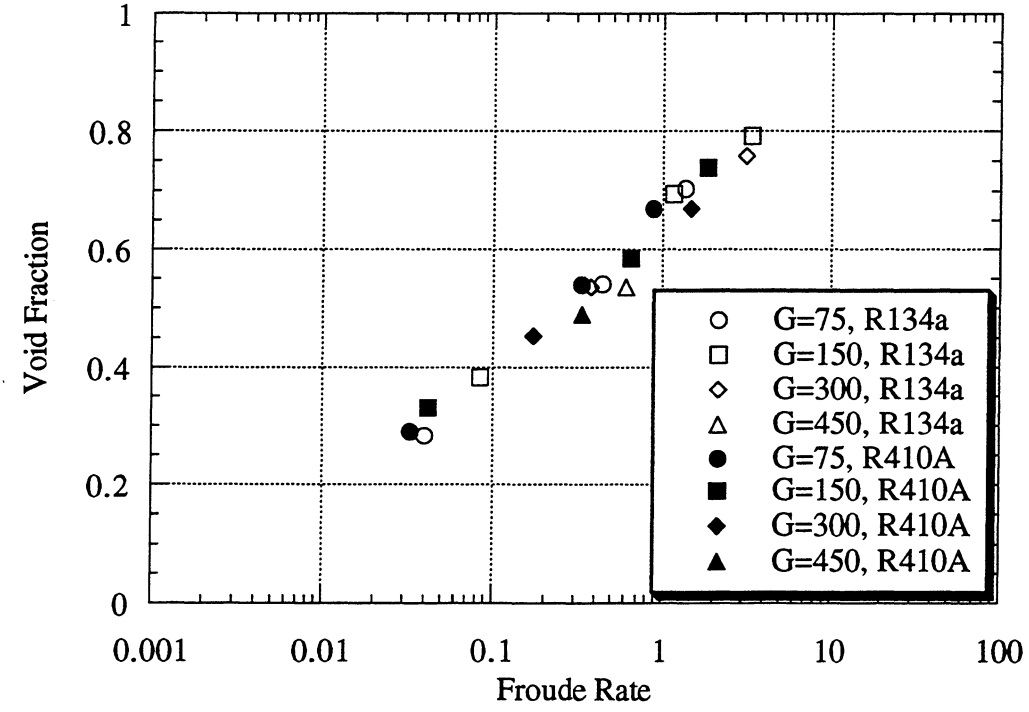

Figure 8.14 Void fraction vs. Froude Rate for the 8.89 mm i.d. axial tube (G is in kg/m^2-s)

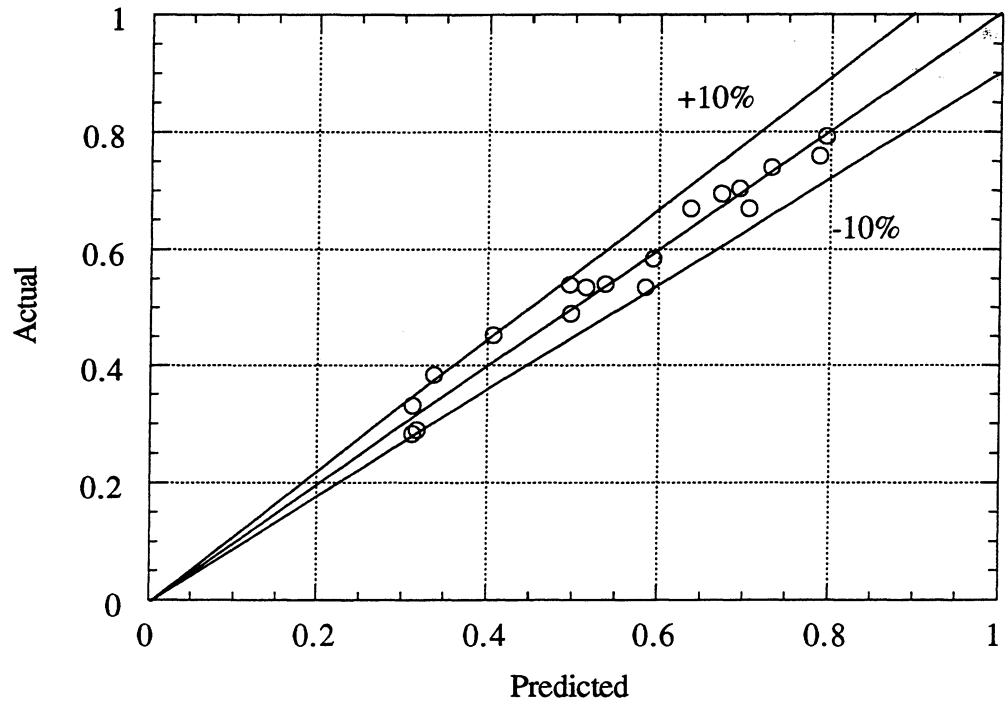

Figure 8.15 Actual void fraction vs. the prediction of the axial tube correlation, Eq. (8.4), for the 8.89 mm i.d. axial tube

Chapter 9

Conclusions

The goal of this study was to study void fraction during refrigerant condensation. A 6.04 mm i.d. smooth tube, 8.93 mm i.d. helical tube, and 8.89 mm i.d. axial tube were all tested with R134a and R410A. The experimental data was collected so that it could be compared to existing correlations, and, if necessary, so that new correlations could be developed. The smooth tube was used as a reference case upon which the grooved tubes could be compared. At an inlet temperature of 35 °C, inlet qualities of 0.1, 0.3, and 0.5 were run with mass fluxes of 75 and 300 kg/m^2-s for the smooth tube and 75, 150, 300, and 450 kg/m^2-s for the grooved tubes.

There were a number of trends observed in each tube tested. It was found that void fraction tends to increase with both inlet and average quality. In addition, it was found that void fraction increases with mass flux as well, with the greatest increases occurring at low average qualities. It is speculated that this is caused by a shift from stratified wavy flow to annular flow as mass flux is increased. R134a was also found to have a higher void fraction than R410A at a given point. This is due to the higher saturation pressure for R410A.

When comparing the data of the 6.04 mm smooth tube to that of the 7.04 mm i.d. smooth tube used in Graham's companion study, it seemed that the larger tube had slightly lower void fractions. The axial tube had consistently lower void fractions than the smooth tube, but slightly higher void fractions than the helical tube. These trends, too, may be attributed to a change in the flow regime caused by the grooves.

The experimental data was also compared to the homogenous, Zivi, Smith, Rigot, Ahrens-Thom, Baroczy, Wallis, Hughmark, Premoli, Tandon, and Graham correlations. With the exception of Graham's correlation, all the aforementioned correlations deviated strongly from the data obtained in this study.

Since Graham's correlation collapsed the data reasonably well with the Froude Rate, a similar format was used to correlate the 6.04 and 7.04 mm i.d. smooth tube data. The correlation obtained had an average deviation of 3.73%. This correlation was also compared to the experimental data of Paul Sacks, and it fit most data within 10%.

In an effort to attain conformity, a variation of the smooth tube correlation was also used to correlate the helical and axial tube data. The helical correlation had an average deviation of 5.95% and the axial had an average deviation of 5.11%.

Bibliography

Ahrens, F. W. 1983. "Heat pump modeling, simulation and design." *Heat Pump Fundamentals. Proceedings of the NATO Advanced Study Institute on Heat Pump Fundamentals, Espinho, Spain, 1980.* J. Berghmans, ed. The Hague, Netherlands: Martinus Nijhoff Publishers.

Anderson, G. H. and B. G. Mantzouranis. 1960. "Liquid entrainment; measuring local mass flow density of liquid drops and their velocity." *Chem. Engrng Sci.*

Bankoff, S. G. 1960. "A variable density single-fluid model for two-phase flow with particular reference to steam-water flow." *Transactions ASME, Journal of Heat Transfer,* Vol. 82, pp. 265-272.

Baroczy, C. J. 1965. "Correlation of liquid fraction in two-phase flow with application to liquid metals." *Chemical Engineering Progress Symposium Series*, Vol. 61, No. 57, pp. 179-191.

Dobson, M. K. 1994. "Heat transfer and flow regimes during condensation in a horizontal tube." Ph.D. Dissertation, University of Illinois.

Dobson, M. K. and J. C. Chato. 1998. "Condensation in smooth horizontal tubes." *Transactions ASME, Journal of Heat Transfer*, Vol. 120, pp. 193-212.

Domanski, P., and D. Didion. 1983. *Computer Modeling of the Vapor Compression Cycle with Constant Flow Area Expansion Device.* NBS Building Science Series 155.

Gaibel, J. A., et al. 1994. "Condensation of a 50/50 blend of R-32/R-125 in horizontal tubes with and without oil." *University of Illinois Air Conditioning and Refrigeration Center Technical Report* , 56.

Graham, D. M. 1998. "Experimental investigation of void fraction during refrigerant condensation." M.S. Thesis, University of Illinois.

Haywood, R. W., Knights, G. A., Middleton, G. E. and J. R. S. Thom. 1961. "Experimental study of the flow conditions and pressure drop of steam-water mixtures at high pressures in heated and unheated tubes." *Proc. Instn. Mech. Engrs.*

Hinde, D. K., M. K. Dobson, J. C. Chato, M. E. Mainland and N. L. Rhines. 1992 "Condensation of refrigerants 12 and 134a in horizontal tubes with and without oils." *University of Illinois Air Conditioning and Refrigeration Center Technical Report* , 26.

Hughmark, G. A. 1962. "Holdup in gas-liquid flow." *Chemical Engineering Progress,* Vol. 58, No. 4, pp. 62-65.

Hurlburt, E. T. and T. A. Newell. 1997. "Prediction of the circumferential film thickness distribution in horizontal annular gas-liquid flow." Submitted to Int. J. Multiphase Flow.

Isbin, H. S., Shear, N. C. and K. C. Eddy. 1957. "Void fractions in two-phase steam-water flow." *A.I.Ch.E. Jl*, Vol. 3, pp. 136-142.

Kenney, P. J., et al. 1994, "Condensation of a zeotropic refrigerant R-32/R-125/R-134a (23% / 25% / 52%) in a horizontal tube." *University of Illinois Air Conditioning and Refrigeration Center Technical Report*, 62.

Larson, H. C. 1957. "Void fractions of two-phase steam water mixtures." M.S. Thesis, University of Minnesota.

Lockhart, R. W. and R. C. Martinelli. 1949. "Proposed correlation of data for isothermal two-phase, two-component flow in pipes." *Chemical Engineering Progress*, Vol. 45, No. 1, pp. 39-48.

Maurer, G. 1960. "A method for predicting steady-state boiling vapor fractions in reactor coolant channels." Bettis Technical Review, WAPD-BT-19.

Martinelli, R. C., and D. B. Nelson. 1948. "Prediction of pressure drop during forced-circulation boiling of water." *Transactions ASME*, Vol. 70, pp. 695-702.

Ponchner, M. 1995. "Condensation of HFC-134a in an 18° helix angle micro-finned tube." M.S. Thesis, University of Illinois.

Polaski, M. 1993. "Comparison of the accuracy of thermocouple mounting techniques on concentric tube heat exchangers." Independent Study Project, University of Illinois.

Premoli, A., D. Francesco, and A. Prina. 1971. "A dimensional correlation for evaluating two-phase mixture density." *La Termotecnica*, Vol. 25, No. 1, pp. 17-26.

Rice, C.K. 1987. "The effect of void fraction correlation and heat flux assumption on refrigerant charge inventory predictions." *ASHRAE Transactions*, Vol. 93, Part 1, pp. 341-367.

Rouhani, S.Z. and K.M. Becker. 1963. "Measurements of void fraction for flow of boiling heavy water in vertical round duct." *Aktebolaget Atomenergie Rep.*, No. AE-106.

Sacks, P.S. 1975. "Measured characteristics of adiabatic and condensing single-component two-phase flow of refrigerant in a 0.377-In. diameter horizontal tube." ASME Winter Annual Meeting, Houston, TX, 75-WA/HT-24.

Smith, S. L. 1969. "Void fractions in two-phase flow: a correlation based upon an equal velocity head model." *Proc. Instn. Mech Engrs.*, London, Vol. 184, Pt. 1, No. 36, pp. 647-664.

Sweeney, K. A. 1996. "The heat transfer and pressure drop behavior of a zeotropic refrigerant mixture in a microfinned tube." M.S. Thesis, University of Illinois.

Tandon, T. N., H. K. Varma, and C. P. Gupta. 1985. "A void fraction model for annular two-phase flow." *International Journal of Heat and Mass Transfer*, Vol. 28, No. 1, pp. 191-198.

Thom, J. R. S. 1964. "Prediction of pressure drop during forced circulation boiling of water." *International Journal of Heat and Mass Transfer*, Vol. 7, pp. 709-724.

Wallis, G. B. 1969. *One-Dimensional Two-Phase Flow*. New York: McGraw-Hill, pp. 51-54.

Wilson, M. J. 1998. "Experimental investigation of void fraction during horizontal flow in larger diameter applications." M.S. Thesis, University of Illinois.

Yashar, D. A. 1998. "Experimental investigation of void fraction during horizontal flow in smaller diameter refrigeration applications." M.S. Thesis, University of Illinois.

Zivi, S. M. 1964. "Estimation of steady-state steam void-fraction by means of the principle of minimum entropy production." *Transactions ASME, Journal of Heat Transfer*, Series C, Vol. 86, May, pp. 247-252.

Appendix A

Experimental Data

This appendix contains the raw experimental data for all three tubes which were tested, as well as how the data compares to the various correlations given in Chapter 8. Graham's smooth tube data is also listed since it was used to develop the smooth tube correlation. The mass flux is given in kg/m^2-s. Generally, the mass flux was within 2.5% of the value in the tables. The average quality is reported, as well as the Froude Rate, which was defined in Chapter 2.

Table A.1

6.04 mm i.d. Smooth Tube Data and Correlation Values

Refrigerant	G	x	α-measured	Ft	α-predicted	% difference
R134a	75	0.067	0.356	0.127	0.414	-16.38
R134a	75	0.184	0.616	0.619	0.615	0.15
R134a	75	0.397	0.772	2.276	0.771	0.05
R134a	300	0.080	0.636	0.677	0.627	1.41
R134a	300	0.248	0.844	3.995	0.824	2.33
R134a	300	0.374	0.877	8.126	0.876	0.11
R410A	75	0.011	0.326	0.004	0.649	-99.10
R410A	75	0.166	0.521	0.276	0.505	2.97
R410A	75	0.378	0.680	1.109	0.690	-1.46
R410A	300	0.045	0.484	0.146	0.429	11.40
R410A	300	0.223	0.738	1.744	0.743	-0.70
R410A	300	0.369	0.874	4.456	0.833	4.72

Table A.2

6.04 mm i.d. Smooth Tube Data for Adiabatic Tests and Correlation Values

Refrigerant	G	x	α-measured	Ft	α-predicted	% difference
R134a	75	0.077	0.510	0.158	0.437	14.29
R134a	75	0.273	0.730	1.197	0.699	4.22
R134a	300	0.094	0.682	0.869	0.659	3.35
R134a	300	0.296	0.865	5.396	0.848	2.01
R410A	75	0.064	0.454	0.062	0.364	19.74
R410A	75	0.256	0.662	0.567	0.603	8.98
R410A	300	0.092	0.594	0.447	0.570	3.96
R410A	300	0.308	0.835	3.031	0.799	4.24

Table A.3

6.04 mm i.d. Smooth Tube Data for Evaporation Tests and Correlation Values

Refrigerant	G	x	α-measured	Ft	α-predicted	% difference
R410A	75	0.258	0.636	0.595	0.609	4.26
R410A	75	0.447	0.768	1.656	0.737	4.01
R410A	300	0.160	0.717	1.146	0.694	3.26
R410A	300	0.329	0.852	3.337	0.808	5.10

Table A.4

Graham's 7.04 mm i.d. Smooth Tube Data and Correlation Values

Refrigerant	G	x	α-measured	Ft	α-predicted	% difference
R134a	75	0.071	0.413	0.131	0.417	-0.92
R134a	75	0.174	0.562	0.518	0.591	-5.15
R134a	75	0.412	0.714	2.267	0.771	-7.97
R134a	75	0.545	0.818	3.923	0.822	-0.58
R134a	75	0.721	0.880	7.880	0.874	0.69
R134a	150	0.112	0.603	0.524	0.592	1.75
R134a	150	0.245	0.760	1.857	0.750	1.30
R134a	150	0.473	0.881	5.948	0.855	2.98
R134a	150	0.668	0.924	12.790	0.902	2.30
R134a	150	0.86	0.947	28.066	0.936	1.10
R134a	300	0.115	0.736	1.111	0.690	6.15
R134a	300	0.264	0.830	4.326	0.831	-0.08
R134a	300	0.491	0.887	12.510	0.901	-1.65
R134a	300	0.678	0.926	25.457	0.933	-0.70
R134a	300	0.885	0.947	63.396	0.959	-1.32
R134a	450	0.117	0.754	1.665	0.738	2.07
R134a	450	0.295	0.855	7.594	0.872	-2.03
R134a	450	0.466	0.898	17.574	0.918	-2.19
R134a	450	0.658	0.940	37.432	0.945	-0.56
R134a	450	0.846	0.958	78.506	0.963	-0.56
R410A	75	0.054	0.329	0.044	0.358	-8.79
R410A	75	0.215	0.514	0.381	0.549	-6.79
R410A	75	0.412	0.701	1.167	0.696	0.69
R410A	75	0.554	0.757	2.133	0.765	-1.07
R410A	75	0.769	0.861	4.709	0.837	2.70
R410A	150	0.075	0.406	0.149	0.431	-6.09
R410A	150	0.262	0.650	1.062	0.685	-5.40
R410A	150	0.439	0.780	2.676	0.788	-0.94
R410A	150	0.629	0.851	5.462	0.849	0.20
R410A	150	0.842	0.929	13.356	0.904	2.58
R410A	300	0.093	0.488	0.419	0.562	-15.03
R410A	300	0.26	0.738	2.509	0.781	-5.89
R410A	300	0.424	0.828	5.176	0.845	-2.06
R410A	300	0.639	0.904	11.641	0.897	0.70
R410A	300	0.878	0.951	32.082	0.941	1.07
R410A	450	0.095	0.611	0.637	0.618	-1.22
R410A	450	0.271	0.760	3.480	0.812	-6.91
R410A	450	0.467	0.848	9.296	0.885	-4.27
R410A	450	0.659	0.911	19.309	0.922	-1.14
R410A	450	0.839	0.953	40.437	0.948	0.54

Table A.5

8.93 mm i.d. Helical Tube Data and Correlation Values

Refrigerant	G	x	α-measured	Ft	α-predicted	% difference
R134a	75	0.039	0.208	0.045	0.278	-33.76
R134a	75	0.154	0.448	0.385	0.494	-10.26
R134a	75	0.297	0.681	1.129	0.654	3.94
R134a	150	0.036	0.306	0.081	0.301	1.58
R134a	150	0.186	0.657	1.039	0.643	2.24
R134a	150	0.352	0.771	3.026	0.774	-0.44
R134a	300	0.039	0.384	0.180	0.384	0.07
R134a	300	0.226	0.738	2.847	0.768	-4.01
R134a	300	0.360	0.788	5.108	0.824	-4.59
R134a	450	0.060	0.557	0.536	0.545	2.11
R410A	75	0.007	0.179	0.002	0.796	-345.93
R410A	75	0.144	0.435	0.184	0.387	11.11
R410A	75	0.255	0.556	0.463	0.522	6.01
R410A	150	0.038	0.302	0.048	0.279	7.79
R410A	150	0.201	0.597	0.625	0.568	4.81
R410A	150	0.376	0.714	1.805	0.716	-0.15
R410A	300	0.066	0.426	0.218	0.410	3.68
R410A	300	0.239	0.659	1.565	0.698	-5.81
R410A	450	0.076	0.482	0.405	0.502	-4.30

Table A.6

8.89 mm i.d. Axial Tube Data and Correlation Values

Refrigerant	G	x	α-measured	Ft	α-predicted	% difference
R134a	75	0.036	0.283	0.040	0.314	-10.90
R134a	75	0.167	0.540	0.436	0.537	0.55
R134a	75	0.329	0.702	1.344	0.694	1.23
R134a	150	0.037	0.383	0.085	0.338	11.69
R134a	150	0.197	0.695	1.139	0.672	3.26
R134a	150	0.374	0.792	3.329	0.795	-0.31
R134a	300	0.062	0.535	0.372	0.514	3.96
R134a	300	0.240	0.758	3.104	0.788	-3.92
R134a	450	0.065	0.536	0.600	0.584	-8.91
R410A	75	0.048	0.290	0.033	0.319	-10.12
R410A	75	0.207	0.539	0.327	0.496	8.06
R410A	75	0.369	0.670	0.874	0.637	4.92
R410A	150	0.036	0.331	0.042	0.314	5.08
R410A	150	0.205	0.585	0.640	0.593	-1.39
R410A	150	0.385	0.739	1.827	0.731	1.06
R410A	300	0.057	0.452	0.171	0.408	9.77
R410A	300	0.231	0.669	1.467	0.704	-5.25
R410A	450	0.067	0.489	0.330	0.497	-1.69

Appendix B

Correlation Predictions for the Helical Tube

In this appendix, the figures comparing correlations to actual data for the 8.93 mm i.d. helical tube are shown.

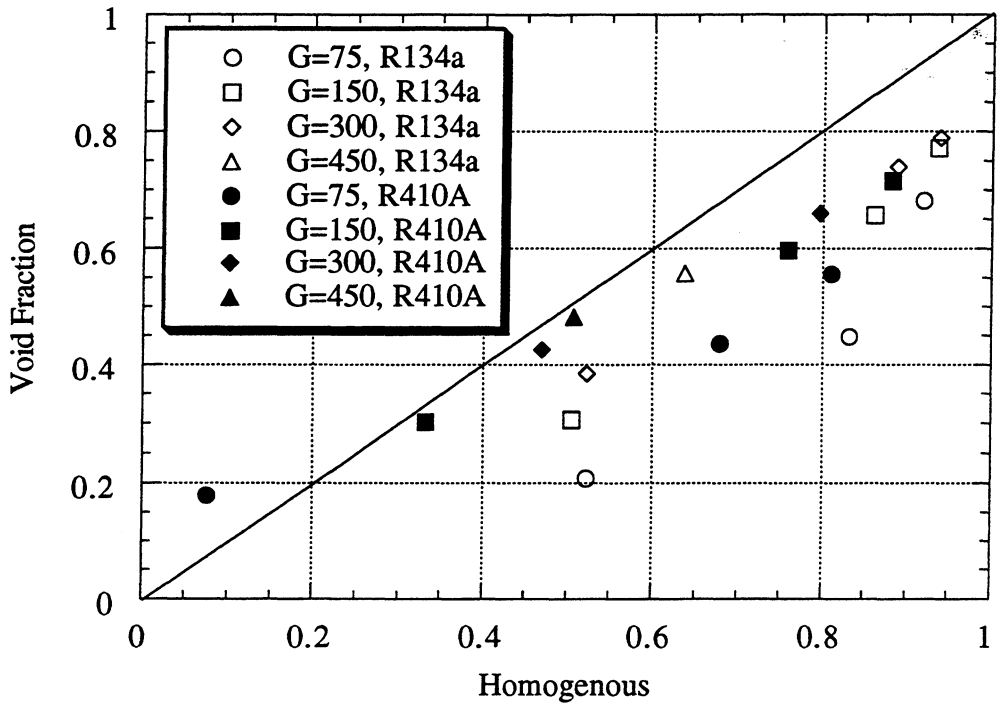

Figure B.1 Actual void fraction vs. homogenous prediction for the 8.93 mm i.d. helical tube (G is in kg/m^2-s)

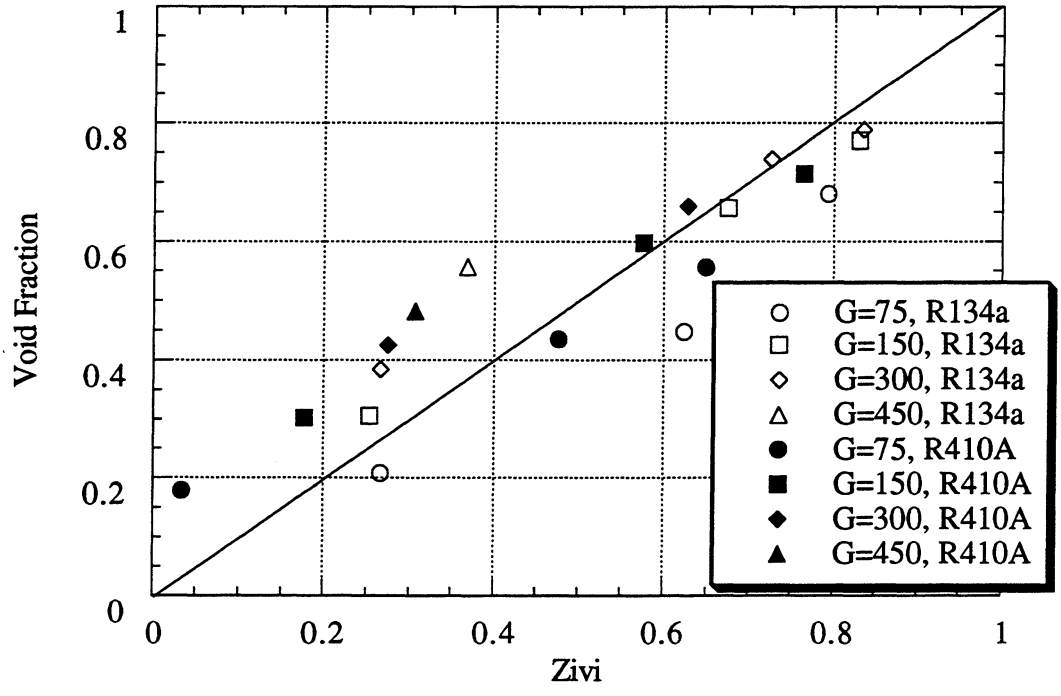

Figure B.2 Actual void fraction vs. Zivi prediction for the 8.93 mm i.d. helical tube (G is in kg/m^2-s)

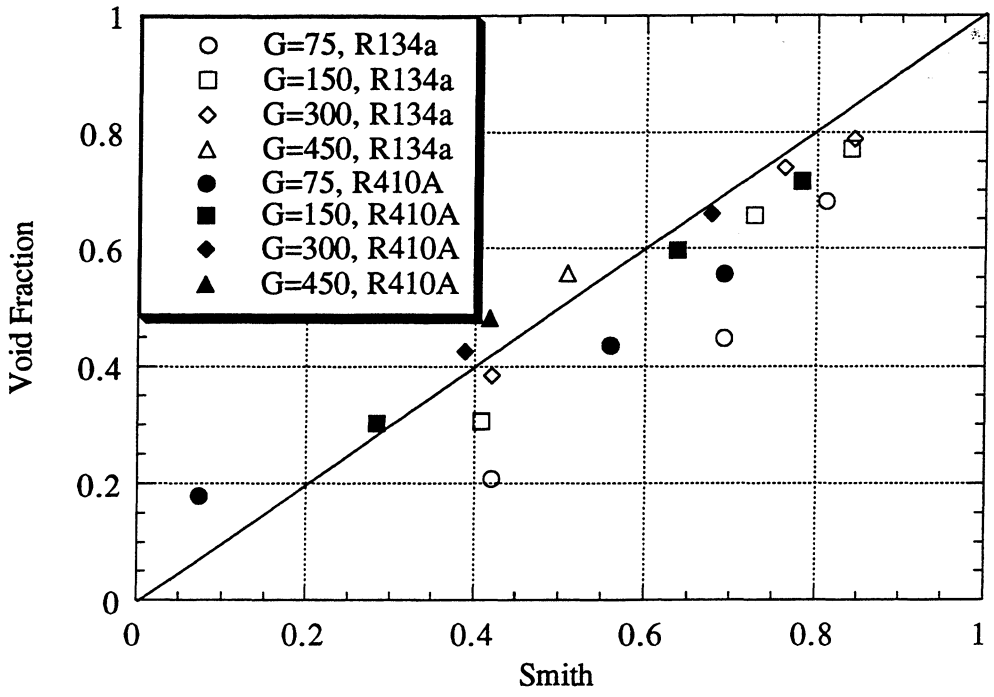

Figure B.3 Actual void fraction vs. Smith prediction for the 8.93 mm i.d. helical tube (G is in kg/m^2-s)

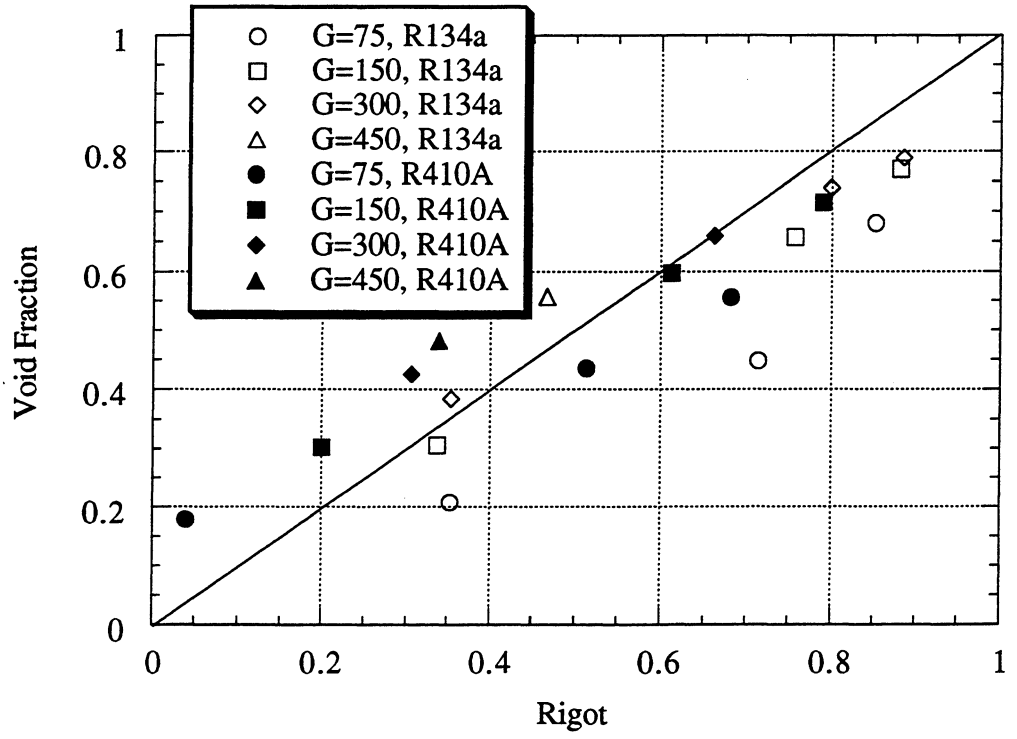

Figure B.4 Actual void fraction vs. Rigot prediction for the 8.93 mm i.d. helical tube (G is in kg/m^2-s)

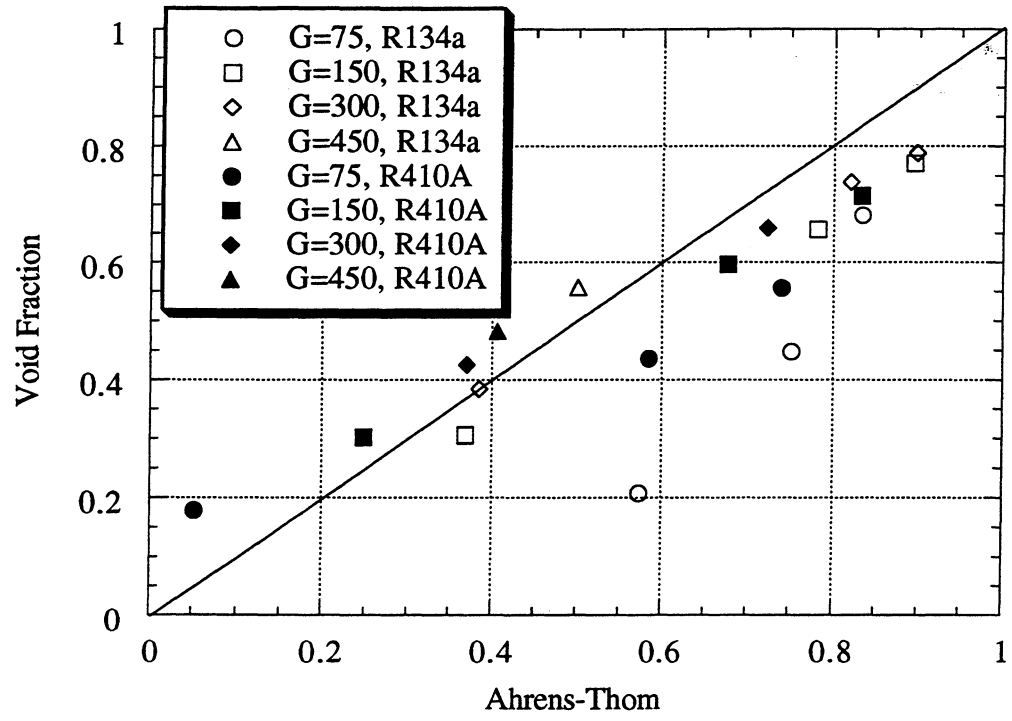

Figure B.5 Actual void fraction vs. Ahrens-Thom prediction for the 8.93 mm i.d. helical tube (G is in kg/m^2-s)

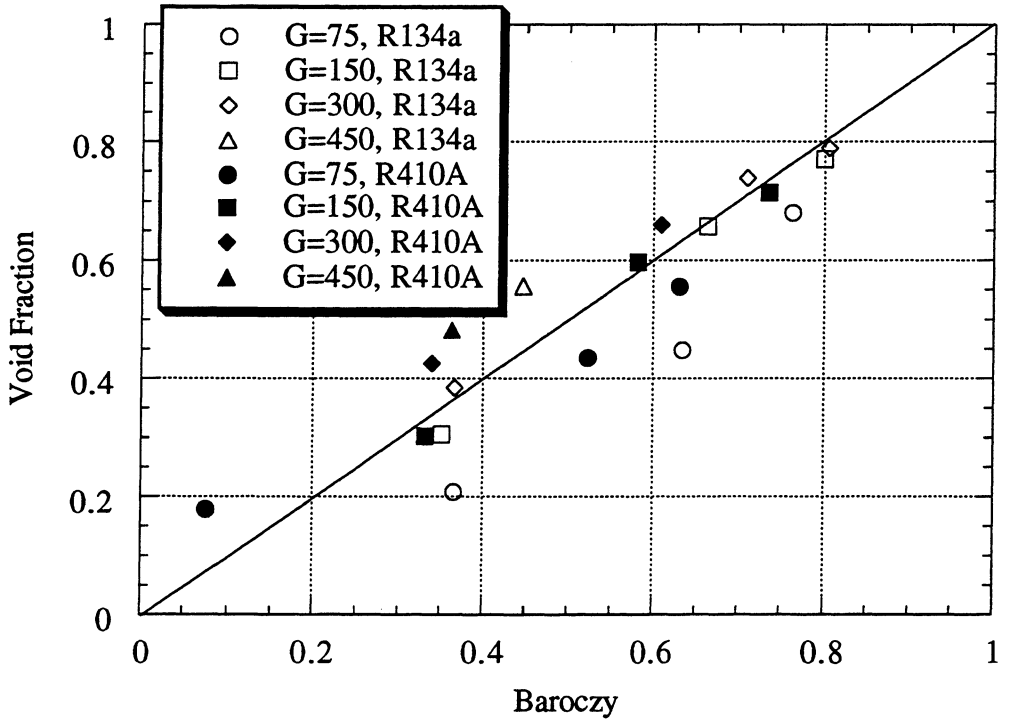

Figure B.6 Actual void fraction vs. Baroczy prediction for the 8.93 mm i.d. helical tube (G is in kg/m^2-s)

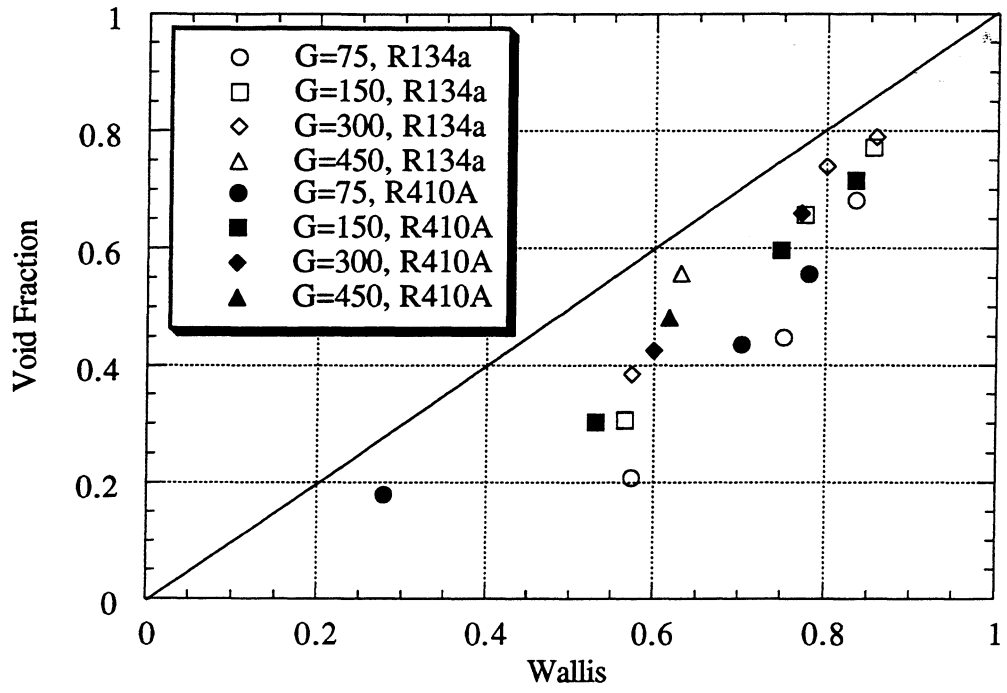

Figure B.7 Actual void fraction vs. Wallis prediction for the 8.93 mm i.d. helical tube (G is in kg/m^2-s)

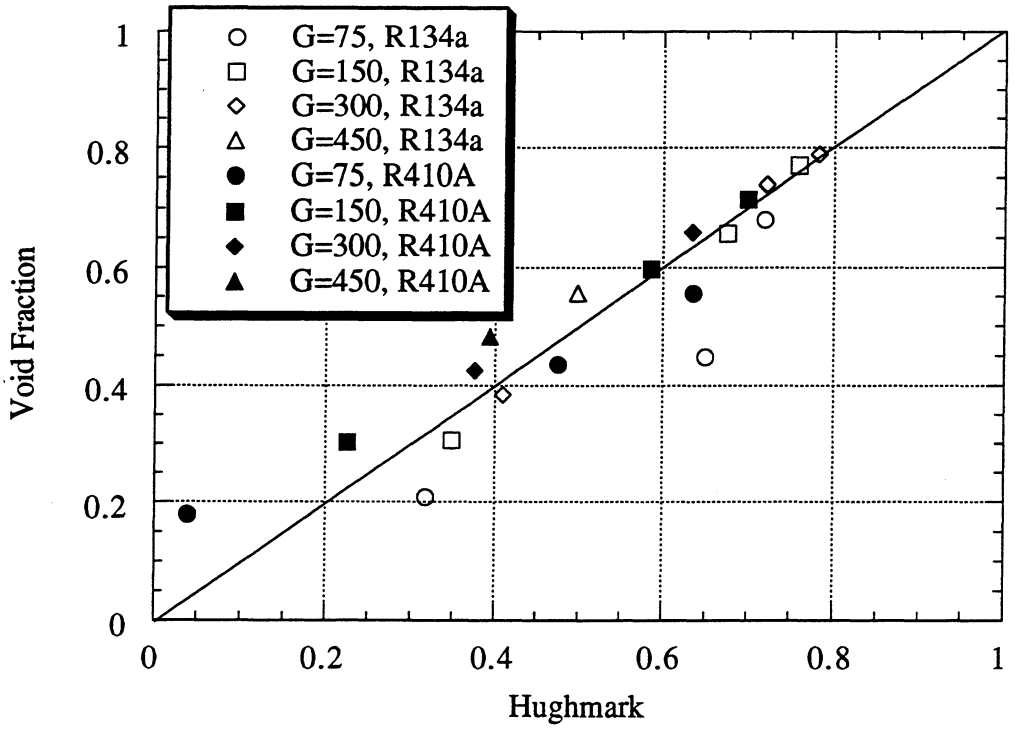

Figure B.8 Actual void fraction vs. Hughmark prediction for the 8.93 mm i.d. helical tube (G is in kg/m^2-s)

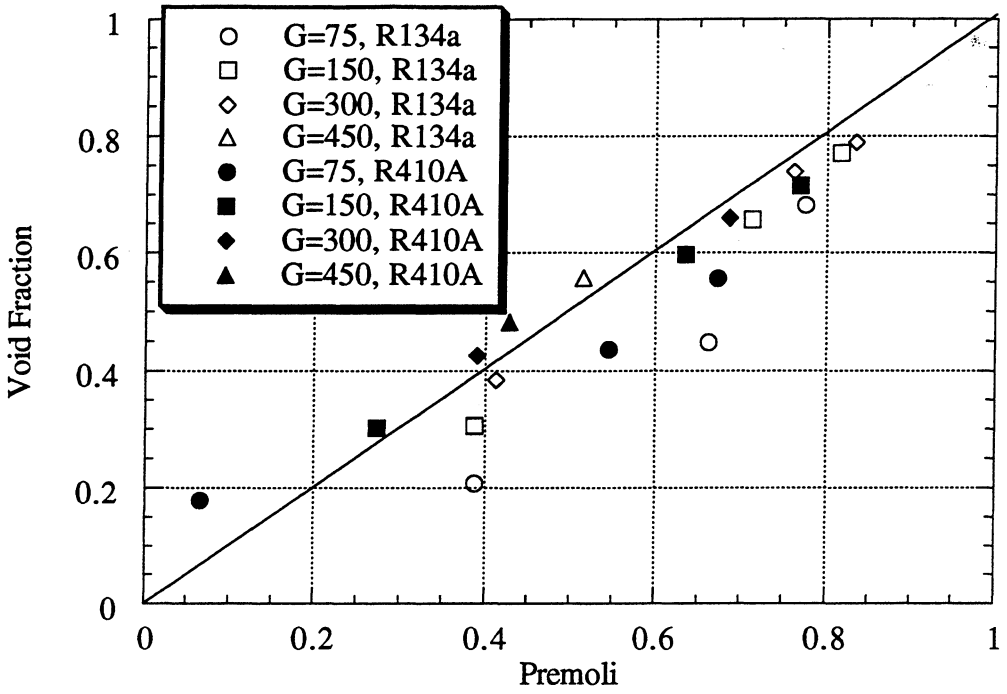

Figure B.9 Actual void fraction vs. Premoli prediction for the 8.93 mm i.d. helical tube (G is in kg/m^2-s)

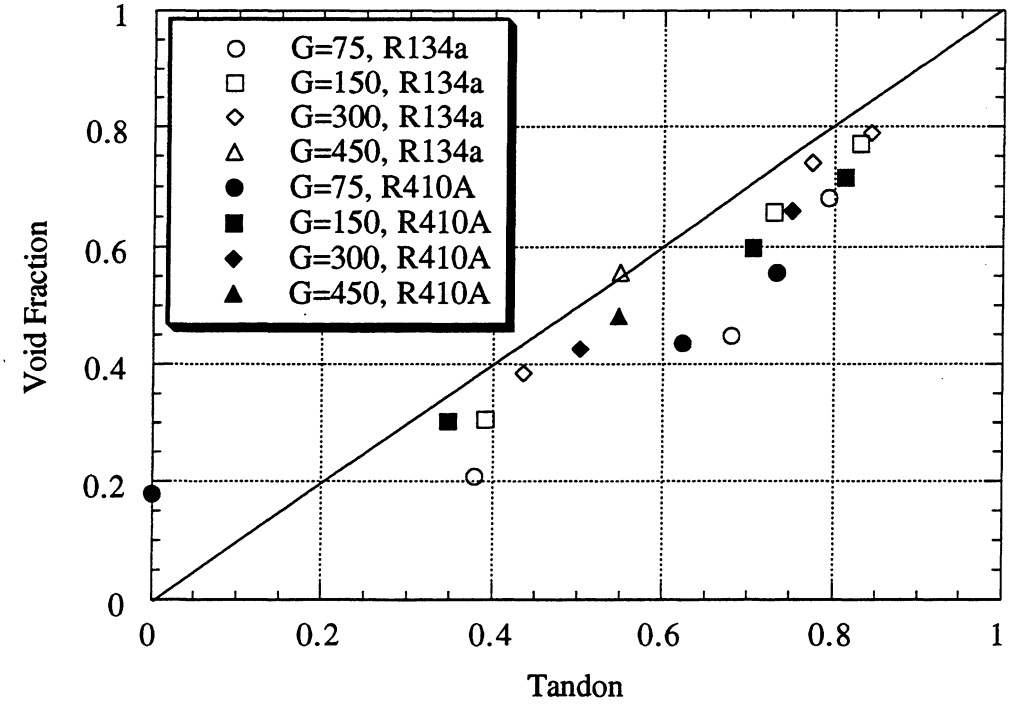

Figure B.10 Actual void fraction vs. Tandon prediction for the 8.93 mm i.d. helical tube (G is in kg/m^2-s)

Table B.1

Correlation Prediction Errors for the 8.93 mm i.d. Helical Tube

Correlation	Average Error (%)
Homogenous	38.75
Zivi	22.04
Smith	21.92
Rigot	24.33
Ahrens-Thom	25.91
Baroczy	17.82
Wallis	43.20
Hughmark	16.17
Premoli	19.42
Tandon	25.85

Appendix C

Correlation Predictions for the Axial Tube

In this appendix, the figures comparing correlations to actual data for the 8.89 mm i.d. axial tube are shown.

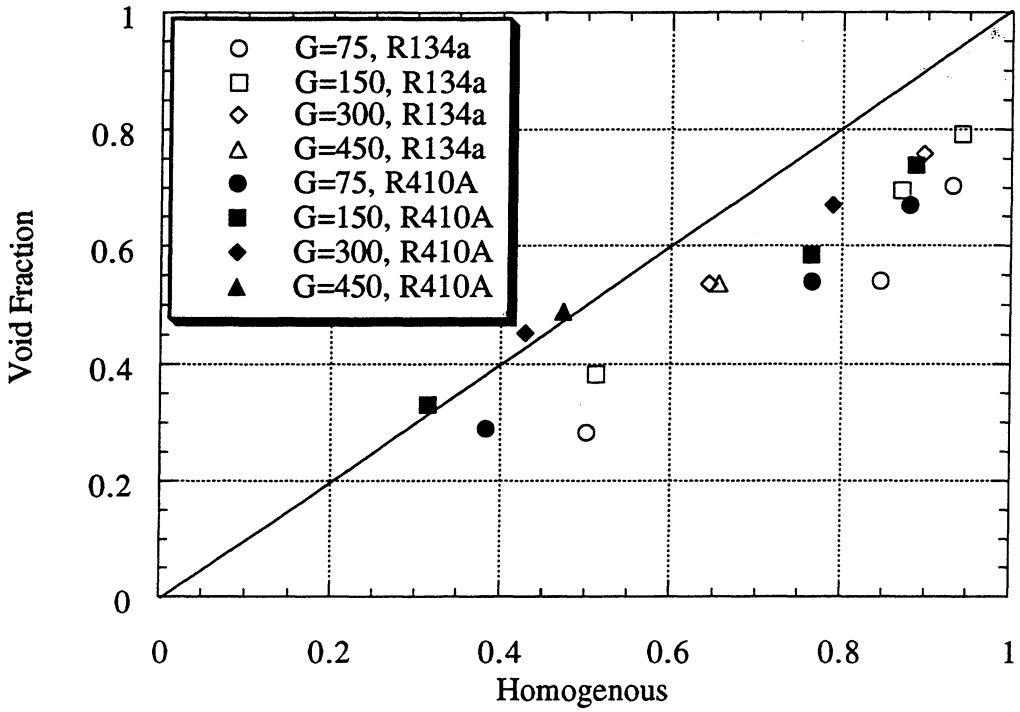

Figure C.1 Actual void fraction vs. homogenous prediction for 8.89 mm i.d. axial tube (G is in kg/m^2-s)

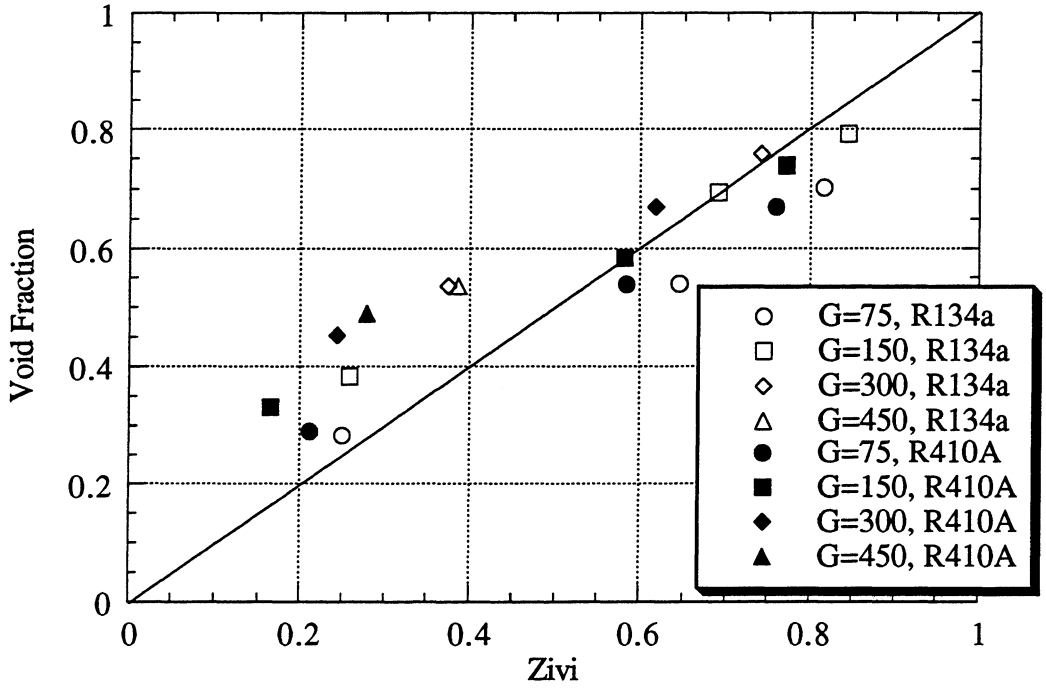

Figure C.2 Actual void fraction vs. Zivi prediction for the 8.89 mm i.d. axial tube (G is in kg/m^2-s)

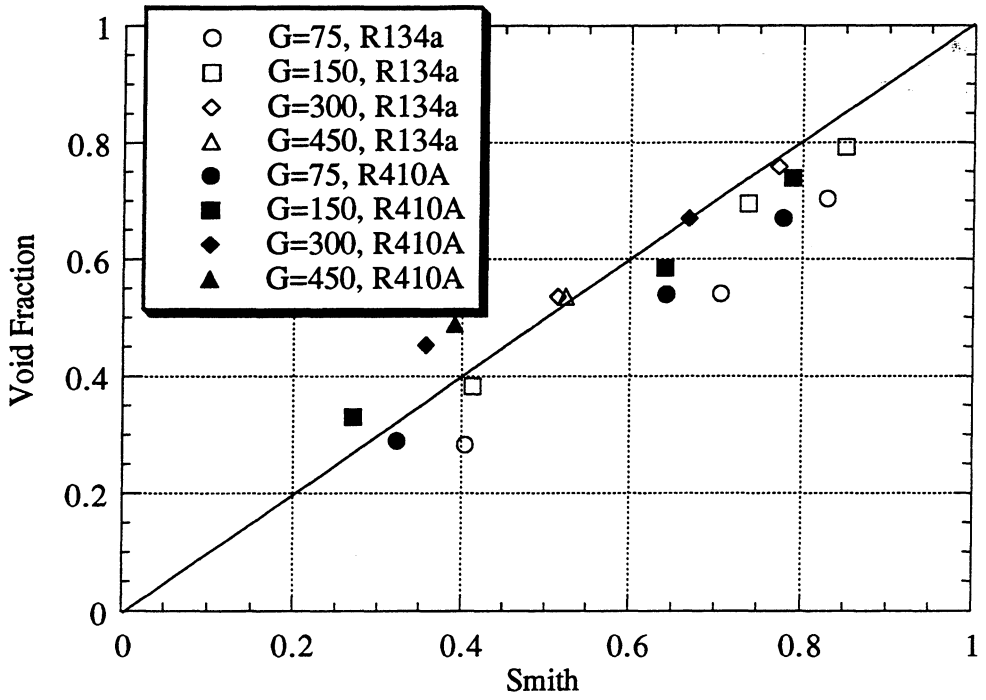

Figure C.3 Actual void fraction vs. Smith prediction for the 8.89 mm i.d. axial tube (G is in kg/m^2-s)

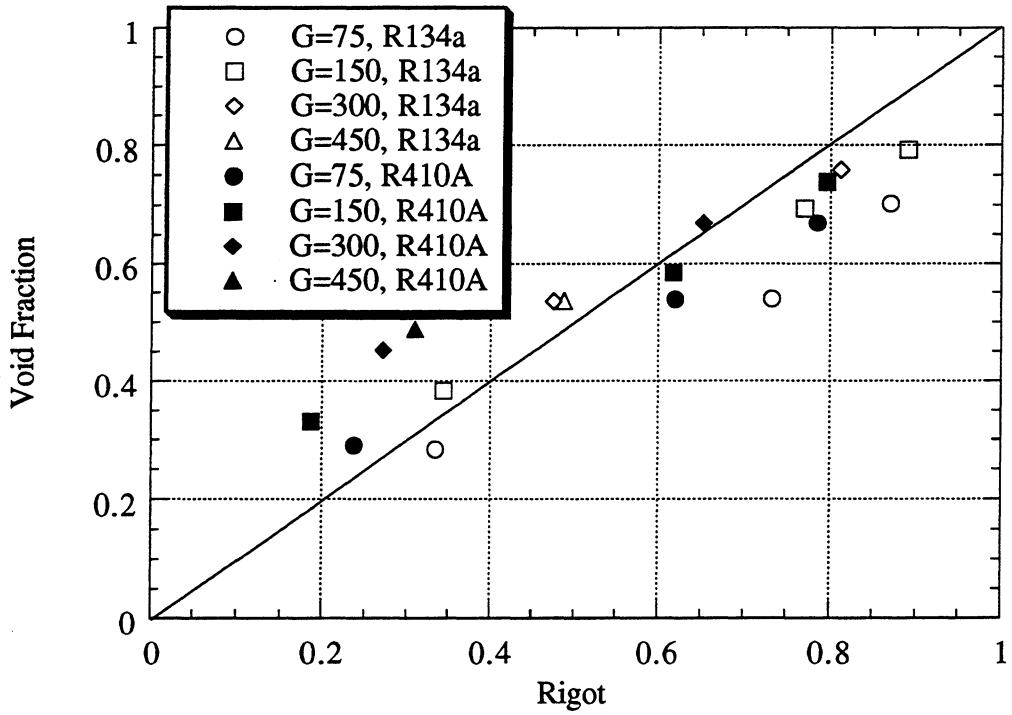

Figure C.4 Actual void fraction vs. Rigot prediction for the 8.89 mm i.d. axial tube (G is in kg/m^2-s)

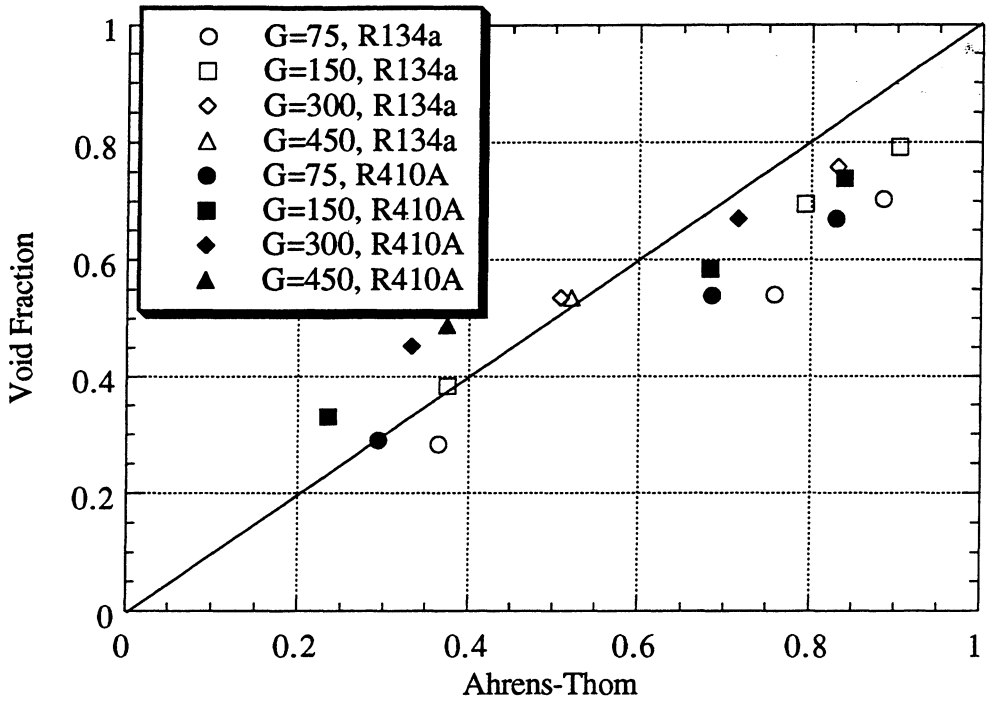

Figure C.5 Actual void fraction vs. Ahrens-Thom prediction for the 8.89 mm i.d. axial tube (G is in kg/m^2-s)

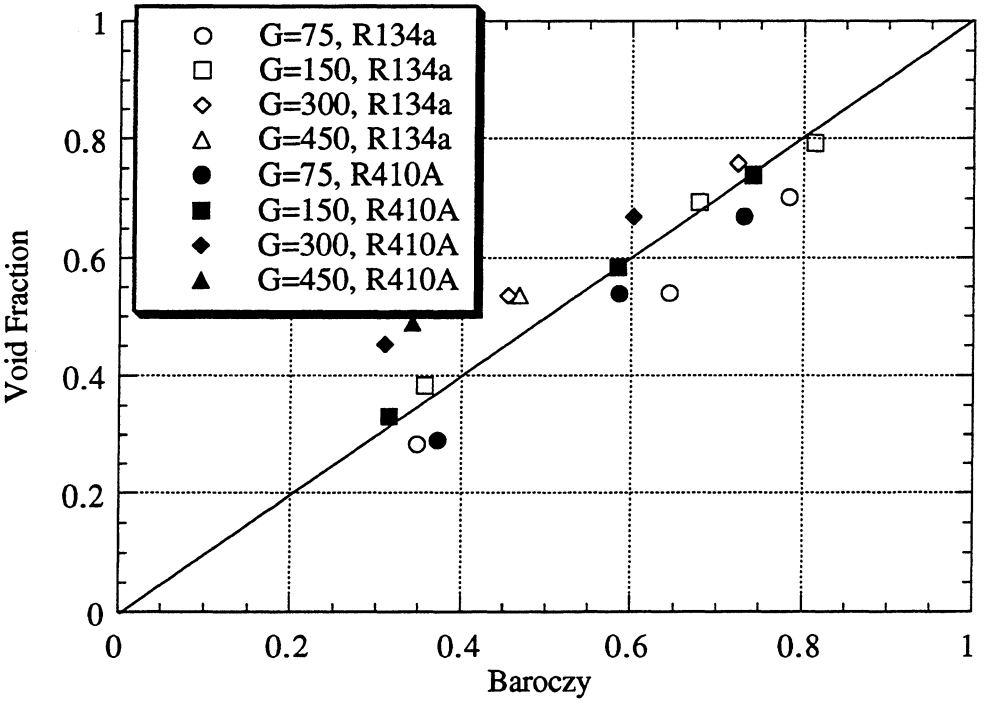

Figure C.6 Actual void fraction vs. Baroczy prediction for the 8.89 mm i.d. axial tube (G is in kg/m^2-s)

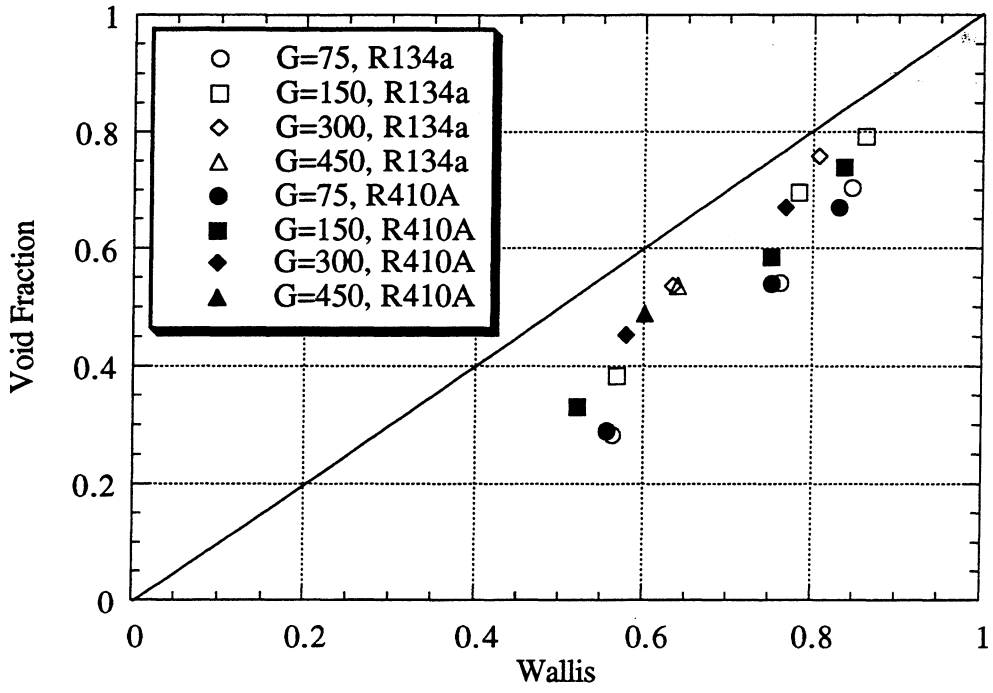

Figure C.7 Actual void fraction vs. Wallis prediction for the 8.89 mm i.d. axial tube (G is in kg/m^2-s)

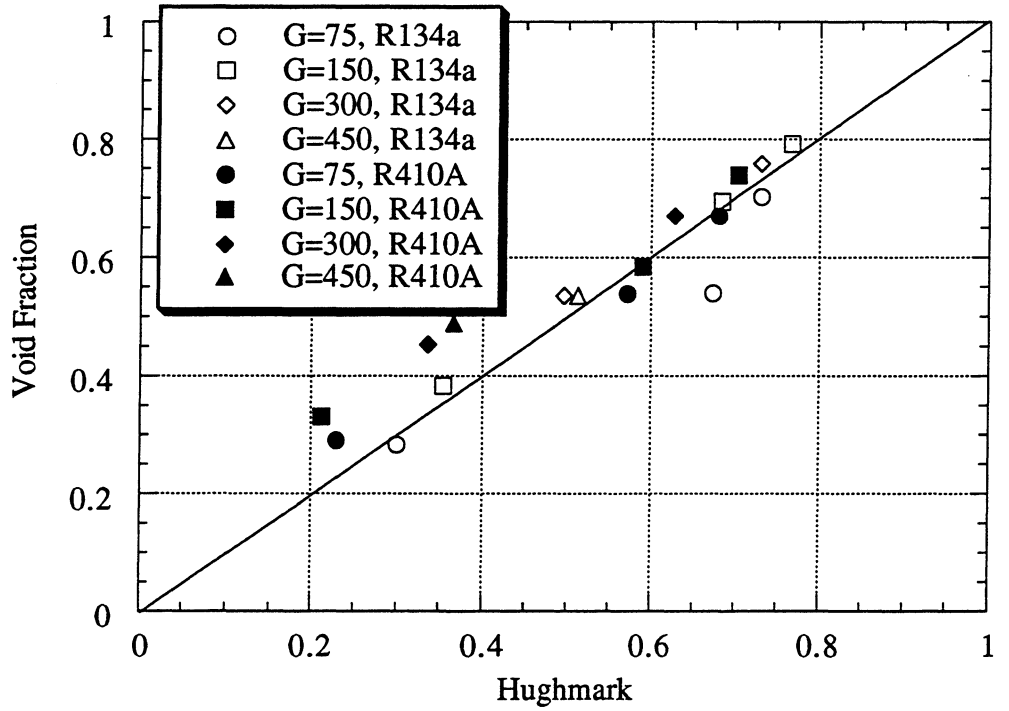

Figure C.8 Actual void fraction vs. Hughmark prediction for the 8.89 mm i.d. axial tube (G is in kg/m^2-s)

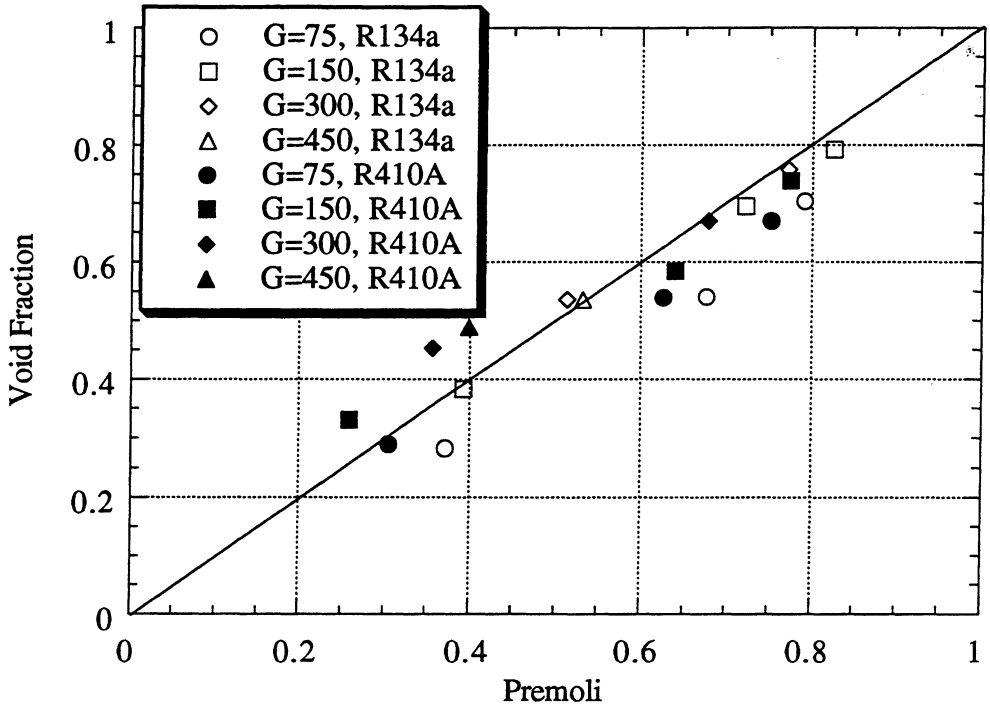

Figure C.9 Actual void fraction vs. Premoli prediction for the 8.89 mm i.d. axial tube (G is in kg/m^2-s)

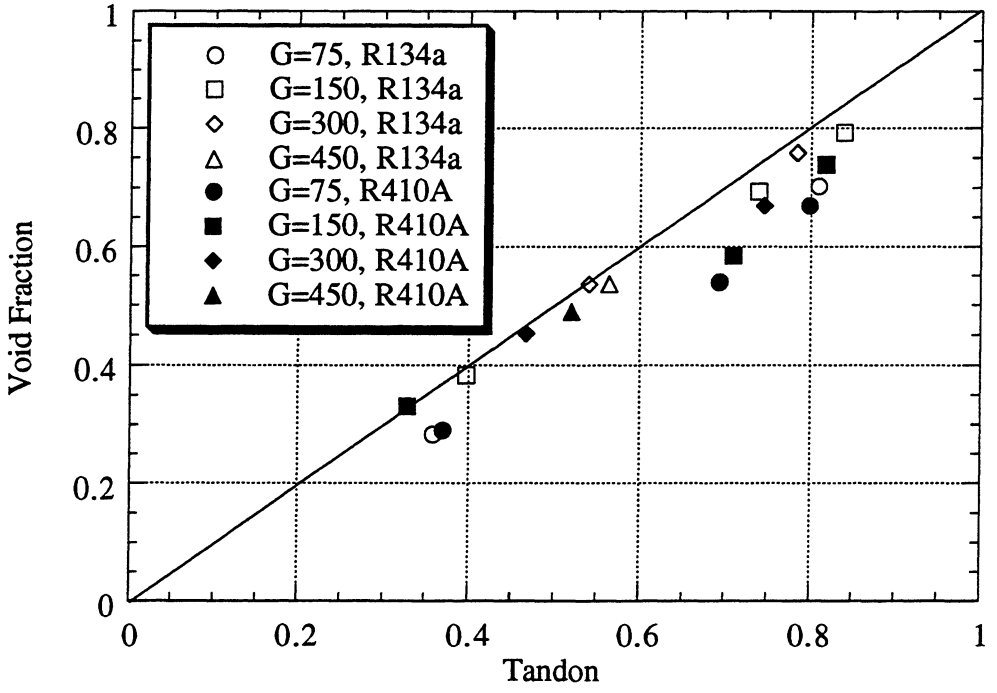

Figure C.10 Actual void fraction vs. Tandon prediction for the 8.89 mm i.d. axial tube (G is in kg/m^2-s)

Table C.1

Correlation Prediction Errors for the 8.89 mm i.d. Axial Tube

Correlation	Average Error (%)
Homogenous	27.36
Zivi	19.29
Smith	13.56
Rigot	18.02
Ahrens-Thom	17.28
Baroczy	12.28
Wallis	33.12
Hughmark	10.48
Premoli	10.97
Tandon	12.56